KINETIC MECHANISM STUDY AND WASTE TYRE CHARACTERISATION FOR VALUABLE CHEMICALS PRODUCTION

by

Mwelwa Katambwa Maxwell

Submitted in fulfilment of the academic requirements of the Master of Science Degree in Chemical Engineering,

College of Agriculture, Engineering and Science,

University of KwaZulu-Natal, Durban, South Africa

February 2022

Supervisor: Dr N.M. Mkhize

Co-supervisor: Dr S.A. Iwarere

As the candidate's supervisor and co-supervisor, we have approved this thesis/dissertation for submission.

[redacted]

Dr N.M. Mkhize

09/02/2022

Date

[redacted]

Dr S.A. Iwarere

09/02/2022

Date

DECLARATION 1 - PLAGIARISM

I, Mwelwa Katambwa Maxwell, declare that

1. Unless otherwise stated, all of the research presented in this thesis is my own.
2. This thesis has not been submitted to any other university for a degree or examination.
3. This thesis does not contain other persons' data, pictures, graphs, or additional information unless expressly acknowledged as being sourced from other persons.
4. Unless explicitly mentioned as being derived from other authors, this thesis does not contain other people's writing. When other written sources are cited, then:
   a. Their words have been rewritten, but the broad information that they are credited with has been referenced.
   b. Where their precise words were used, their text was italicised, enclosed in quotation marks and referenced.
5. Unless explicitly acknowledged and the source described in the dissertation and References, this thesis does not contain text, tables or graphics copied and pasted from the Internet.

[redacted]

Mwelwa Katambwa Maxwell

09/02/2022

Date

DECLARATION 2 – PUBLICATION

This dissertation includes one unpublished review paper. The development and writing of the paper were my principal responsibility. The initiation and reviewing of the review paper were at the contribution of co-authors Dr Samuel Ayodele Iwarere and Dr Ntandoyenkosi Malusi Mkhize.

Manuscript: Advances in understanding mechanisms underlying tyre valorisation.

09/02/2022

Mwelwa Katambwa Maxwell — Date

Abstract

Researchers have extensively investigated waste tyre pyrolysis kinetics and mechanisms. However, available literature shows limitations as the studies were primarily aimed at tracking the devolatilisation of the main components of the feedstock than the formation of chemicals. In the present study, truck tyre crumbs of less than 1 mm were pyrolysed in a multi-shot pyrolyser connected to a mass spectrometer. The aim is to investigate the kinetics and reaction pathways that favour the formation of specific valuable chemicals (such as limonene and indene) in tyre-derived oil to maximise their production and content.

The multi-shot pyrolyser (EGA/PY-3030D) equipment and accessories have been used to track the temperature and heating rate influence on the formation of chemicals. For temperature influence, experiments were conducted in single-shot mode and at different temperatures (400, 500, 600, and 700 °C), based on thermogravimetric analysis data. Chromatograms analysed regarding the area % of the considered chemicals proved that the selectivity to limonene decreases as temperature increases, reaching a minimum of 28.5% around 700 °C. In contrast, there was no discernible effect of temperature on indene in the considered range of temperature. The selectivity ratios of limonene to isoprene and indene to styrene presented a plateau between 400 and 600 °C. This trend evidenced that several equilibrated reactions steps could have taken place between limonene and isoprene as well as indene and styrene. Above 600 °C, the selectivity ratio of limonene to isoprene decreases, characteristic of cyclisation, hydrogenation and aromatisation reactions.

The influence of heating rate on the production of the chemicals was conducted through Direct Evolved Gas Analysis (EGA) experiments at heating rates of 20, 30, 40, 50 and 100 °C /min and optimum temperature of 500 °C, obtained from temperature influence on the production of the chemical. The selectivity to limonene presented a continuous increase with the increase of heating rate from 30.8 % at 20 °C /min to 37.8 % at 50 °C /min and 42.7% at 100 °C /min. Hence, limonene formation is maximised at higher heating rates.

The kinetic study conducted through combined model fitting and model-free approaches presented values in the range of 122 and 145 $kJ.mol^{-1}$. The highest value has been obtained using the differential method (144.4 $kJ.mol^{-1}$) with a difference of about five units with the two model-free methods of Kissinger (138.5 $kJ.mol^{-1}$) and Starink's (139.7 $kJ.mol^{-1}$). The Friedman's (122.0 $kJ.mol^{-1}$) and Coats-Redfern (130.6 $kJ.mol^{-1}$) methods present lower activation energy values with a difference of about 22 and 16 with the differential method. Therefore, a simplified reaction map has been presented and includes equilibrated reactions that contribute to the production of limonene-isoprene and styrene-indene.

Preface

Under the supervision of Dr Ntandoyenkosi Malusi Mkhize and Dr Samuel Ayodele Iwarere, the experimental work of the present dissertation was conducted at the University of KwaZulu-Natal, College of Agriculture, Engineering and Science (CAES), Department of Chemical Engineering, Howard College Campus (Durban) and from February 2020 to February 2022.

Acknowledgement

The following people are thanked for their substantial contributions to this study:

First and foremost, Jesus Christ, my Lord and Saviour for his love and faithfulness. Lord, I am forever thankful, and to You only be the glory!

My supervisors, Dr N.M. Mkhize of the University of KwaZulu-Natal, Durban, South Africa and Dr S.A. Iwarere of the University of Pretoria, Pretoria, South Africa, for their guidance and support.

The technical staff of the analytical laboratory at the University of KwaZulu-Natal for their technical assistance during experimental measurements,

Friends and family members, for their prayers and support of all kinds throughout the entire research period,

My late parents, Mwelwa Nsambi Dieudonne and Katambwa Kalenge Astride, for their unconditional love and support. You always believed in my ability to be successful in the academic area. You are gone, but your belief in me has made this journey possible,

Last but not least, my fiancée and wife to be Ngobela Kayambi Nana, for her love, understanding, patience and support.

Table of Contents

List of Tables

List of Figures

List of Abbreviations

Abbreviation	Description
TT	Truck Tyre
NR	Natural rubber
SBR	Styrene Butadiene Rubber
BR	Butadiene Rubber
TDO	Tyre Derived Oil
TGA	Thermogravimetry Analysis
DTG	Differential Thermogravimetric
FTIR	Fourier Transform Infrared Spectroscopy
Py	Pyrolyser
GCMS	Gas Chromatographic - Mass Spectroscopy
EGA	Evolved Gas Analysis
Wt.%	Weight percentage
min	Minute
s	Second
L	Litre
kJ	Kilo Joule
ASTM	American Society for Testing Materials
ISO	International Organisation for Standardisation
BTXE	Benzene Toluene Xylene Ethylbenzene
R time	Retention time

1. Introduction

The global production rate of tyres has been estimated at 1.5 billion per year (Parthasarathy et al., 2016). These products end up eventually as waste. However, only 15 – 20 % of waste tyres (WT) are recycled whilst the remaining 85 – 80 % are merely dumped into landfill sites. Due to tyres high resistance to degradation under typical environmental conditions, the technique of landfilling results in environmental problems such as water and soil pollution, venomous insect breeding grounds, and increased pollution emissions from fires (Parthasarathy et al., 2016, Mkhize, 2018).

Various solutions aimed at recycling waste tyres have been developed as alternatives to waste tyre management. Traditional methods for reducing waste tyre stocks include combustion for power and/or steam generation, blending tyre crumb with asphalt for civil works, and reusing in the manufacture of plastic and rubber products, such as filler. These techniques, however, cannot keep up with the rate of waste tyre generation. As a result, devulcanisation and thermal decomposition (incineration and pyrolysis) techniques for WTs have sparked a lot of interest. The pyrolysis of WTs, which recovers both energy and valuable chemicals from the products, is a potential alternative strategy among all approaches (Williams, 2013, Mkhize, 2018).

Pyrolysis is described as the thermal decomposition of materials into simpler constituents in an oxygen-free environment. Organic materials' pyrolysis at high temperatures, on the other hand, is a theoretically possible way for recovering valuable products from waste tyres, such as chemicals and fuels, combustible gases, and activated carbons. Furthermore, among the three waste tyre pyrolysis products, tyre derived oil (TDO), gas, and char, the TDO is the most essential fraction for energy (engine fuels) and valuable chemical products recovery (Quek and Balasubramanian, 2012, Mkhize, 2018).

Pyrolytic oil, a dark brown or black oil with medium viscosity and sulfurous/aromatic smell, contains over 100 chemical components. Aromatic hydrocarbons (such as benzene, toluene, xylenes, styrene, ethylbenzene and cymene), polyaromatic hydrocarbons (such as naphthalene), aliphatic hydrocarbons (such as dodecane and tridecane) and monoterpenes (such as limonene and indene) utilised in the chemical industry, are the components present in higher concentration in pyrolytic oil (Quek and Balasubramanian, 2012).

This project, a micro-scale analytical and experimental work, focuses on the kinetic mechanistic study of reaction pathways that favour the formation of valuable chemicals (limonene and indene) from waste tyre crumb pyrolysis.

1.1. Contextual background

Pyrolysis is a practically feasible method of recovering valuable materials from waste tyres. However, despite repeated attempts to commercialise the process, the pyrolysis of tyres remains unprofitable (Quek and Balasubramanian, 2012).

Several researchers investigated the influence of pyrolysis parameters on the production of oil from waste tyres (Parthasarathy et al., 2016). Temperature, heating rate, pressure, particle size, inert gas flow rates, pyrolysis environment types, reactor layout, and catalyst use are all parameters to consider. However, the association between oil output and these parameters has not been found to be consistent across the studies (Quek and Balasubramanian, 2012, Parthasarathy et al., 2016).

Therefore, over the years, numerous academics have studied the WT pyrolysis process in depth. They attempted to figure out the kinetics and mechanisms using one popular approach: developing appropriate mathematical models from data of the thermogravimetric analyser (TGA), a typical thermal method of material analysis.

Some researchers attempted to relate the thermogravimetric data to main components found in tyres. For instance, Williams and Besler (1995) used three tyres at various heating rates and compared the results to thermograms of three rubber compounds (NR, BR, and SBR). They discovered that weight loss profiles of one or more of the three rubbers correspond to regions of drastic weight loss on the thermograms. Using the Arrhenius and its variant equations, they were also able to extract kinetic parameters. Tyres are comprised of three primary components, according to Seidelt et al. (2006): natural rubber, styrene-butadiene rubber copolymer, and additives such as sulfur, zinc oxide and carbon black. The derivative thermogravimetric (DTG) curves of these components were placed on DTG curves of tyres understudy using a trial-and-error approach. They used a similarity merging to prove that the kinetic parameters generated for each component were in good agreement with the experimental data.

To further understand the mechanism of WT pyrolysis, Han et al. (2018) used a thermogravimetric analyser in conjunction with a mass spectrometer. They discovered that WT pyrolysis DTG curves featured a bimodal peak between 250 and 500 °C, as well as a modest peak between 600 and 800 °C. In addition, the development of gaseous products detected using a mass spectrometer and the functional groups on the surface of the residue char detected with a Fourier-transform infrared (FTIR) spectrometer indicated that tyre pyrolysis could be partitioned into four different stages. The first stage occurs when the temperature is below 320 °C, the second when the temperature is between 320 and 400 °C, the third when the temperature is between 400 and 520 °C and the fourth when the temperature is above 520 °C. Using the Master Plots method, Aslan et al. (2017) probed the most appropriate reaction model for waste tyre pyrolysis.

Isoconversional methods were used to determine the averaged activation energy of 162.8 ± 23.2 $kJ.mol^{-1}$ throughout a mass fraction conversion interval of 0.20 to 0.80. The reaction order of three was found to better describe the pyrolytic decomposition.

The above research works mainly focused on studying the devolatilisation mechanism of waste tyre components rather than the tracking of valuable chemicals formation with pyrolysis operating conditions, which constitutes the novelty of the present study.

However, more recently researchers conducted studies to optimize pyrolysis process parameters and establish mathematical modelling to bring more insights into understanding kinetic mechanism for producing specific products. Among them, Ngxangxa (2016) devised the qualitative and quantitative gas chromatography-mass spectrometric (GC-MS) and comprehensive two-dimensional gas chromatography (GC×GC) approaches for tyre derived oil (TDO) characterisation of selected market-value chemicals in TDOs. They reported that dl-limonene, p-cymene, benzothiazole, ethylbenzene, toluene, p-xylene, 3-ethyl toluene and α-terpinolene were the most prevalent TDO constituents. Mkhize et al. (2019) investigated the influence of heating rate on the synthesis of isoprene and dl-limonene during WT pyrolysis. They used a thermogravimetric analyser in conjunction with mass spectrometry (TGA/MS). They reported that the peak temperature of both the isoprene and dl-limonene synthesis reactions increased as the heating rate was increased. The latter is more significant for dl-limonene than isoprene. In addition, the authors showed that when the heating rate rose, the maximum dl-limonene formation rate was higher than the maximum isoprene formation rate. Furthermore, activation energies of around 133 and 115 $kJ.mol^{-1}$ for isoprene and dl-limonene synthesis reactions, respectively, were estimated using the Kissinger approach.

Recently, Menares et al. (2020) published a paper on fast WT pyrolysis using quasi-isothermal thermogravimetric analysis, kinetic modelling and an analytical pyrolyser with gas chromatography/mass spectrometry (Py-GC/MS). They found that devolatilisation/condensation and depropagation processes characterise WTs pyrolysis up to 482°C, while cyclisation and aromatisation of primary products create predominantly monoaromatics at higher temperatures. Isoprene (20.5 %) and limonene (51 %) were the most common chemicals found at temperatures below 500°C. Monoaromatics and gases were formed more readily at higher temperatures (over 600°C), with the equilibrated Diels-Alder reaction governing limonene and isoprene composition. Furthermore, the model-based and isoconversional approaches yielded kinetic parameters in high agreement (101 – 176 $kJ.mol^{-1}$).

Previous kinetic mechanism studies on the thermochemical treatment of waste tyres show that studies are not merely insufficient. They, however, present limitations as they mainly focus on

the profiling/tracking devolatilisation of the main components of the feedstock instead of tracking the formation of the chemicals (limonene and indene), which forms the basis of this study.

1.2. Research aim and objectives

Waste tyre crumb is categorised as high promising material for synthesising valuable chemicals and energy recovery due to availability, not competing with the food market, abundant carbon and hydrogen components and reduced water content. The major goal of this research is i) to investigate the kinetics of truck tyre crumb thermal degradation to maximise commercial production of chemicals such as limonene and indene ii) to propose a simplified tyre devolatilisation reaction map with respect to the first aim.

Hence, the study will focus on the following objectives:

i) Estimation and analysis of kinetic parameters through a combined model-free and model-fitting approach,
ii) Optimization of waste tyre pyrolysis parameters such as temperature and heating rate to enhance the production of limonene and indene,
iii) Characterization of materials and analysis of chemical compositions of the pyrolytic products and then propose the simplified reaction map.

1.3. Thesis layout

This section presents the several chapters that make up the thesis, as well as some of the subtopics.

Chapter 1 is an introduction. This chapter analyses major waste tyre issues and presents some challenges in mitigating those problems while taking advantage of waste tyres products.

Chapter 2 reviews the literature on attempts to better understand waste tyre pyrolysis mechanisms as well as different approaches adopted by previous researchers.

Chapter 3 describes the materials and methods used in the present study. The characterisation procedure of the truck tyre sample, the kinetic approach adopted as well as the pyrolysis and compounds analysis equipment, are all covered in this chapter.

Chapter 4 is composed of results and comments. The findings of material characterisation, kinetic study and pyrolysis coupled to Py-GC/MS are presented in this chapter while providing pertinent observations and remarks about the study objectives.

Chapter 5 is constituted of the conclusion and possible improvements. On the basis of key observations from the experiments, concluding remarks and guidelines for further studies are provided in this section.

2. Literature review

Advances in understanding mechanisms underlying tyre valorisation

Abstract

The depletion of natural resources and the need to minimise solid waste in metropolitan areas have necessitated the incorporation of used materials, especially waste tyres (WT), into manufacturing processes to valorise this form of the garbage while reducing natural resources. As a result, techniques and recycling methods have been established to use tyres as feedstock for marketable products due to their high calorific value and significant amount of carbon black. Among several techniques, pyrolysis has emerged as the most appealing for treating WTs. This technique allows the recovery of valuable products like combustible gases, fuels and chemicals, and activated carbon. Studies have focused on understanding the mechanism underlying the WT pyrolysis through the establishment of mathematical models and reaction patterns to valorise WTs and efficiently produce marketable chemicals. This paper presents an overview of recent developments in understanding WT pyrolysis mechanisms. A general mechanism observed involves a first depolymerisation and condensation of rubbers, then a decomposition of the consolidated products, and finally a devolatilisation of additives. Based on the limited information available on the chemicals' formation mechanisms, it is assumed that limonene and isoprene are derived from natural rubber via a series of polyisoprene β-scission and depropagation reactions and monomeric isoprene intramolecular cyclisation and scission, respectively, with an equilibrium step of Diels-Alder reaction.

2.1. Introduction

Renewable energy sources and waste recycling and reuse techniques are gaining interest due to several factors, including the need to reduce global warming and society's reliance on finite fossil fuels and important raw materials. Furthermore, the rapid growth in the number of vehicles on the road worldwide, combined with insufficient practical and economic waste tyre recycling methods, have led waste tyres to be considered one of the most severe pollution problems in waste disposal (Martinez et al., 2013).

However, the global market for light automobiles is rapidly expanding. Global car manufacturing reached 98.1 million units in 2018, with a future growth expected to reach 110 million units in 2025. As a result, the need for tyres will rise, providing a substantial issue in terms of reusing or disposing of this sophisticated material once it has been used (ACEA, 2019, Menares et al., 2020).

Rubber (60 – 65 wt.%), mostly a mix of natural rubber (NR) and synthetic rubber (SR), carbon black (25 – 35 wt.%), accelerators and fillers added throughout the manufacturing process make up the tyre (Martínez et al., 2013, Rowhani and Rainey, 2016). On the other hand, waste tyres (WT) are a problematic waste that belongs to a type of solid waste named "bulky" in waste management. They refer to tyres that have exceeded their useful lifespan in roadworthiness (Ishola Felix et al., 2018). The necessity to minimise solid waste in cities and the depletion of natural resources have necessitated the incorporation of scrap material into productive processes; thereby providing value to what would otherwise be considered garbage and lowering natural resource use (Ramirez-Canon et al., 2018).

Therefore, researchers have been interested in creating waste tyre recycling procedures and techniques. These initiatives try to reduce the environmental impact of waste tyres by using them as feedstock for commercial products, since they have a higher calorific value than coal and a significant percentage of carbon black when the char is significantly refined. Waste tyre management methods may be classified into three categories: i.e., i) direct disposal (stockpiling and landfilling); ii) material recycling and reuse (milling/grinding, re-treading, devulcanisation and civil engineering applications); and iii) thermal treatment with energy recovery (incineration, gasification and pyrolysis) (Isayev, 2005, Rowhani and Rainey, 2016, VIGLASKY et al., 2017).

Waste tyres thermochemical conversion is one of the attractive processes used for valorisation or disposal. In conventional coal-based plants, waste tyre combustion and incineration are attractive options for producing heat and power. These processes, however, are considered inefficient because they do not account for the recovery of important chemicals from various tyre fractions (Menares et al., 2020).

Pyrolysis is a technically appealing method for the thermochemical treatment of WTs that enables for recovery of important products like as flammable gases, fuels, chemicals, and activated carbons. Pyrolysis is a thermal decomposition of organic materials into simpler substances when exposed to intense heat in an oxygen-free environment (Quek and Balasubramanian, 2013).

The pyrolysis compounds from the WT include a liquid (TDO), which is the most important component for energy recovery and recovery of valuable chemical compounds like limonene, benzene, toluene and xylene. Gas and solid are also obtained, with the first being primarily used to provide the pyrolysis process' energy requirements. The solid output, also called char, can be used for producing carbon black as an ingredient for better asphaltic and concrete mixtures, as well as in tyre production (McCullough et al., 2015, Menares et al., 2020).

Despite the fact that waste tyre pyrolysis appears to be a simple concept, the end products are frequently low-value mixes of hydrocarbons with a wide compositional range, spanning from light alkane gases to coke. The composition of various pyrolysis products is determined by the pyrolysis parameters as well as the tyre's composition. As a result, the best conditions for the type of feedstock and process operating parameters must be determined depending on the pyrolysis' final goal (Martínez et al., 2013, Acevedo and Barriocanal, 2015).

Several studies looked into the impact of WT pyrolysis variables on rubber components devolatilisation pathways. Temperature, heating rate, pressure, particle size, inert gas flow rates, sorts of pyrolysis environment, reactor layout and catalyst use are all variables or parameters to consider. Nevertheless, no final consensus on the relation between product yields and these variables could be observed among these studies (Quek and Balasubramanian, 2012, Parthasarathy et al., 2016).

Researchers have investigated the mechanisms of solid-state materials pyrolysis in an endeavour to valorise waste tyres. The approach entails developing appropriate mathematical models and reaction patterns from the thermogravimetric analyser (TGA) data, a typical thermal method of material analysis. As a result, various models, such as kinetic, mass transfer, and heat diffusion models, have been used (Khiari et al., 2018).

The advancements of the waste tyre pyrolysis process was reviewed for the very first time in decades by Martínez et al. (2013). They provided a detailed overview of the process by describing the effects of the key process variables, such as feedstock size and content, on the pyrolysis product distributions and physicochemical characteristics. Furthermore, they highlighted the key features of the pyrolytic compounds, with a focus on the liquid fraction's potential as an alternative fuel in internal combustion engines. However, Williams (2013), in their review of the WT pyrolysis process, presented the reactors range used so far by pointing out the influence of the reactors configuration on the pyrolysis products characteristics. They also showed the principal gases produced from the pyrolysis of waste tyres to be H_2, C_1 - C_4 hydrocarbons, CO_2, CO and H_2S. In addition, they reported on the upgrading of char to higher-quality carbon black and activated carbon. Catalysts were also utilised to convert the oil into an aromatic-rich chemical feedstock or hydrogen from WTs. Nkosi and Muzenda (2014) also presented a review of the pyrolysis process by highlighting the impact of the operating parameters and discussing the pyrolytic products. Moreover, they analysed the pyrolysis products market and the success and failures of the process.

Recently, Singh (2015) reviewed and discussed the tyre pyrolysis process and the applications of the derived products. They reported the characteristics of used tyres materials and recycling methods, the types and principles of pyrolysis, the pyrolysis products and their composition, concluding by the advantages of a waste tyre pyrolysis plant.

From the above, since pyrolysis of waste tyres has received particular attention in the 1990s, the kinetic notion was in quite a state of disarray and the tyre pyrolysis devolatilisation mechanisms were still in their embryonic stages. Since then, our understanding of the reaction mechanisms involved in pyrolytic processes has advanced significantly, and the kinetic schemes that describe the entire pyrolysis process have been refined to properly characterise the process. Given this, the purpose of this work is to present a succinct review of recent progress in understating the mechanisms underlying the pyrolysis of waste tyres.

In addition, the composition of waste tyre pyrolysis products is discussed in this research. The mechanisms of waste tyre pyrolysis are described in depth. Also are reviewed and discussed, the studies on pyrolysis kinetics and modelling approaches.

2.2. Waste tyre pyrolysis

2.2.1. Process description

Pyrolysis is the thermal decomposition of organic molecules in the absence of oxygen, which results in the breakdown of complex organic compounds into simpler organic compounds. It breaks chemical bonds with the addition of heat, allowing organics to disintegrate and evaporate. The majority of tyre pyrolysis processes operate between 250 and 500 °C, while some have been claimed to function at temperatures as high as 900 °C. Crumbed tyres emit more liquid products and gases at temperatures exceeding 250 °C. Oil and char yield, on the other hand, may decrease at temperatures exceeding 400 °C, compared to gas generation (Antoniou and Zabaniotou, 2013).

In the reactor, the rubber softens, and the rubber polymeric materials break down into smaller molecules, which finally evaporate and escape the reactor. The hot volatiles compounds can either be burnt immediately to generate electricity or condensed into pyrolysis oil, an oily liquid. Relatively small particles that can't condense stay as gas and are burnt as fuel. Sulfur compounds, zinc oxides and other minerals in the tyre are solidified and removed (VIGLASKY et al., 2017).

When properly carried out, the pyrolysis of tyres can have low emissions or waste. When the temperature approaches 450 °C, the principal product is liquid, which is a combination of hydrocarbons based on the original composition of the waste material. A mixture of carbon monoxide and hydrogen (synthetic gas) emerges as major product at temperature above 700 °C, due to additional cracking of liquids (VIGLASKY et al., 2017).

The qualities of pyrolysis products are thus determined by the type of the feedstock and process variables. Whole tyres, for example, include both fibres and steel, whereas shredded tyres have the majority of the steel and, in some cases, the majority of the fibre removed. The reactor is also an important component of the pyrolysis process. Fixed-bed, fluidized-bed, rotary kiln, screw kiln, and spouted bed reactors have all been employed for scrap tyre pyrolysis (Rowhani and Rainey, 2016, VIGLASKY et al., 2017). Depending on the applied pressure, such as atmospheric or vacuum, the process might be batch or continuous. Direct-fired fuel, electrical induction, and/or microwaves can all be used to provide the required energy for thermal devolatilisation of waste tyres. As a carrier gas, nitrogen or another inert gas as carrier gas is used. To some extent, the pyrolysis may require the use of a catalyst to speed up the process (VIGLASKY et al., 2017).

Liquid, gas and char are the end products of pyrolysis. For its energy and economic importance, the liquid is the most prized portion (Hita et al., 2016). As a result, the most lucrative reactor designs and process operating conditions allow higher liquid yields. Figure 2.1 depicts the WT pyrolysis process schematically.

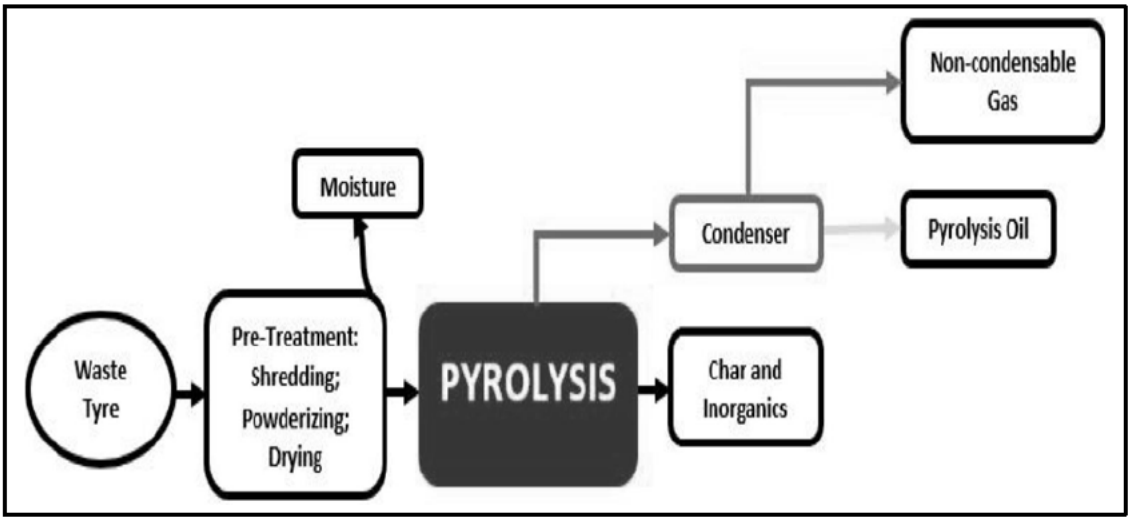

Figure 2.1: Waste tyre pyrolysis process schematic

2.2.2. Operating parameters

Temperature in the reactor maintains the endothermic process of waste tyre pyrolysis. Temperature emerges as an important operating parameter that most influences product distribution and conversion grade.

Therefore, the temperature is the parameter that significantly influences the pyrolysis process and the WT pyrolysis mechanisms. In heat transfer phenomena, the heating rate and particle size directly interact with the distribution of liquid, gas, and solid fractions and their physicochemical characteristics (Martínez et al., 2013).

Secondary pyrolysis reactions such as thermal cracking, repolymerisation, recondensation and char formation are controlled by the carrier gas flow and atmosphere type in the process (Martínez et al., 2013). Other variables of the process, such as pyrolysis time and hot volatiles retention time, have a significant impact.

The pyrolysis temperature has an impact on the makeup the three phases that result from the WT pyrolysis process. In addition, since 100 % of tyre conversion is achieved at 500 °C, this appears to be the ideal temperature at atmospheric pressure (Aylón et al., 2005, Laresgoiti et al., 2000). At lower temperatures, the main tyre compounds (NR, BR and SBR) stay in the pyrolytic carbon black, which has a heterogeneous sticky-gummy appearance (Martínez et al., 2013). The volume and properties of the pyrolysis products are almost unaffected by higher temperatures (Laresgoiti et al., 2000, González et al., 2001).

Due to significant thermal cracking at high temperature, gas yield rises as temperature rises (Zabaniotou and Stavropoulos, 2003). Secondary reactions, such as thermal cracking and heterogeneous reactions affecting a tyre's inorganic compounds, might cause gas compounds and yields to be compromised. As a result, the behaviour of the gas portion regarding the composition, calorific value, and yield varies widely among studies (Martínez et al., 2013). Longer chain hydrocarbons are projected to decrease as temperature rises, favouring lighter hydrocarbons and H_2.

When the pyrolysis temperature is raised, no substantial changes in yield are expected on the solid fraction. As a result, the solid proportion must be roughly equal to the total of the original char and ash content. However, additional processes such as tar and char synthesis can cause the solid fraction to be larger than predicted. When the carrier gas contains oxygen (CO_2 or steam), however, a rise in temperature can result in lesser char production due to the occurrence of gasification reactions (Betancur et al., 2009, Martínez et al., 2013).

The liquid yield of pyrolysis, on the other hand is essentially constant or reaches a peak at around 450 - 500 °C and then drops as the temperature rises. The aromatic chemicals in the liquid fraction increase at the same time. As previously stated in relation to the influence on gas products, the rise in aromatic compounds is related to secondary reactions that affect the chemical characteristics and yields of the products. Moreover, Xu et al. (2018) reported that the primary pyrolysis products of gases, aromatics and alkenes alter drastically with temperature variation. The fraction of alkenes decreases with temperature increase due to secondary cracking of pyrolysis products between 600 and 800 °C, and then increases when the temperature reaches 800 °C and higher. The latter could be ascribed to aromatics decomposing into alkenes at higher temperatures.

The yield of limonene, one of the alkenes' main products, increases at higher temperature (around 450 °C) and decreases when the temperature reaches 800 °C. The decreasing of limonene content is attributed to the decomposition of D-limonene into aromatics due to secondary reactions such as cyclization and aromatisation at high temperatures (Mkhize et al., 2016, Xu et al., 2018). Nevertheless, the content of D-limonene shows an increase when the temperature is raised from 800 °C to 1000 °C due to some reactions such as the Diels-Alder reaction of isoprene (Xu et al., 2018).

The previous observation was made for another chemical of tyre oil, i.e., indene. The yield of indene shows an increase with temperature increase up to 500 °C then decreases at higher temperatures.

Next to temperature, heating rate is an important factor in pyrolysis products yield control. The weight loss profile in the thermogravimetric study switches to higher temperatures as the heating rate is increased. According to Leung and Wang (1998), the weight loss regions migrate to a higher temperature range as the heating rate increases, the weight loss rate increases, and the reaction time shortens quickly, with no significant difference in the total weight loss. With increased heating rate, the apparent activation energy and frequency factor both rise, complicating the pyrolysis reaction.

Pressure is another parameter that influences the production of chemicals from pyrolysis. Decreasing the pyrolysis pressure decreases the residence time (Roy et al., 1997). Hence, the formation of undesired products and the destruction of desirable chemicals, such as limonene, are minimised. According to Roy et al. (1997), *dl*-limonene concentrations declined as pyrolysis pressure increased. Therefore, it is preferable to perform rubber pyrolysis at low pressures to produce chemicals of higher commercial value.

Table 2.1 summarises the influence of pyrolysis parameters on WT pyrolysis reaction mechanism by highlighting differences in products yields and some chemical concentrations from the literature.

Table 2.1: Influence of WT pyrolysis parameters on products and chemicals production

Ref.	Material	Reactor configuration	Pyrolysis parameters			Tyre pyrolysis products			Chemicals yields in Pyrolytic oil	
			Temperature / Time	Heating rate	Pressure	Gas %	Solid %	Liquid %	Limonene %	Indene %
Roy et al. (1997)	Pure isoprene (2 cm^3) and polyisoprene rubber (2 cm^3)	Batch reactor	500 500 500 500	15°C/min	0.8 kPa 28.0 0.8 6.4	2.6 5.9 1.0 3.2	0.1 3.8 36.8 35.1	97.3 90.3 62.2 61.7	16.6 11.9 5.0 4.2	-
Cunliffe and Williams (1998)	Shredded scrap tyres (3x1.5 cm)	Static-bed batch reactor	450 475 500 525 560 600	-	-	4.5 4.5 5.5 5.2 6.5 8.9	37.4 37.3 38.3 37.8 38.1 38.0	58.1 58.2 56.2 56.9 55.4 53.1	3.13 3.03 2.90 2.89 2.45 2.51	0.22 0.26 0.32 0.31 0.31 0.16
Dai et al. (2001)	Tyre powder (0.32 and 0.8 mm)	Circulating fluidized bed	500	-	Slight vacuum	~16	~27	~50	23.9 max	
Conesa et al. (2004)	Tyre (4 mm)	Fixed Bed	450 750 1000	-	-	- - 25.1/22.15	35.2/13 37.2/14.8 37.6/16.5	37.8/25.7 10.9/13.1 <0.01	6.9/4.1g/kg 0.2/1.1g/kg -	0.3/0.4g/kg 1.6/1.8g/kg
Li et al. (2004)	Shredded scrap tyres (13 – 15 mm)	Rotary Kiln	450 500 550 600 650	-	-20 to -10 Pa	13.1 13.6 15.5 18.0 18.3	43.0 41.3 39.3 39.3 38.8	43.0 45.1 44.6 42.9 53.7	5.440 1.883 0.419 0.122 0.070	0.831 0.381 0.900 0.447 0.382
Laresgoiti et al. (2004)	Car tyre (2-3 cm wide)	Autoclave	300 400 500 600 700	15 °C/min	-	7.6 19.3 17.2 17.6 17.8	87.6 55.9 44.8 44.2 43.7	4.8 24.8 38.0 38.2 38.5	21.07 8.22 5.12 3.19 3.29	0.77 0.43 0.90 0.64 0.60
Rofiqul et al. (2007)	Heavy automotive waste tyre (2, 4 and 12 cm^3)	Fixed-bed fire-tube heating reactor	425 475 525 575	15 °C/min optimal	Slightly above the atmospheric	8 9 12.5 18.6	39.5 37 35.5 33	52 55 51 48	50.8 50.86 24.84 21.24	-
Arabiourrutia et al. (2007)	Scrap car tyres (0.63 – 1 mm)	Conical spouted bed reactor	425 500 550 610	-	-	0.70 3.50 3.05 3.18	34 34	30.48 29.30 27.29 23.70	23.93 16.94 13.59 6.34	0.46 1.94 1.15 1.40

Zhang et al. (2008)	WT Granules with: No additive NaOH Na_2CO_3	Stainless steel reactor	500 500 500	20 °C/min	3.5 – 4 kPa	21.8 13.3 15.3	36.1 38.6 42.7	42.1 48.1 42.0	11.73 11.95 12.39	
Lopez et al. (2010)	Tyre (3 g/min)	Conical Spouted Bed	425 600			~2 ~7.5	33.9 35.8		19 <1	-
Bajus and Olahová (2011)	Automotive scrap tyres (1 – 3 cm^2)	Batch reactor	450 570	16.5, 9 and 7.5 °C/min	-	11.1 9.3	46.3 40.7	42.6 50.0	9.0 4.6	-
Islam et al. (2011)	Waste Truck tyre (4 cm^3)	Fixed Bed	375 425 475 525 575	-	-	7.5 8 9 12.5 18	45 39 36 35 35	47 53 55 52 47	50.86	-
Banar et al. (2012)	Tyre derived Oil mixtures (1 – 4 mm)	Fixed bed reactor	400	5 °C/min 35 °C/min	-	27.2 33.8	34.0 35.1	38.8 35.0	11.06 ppm 219.9 ppm	-
Acevedo and Barriocanal (2014)	Tyre crumbs	Rotary Oven Fixed bed	850 850	5 °C/min	-	35 3.5	28 38	25 55	5.12 21.58	9.74 3.85
Choi et al. (2016)	Scrap tyre rubber (1 – 2 mm)	Auger Fluidised Bed	229 334 454 506 511 516	-	-	3.0 2.7 7.1 6.8 9.4 4.8	1.2 2.5 3.9 34.9 33.5 34.1	1.6 3.5 5.0 48.0 46.6 42.1	- 1.5 2.5 7.0 4.1 3.5	-
Mkhize et al. (2016)	Crumb waste truck tyres (max 5 mm)	Fixed-bed	350 550 350 550 450 309 591 450 450	5 °C/min 5 °C/min 25 °C/min 25 °C/min 15 °C/min 15 °C/min 15 °C/min 0.86 °C/min 29.14 °C/min	-	11.54 19.86 17.15 20.37 19.66 4.36 17.79 23.04 18.44	61.26 36.64 60.26 36.20 36.64 83.67 36.37 37.35 36.66	27.20 43.50 22.59 43.43 43.70 11.97 45.84 39.60 44.90	7.17 6.88 4.67 6.70 7.14 2.10 6.49 4.14 7.62	-

Alvarez et al. (2017)	Waste truck tyre (2.8 – 3.3 mm)	Conical spouted bed reactor	425 475 575	$10^3 – 10^4$ °C/s	-	3.7 5.9 10.1	37.9 35.9 35.9	58.4 58.2 54.0	21.05 22.84 7.04	0.26 0.30 1.09
Song et al. (2017)	Tyre rubber powder (0.6 mm)	Microwave	10 min 20 min 30 min	-	-	9.4 11 12	54 44.8 43	36 44 45	8.61 9.92 9.83	1.01 1.47 1.58
Singh et al. (2018)	LVT MVT HVT	Batch reactor	650 750 750	20 °C/min	Max 3 atm	8.5 12 9	39 42 27	51 45.5 63.5	11.11 21.22 12.75	0.45 0.80 0.44

2.3. Waste tyre pyrolysis mechanisms

2.3.1. Introduction

Pyrolysis is the thermal treatment of WTs in the absence of oxygen to produce pyro-gas, TDO and char. The gas is utilised as a fuel in the endothermic pyrolysis process as well as in a variety of other applications. TDO's high hydrogen and carbon contents, as well as its high concentration of valuable chemicals (such as dl-limonene, terpinolene and p-cymene), distinguish it as a potential liquid fuel feedstock for the synthesis of useful chemicals (Mkhize et al., 2019).

Several researchers have studied the pyrolysis process of WTs in depth over the decades, employing a variety of methodologies (Table 2.2) to better understand its kinetics and mechanisms.

For instance, Chen et al. (2001) thermogravimetrically analysed the kinetics of the passenger car tyre and truck tyre pyrolysis in N_2 for heating rates values of 5, 10, 20 and 30 °C /min and temperature in the range of 100 to 900°C. They found that the pyrolysis process starts with the dehydration and devolatilisation of processing oils, with a subsequent devolatilisation of natural rubber or butadiene rubber. Using Friedman's method, they also reported the average kinetic parameters of E = 147.95±0.21 kJ.mol^{-1}, A = (6.295±1.275) x 10^{10} min^{-1}, and n = 1.81±0.18 for the two tyres that they observed to behave similarly in pyrolysis devolatilisation.

In the same way, Iwarere and Mkhize (2019) conducted a kinetic mechanism study of two types of WT (Truck tyre, TT and Passenger car tyre, PCT) pyrolysis based on the rubbery fractions devolatilisation at heating rates 10 to 50 °C/min. They used two model-free methods (Freidman and Kissinger) and observed that the reaction progress profile of the TT matches that of the PCT, with the gradient of the TT profile being steeper compared to the PCT. Moreover, they reported that the TT profile is characterised by one prominent peak attributed to the natural rubber, the main rubbery fraction of the TT. However, two distinctive peaks were identified in the devolatilisation of the PCT. Peak one was sought to be the NR, whereas peak two was associated with synthetic rubber (BR and SBR).

Therefore, the authors concluded that there is a high potential for stepwise pyrolysis of the fractions from tyre rubber, particularly PCT, which may benefit the fractional recovery of the valuable chemicals from the WTs.

According to Seidelt et al. (2006), tyres are formed by three primary components: polyisoprene (NR), styrene-butadiene rubber copolymer (SBR) and additives such as sulfur, zinc oxide (ZnO), and carbon black. They used a trial-and-error technique to superimpose, in the correct ratios, the derivative thermogravimetric (DTG) curves of the three primary components of tyres on the DTG curves of tyres under study. The author used a similarity merging to prove that the kinetic

parameters generated for each component were in agreement with experimental data. Danon et al. (2015) used a combination of model-free and model-based kinetics to evaluate the pyrolytic devolatilisation behavior of four rubbers (NR, Synthetic polyisoprene, BR and SBR) at five heating rates (2, 5, 10, 15 and 20°C/min). They came to the conclusion that the devolatilisation of the rubbers comprised of two distinct weight loss zones: a primary depolymerisation/condensation of the rubbers and a subsequent degradation of the condensed product. They also discovered a third devolatilisation reaction for styrene-butadiene rubber, which they called additive devolatilisation.

To better understand the waste tyre pyrolysis mechanism, Han et al. (2018) used a thermogravimetric analyser in conjunction with a mass spectrometer. They found that waste pyrolysis DTG curves had a highly skewed peak between 250 and 500 °C, and a tiny peak between 600 and 800 °C. In addition, the progression of gas products detected by MS and the functional groups on the surface of the remnant char identified by FTIR demonstrated that tyre pyrolysis could be subdivided into four phases. The first phase took place below 320 °C and was accompanied by slight mass loss due to water vaporisation and plasticiser decomposition. Devolatilisation of natural rubber between 320 and 400 °C was linked to the second phase. The third phase, which took place between 400 and 520 °C, involved the devolatilisation of synthetic rubber, while the fourth phase, which took place above 520 °C, resulted in a negligible weight loss.

Gauthier-Maradei et al. (2019) recently published a study including the estimation of kinetic parameters to forecast tyre rubber pyrolysis in two phases in a fixed bed reactor. To begin, a reaction mechanism for tyre rubber degradation was established utilising a differential scanning calorimetry (DSC) and the decomposition of its three primary polymer components (NR, BR and SBR). Afterwards, using the heat flow collected by DSC, the Borchardt-Daniels method was used to derive the kinetic parameters for each reaction. In the second phase, the authors incorporate the chemical mechanism and associated kinetic parameters into a mathematical model of a fixed bed reactor at a laboratory scale that considered mass and energy balances. They hypothesised a six-step reaction mechanism, three of which are linked with initial pyrolysis (exothermic), two with secondary pyrolysis (endothermic) and one with a post-cracking reaction (exothermic, was observed for NR and SBR). Furthermore, with the model presented at 600 °C, the waste tyre begins to degrade thermally after 11 minutes of reaction, with a maximum liquid generation at 18 minutes. The intermediate chemicals are consumed in their whole.

From the points discussed above, it is clear that there is a considerable body of literature devoted to kinetic mechanism of tyre components devolatilisation. The observations appear to be in agreement. The kinetics of chemicals production, on the other hand, are poorly understood.

Therefore, some recent research has been conducted to optimize pyrolysis process parameters and establish mathematical modelling to bring more insights into understanding the kinetic mechanism for the production of specific products.

Ngxangxa (2016), for example, devised descriptive and analytical gas chromatography-mass spectrometric (GC-MS) and complete two-dimensional gas chromatography (GC×GC) methodologies for the measurement of specific market-value chemicals in tyre derived oils. *Dl-limonene*, *p*-cymene, benzothiazole, ethylbenzene, toluene, *p*-xylene, 3-ethyl toluene and *α*-terpinolene were the most prevalent compounds in the TDO. Mkhize (2018) prototyped novel methods essential to optimising the dl-limonene yield in the pyrolysis oil by modifying the existing WT pyrolysis processes, resulting in an improvement in total TDO yield and quality, high quality characterised by high dl-limonene content and fewer heteroatom compounds (nitrogen-, oxygen- and sulfur-compounds, primarily benzothiazole). In another study, Mkhize et al. (2019) looked at the influence of heating rate on the synthesis of isoprene and dl-limonene during WT pyrolysis. They employed a thermogravimetric analyser in combination with mass spectrometry (TGA/MS) and found that as the heating rate was raises, the peak temperature of both the isoprene and dl-limonene synthesis reactions rose. The latter is more significant than the one in isoprene. In addition, when the heating rate rose, the maximum dl-limonene synthesis rate was found to be higher than the maximum isoprene synthesis rate. Furthermore, using the Kissinger technique to estimate model parameters, activation energies of around 133 and 115 $kJ.mol^{-1}$ were found for isoprene and dl-limonene synthesis reactions, respectively.

Ding et al. (2015) used an analytical pyrolyser in combination with gas chromatography/mass spectrometry (Py-GC/MS) to investigate the primary pyrolysis characteristics of WTs at various temperatures. They discovered that alkenes, not alkanes or aromatics, were the predominant pyrolysis products of WT at 600 °C. The primary compounds of chain alkenes and cyclic alkenes, respectively, were identified to be isoprene (18.7%) and d-limonene (22.9%). The yield and selectivity of alkenes achieved the optimal at 600°C. To further understand the pyrolytic mechanism of WT, d-limonene was pyrolysed in Py-GC/MS to investigate the decomposition procedure.

At low temperatures (≤ 500°C), the isomerisation reaction was shown to control the conversion process. Intrinsic cleavage of the C-C bond, intermolecular hydrogen transfer, and cyclisation to aromatics were prominent when the temperature rose over 600°C. When the temperature was above 650 °C, bicyclic aromatics such as indene and naphthalene were identified. Furthermore, the TG-FTIR results showed that when the temperature increased, WT proceeded through ring-opening and re-cyclisation reactions.

More recently, Menares et al. (2020) used a quasi-isothermal thermogravimetric (TGA) study, kinetic prediction and an analytical pyrolyser combined with gas chromatography/mass spectrometry (Py-GC/MS) to investigate fast pyrolysis of WTs. They reported that at up to 482°C, the WTs pyrolysis is characterised by depropagation and devolatilisation/condensation processes, while at elevated temperatures, initial products undergo cyclisation and aromatisation, resulting in predominantly monoaromatics. Isoprene (20.5 %) and limonene (51 %) were the predominant chemicals present at temperatures below 500°C, (maximum selectivity 71%), as monoaromatics and gases were formed at temperatures above 600°C, with limonene and isoprene concentrations dictated by the evenly balanced Diels-Alder reactions. Moreover, the model-based and isoconversional kinetic parameters were in high agreement (101 – 176 $kJ.mol^{-1}$). The authors also proposed a comprehensible reaction chart for WTs pyrolysis to describe the variations in products composition induced by the temperature variation. They stated that combining TGA, Py-GC/MS and modelling allows for a better appreciation of the reaction pathways governing WTs pyrolysis and, is the foundation for evaluating reliable kinetic parameters.

From the above, the kinetic mechanism researches on the WT thermochemical treatment mainly concentrated on tracking the devolatilisation of the main components of the tyre. A general mechanism can be observed from the literature and involves a first depolymerisation/condensation of the rubbers, a subsequent degradation of the condensed products and lastly, a devolatilisation of additives. An insufficiency has been observed in works tracking the formation of valuable chemicals. Based on the scant evidence available, it is widely assumed that limonene and isoprene are generated from NR by a series of β-scission and depropagation processes of polyisoprene and intramolecular cyclisation and scission of monomeric isoprene, respectively, with an equilibrium step of Diels-Alder reaction, Figure 2.2 (Mkhize et al., 2016, Menares et al., 2020).

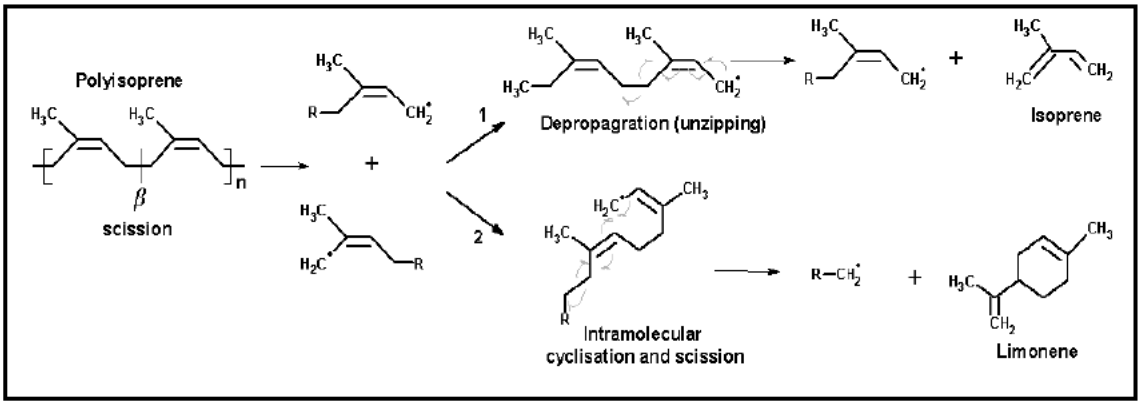

Figure 2.2: Limonene formation mechanism

The following sections discuss various most used methods and models for the solid-state kinetic mechanism study. A particular accent will be on the WTs pyrolysis mechanism study methods.

Table 2.2: Previous works on the kinetics of WTs pyrolysis

Reference	Objective & methods	Operating parameters	Major findings
Williams and Besler (1995)	To determine the effect of tyre structure on thermal devolatilisation, three various tyres were heated in a TGA at three varying heating rates and the findings were compared to thermograms of three distinct rubber compounds (NR, BR, and SBR).	- Particle size < 1 m - Mass ~ 20 mg - Temperature 720 - Heating rates: 5, 20, 40 or 80 K/min	They noticed that regions of considerable weight loss on the thermograms correlate to weight loss patterns of one or more of the three rubbers, and that using the Arrhenius and its related equations, they could obtain kinetic parameters. Furthermore, isoprene, depentene, and other dimers were the primary pyrolysis products for Williams and Besler. A subsequent reaction resulted in the synthesis of a wide range of chemicals, either directly by polymer chain scission or indirectly through isoprene and dipentene breakdown products, or via secondary reactions to generate aromatic compounds.
Conesa et al. (1997)	To investigate the kinetics of WT devolatilisation during thermogravimetric experiments when heated at varied rates.	- Particle size < 1 m - Mass: 4 - 5 mg - Temperature: 20 - 600 ˚C - Heating rates of 1, 5 and 25 ˚C/min N_2 flow rate : 60 cm^3/min	They found that the weight loss of WT in thermobalance can be as high as 65% (35% solid residue), and that the weight loss occurs in three stages, the first of which corresponds to the decomposition of an oil fraction, the second to NR and the third to SBR. They proposed a weight loss model, based on which they concluded that the first fraction defined contributes with $w_{10} = 0.29$ (45.17% of the total weight loss), the second fraction with $w_{20} = 0.23$ (35.885% of the weight loss) and the third fraction with $w_{30} = 0.121$ (18.95% of the total weight loss). Furthermore, the researchers discovered that the first portion decomposes mostly into CO_2 and linear hydrocarbons. In the second stage of decomposition (NR degradation), CO_2 is also produced, whereas SBR mostly yields aromatic chemicals.
Leung and Wang (1998)	Evaluate the thermal devolatilisation kinetics of WTs utilising non-isothermal thermogravimetric approaches. To stimulate the kinetic and process parameters, two new models were used: the three-component-simulation model and the three-elastomer-simulation model.	- Particle sizes: between 1.18 - 2.36 mm, 1.0 - 1.18 mm, 0.5-0.6 mm and 0.335 - 0.425mm - Mass: 8 mg - Temperature: 20 - 600 ˚C - Heating rates : 10, 30, 45 and 60 ˚C/min - N_2 flow rate : 100 mL/min	They discovered that the pyrolysis of tyre powder exhibits three distinct weight-loss areas, each connected to the degradation of different materials and occurring at temperature between 150 and 350, 280 and 440, and 350 and 510 ˚C, respectively. Total weight loss averages around 65%. They also saw a change in weight-loss zones to higher temperatures ranges, as well as a larger weight-loss rate when the heating rate increased. Moreover, the two models were able to mimic the pyrolysis of tyre powder, with simulations matching the real TG and DTG data and providing mechanistic insights into the tyre powder pyrolysis process.
Quek and Balasubramanian (2009)	To construct a new approach to provide understanding into the pyrolysis kinetics of tyres using a method that incorporates two equations, one to account for heat conduction from the outside to the inside of the tyre particle, and the other for mass transfer from within the tyre particle to the surface.	- Particle size: ~ 1 mm - Mass: 5 - 10 mg - T max: 800 ˚C - Heating rates : 10 - 50 K/min N_2 flow rate : 150 mL/min	They observed that the heating rates retained in the reactor had a significant impact on the pyrolysis kinetics and the product composition and development. TGA profiles disclosed an immediate shift in the pyrolysis process at heating rates greater than 30 K/min. The proposed model, on the other hand, assumes that the major components of tyres are extender oil, NR, BR and SBR and that each of these components follows the basic Arrhenius-type equation with a first-order reaction. This model accurately depicted the effect of various kinetic parameters on pyrolysis reactions at various heating rates. As a result, including heat and mass transfer mechanisms into a pyrolytic model helps increase the quantitative knowledge of tyre pyrolysis, as seen by the model findings fitting better at higher rates (>30 K/min).

Al-Salem et al. (2009)	To investigate the feasibility of using pyrolysis on end of life tyres (ELT) in other to utilise the global product yields and amplify preferred ones through an innovative concept in depolymerisation thermal cracking kinetic analysis.	- Particle size < 0.1 mm - Mass: 15 mg - Temperature: 500 ˚C (pre-set as final conversion temp.) - Heating rates: 40 ˚C/min - N_2 flow rate: 100 mL/min - Conversion time: 120 s	Based on a novel engineering kinetics approach, they suggested a thermal cracking strategy with four primary reactions and two secondary reactions. A first-order cracking reaction from ELTS polyisoprene to aromatics, liquids, gases and char, as well as secondary side reaction of fluids to aromatics, form the basis of the method. The depolymerisation kinetics (from primary and secondary reactions) were evaluated and found to be very close to the experimental results, yielding an overall rate constant (k_0) of 8 x 10^{-3} s^{-1}. Furthermore, the examination of kinetic rate constants and products using the thermal cracking model revealed a regression between 0.90 and 0.94.
Cheung et al. (2011)	To investigate the kinetics and heat transport of wide tyre components at different heating rates, using the experimental results from TGA/DTG and DTA.	- Particle size: (2x2x2) mm - Temperature up to 600˚C - Heating rates of 2, 5, 10 & 20 ˚C/min - Carrier gas: N_2	They suggested a multi-stage pyrolysis operating method for the pyrolysis of a single tyre component inside a batch reactor, based on a model that involves mass loss kinetics, exothermic kinetics, and heat flow. The technique begins with a heating phase to initialise the pyrolysis's exothermic processes. An adiabatic stage follows the heating stage, trapping exothermic heat to further promote endothermic reactions. Despite a longer completion time, this technique appears to save 17.29% energy.
Haydary et al. (2012)	To determine kinetic parameters of tyre decomposition by application of different methods, and analyse experimentally and theoretically the effect of particle size on the tyre conversion during the pyrolysis in a flow reactor under isothermal conditions.	- Particle size: 4 to 8 mm (weight of 50 – 500 mg) - Heating rates: 2, 5, 10 and 15 ˚C/min - N_2 flow: 60 ml hr^{-1} - Reactor Temperature: 550˚C - Residence time: 15 to 300 s	Particle size has been found to have a crucial effect on the pyrolysis time of waste tyre. At the temperature of 550 ˚C, when a 5 mm particle is decomposed below 1 min, it has been found that for a complete devolatilisation of a 50 mm particle, time longer than 25 min is required. Moreover, a good coherence was identified between the experimental and mathematical modelling data obtained. However, from the three different methods used for the determination of kinetic parameters, the isoconversional method provided kinetic parameters that describe the trend of experimentally estimated data better than the other two approaches.
Lopez et al. (2013)	To evaluate the thermal devolatilisation kinetics of granulated WTs using TGA/DTG and compare the calculated apparent activation energy and the pre-exponential factor data using the Friedman, Flynn-Wall-Ozawa and Coats-Redfern model-free approaches.	- Particle size: <12 mm dimeter - Mass: 40 mg - Temperature: up to 650 ˚C - Heating rates fixed at 5, 10, 15 and 20 ˚C/min, respectively. - N_2 flow rate : 20 mL/min	According to the researchers, thermal decomposition begins around 290 ˚C and ends around 550 ˚C. The dehydration and devolatilisation of the processing oils is followed by the decomposition of NR and BR. The mean E_a values found using the various model-free approaches were similar, averaging 160 kJ/mol and an A of 2.49×10^{10} min^{-1}. The thermal devolatilisation reaction model, on the other hand, was accounted for by the D3 model, as established using the Coats-Redfern approach. Moreover, the constant activation energy across the α range (0.01 – 0.99) indicates that GST pyrolysis is a multi-step process. They also noticed a difference between the Friedman and the Flynn-Wall-Ozawa approaches for determining A values.
Lanteigne et al. (2013)	The creation of a new WT shreds pyrolysis model that accounts for temperature dependence and forecasts specific product yields (Non-condensable volatiles, condensable volatiles and char). TGA and industrial datasets from the Ecolomondo technique were used to calculate the model parameters. Finally, the researchers compared the model to other pyrolysis	- Mass: 30 mg - Temperature: up to 600 ˚C - Heating rates: 5, 20, 40, and 80 ˚C/min - N_2 flow : 20 mL/min	They created a new predictive kinetics-based model that combines product selectivity information from TG analysis tests with a global single-step decomposition relation term to replicate the nonlinear relationship between product selectivity and temperature. In addition, the energy balance was calculated using a lumped capacitance technique that assumed a completely mixed bed and a constant convection term that included radiation. They compared the model they came up with to three other models they found in the literature (single step, multi-step pseudo components, and parallel and series). None of these models was able to replicate the industrial (Ecolomondo process) pyrolysis kinetics or the product yields. The authors came to the conclusion that the TGA alone is insufficient for calculating pyrolysis kinetics. Furthermore, accurate industrial pyrolysis models require final yield data because they

	models that have been published in the past.		cannot estimate individual product yields (only combined volatiles). The oil production dynamics and yields of the existing industrial process were accurately reflected by the prediction model.
Miranda et al. (2013)	The examination o probable paths for the pyrolysis reaction mechanism of WT rubbers in a micro-autoclave, using both experimental data and various kinetic models.	- Particle size: 2-3 cm - Mass: 20 g - Temperature: up to 350, 370, 390, 410, 430, 450 ˚C - Heating rates : (30±2) ˚C/min - N_2 pressure : 0.48 MPa	They assessed kinetics models using data collected at various temperatures and reaction times. They also created new RT pyrolysis reaction pathways involving a mix of series and parallel reactions, because none of the methods in the literature allowed for numerical modification of the experimental results. The authors proposed the reaction mechanisms based on: i) the physical state of the products obtained, ii) all reactions are elementary first-order and irreversible, iii) temperature dependence of the rate constants is described by the Arrhenius equation and, iv) the reaction medium contains no mass transfer resistances. The authors then compared the experimental and kinetic data. The presented models were well-fitting, allowing multiple reactions for RT's thermal degradation to be proposed.
Danon and Görgens (2015)	To determine the rubber composition of WT crumbs utilising a complex devolatilisation method and a combination of model-free and model-based kinetics.	- Particle sizes: rubbers (<1 mm) and Tyre crumbs (40 mesh) - Mass: 12mg rubbers and 10mg crumbs - Temperature: 110 ˚C (5min) - 600 ˚C - Heating rates : 5, 10 and 20 ˚C/min - N_2 flow rate : 100 mL/min	They used a kinetics model based on a complex mechanism to predict the rubber composition of three distinct WT crumbs, which include two sequential devolatilisation reactions for the rubbers and a single transitional condensed product. The activation energies determined using Friedman's approach were in the range of 220 – 240 kJ/mol for all the combinations. Pre-exponential factors were found to be significantly connected to these values, i.e., higher values of E result in higher values of A in model-based kinetics. However, for lower values of E, the reaction order remains around unity, while for greater values of E, it increases. The model was tested with binary and ternary combinations of three common tyre rubbers (NR, BR and SBR) before being applied to three WT crumbs with various PCT and TT ratios. The model was found to be capable of estimating the natural polyisoprene content accurately.
Danon et al. (2015)	The use a TGA-DTA equipment to investigate the devolatilisation behaviour of four rubbers (NR, PI, BR and SBR) utilising a combination of model-free (Friedman and Kissinger) and model-based kinetics.	- Particle size: <1mm - Mass: 10±0.5 mg - Temperature: 110 ˚C (5min) - 600 ˚C - Heating rates : 2, 5, 10, 15 or 20 ˚C/min - N_2 flow rate : 100 mL/min	They found that all four rubbers had two separate weight reduction regions. These zones were the primary depolymerisation/condensation and the secondary degradation of the condensed product. Moreover, DTG and DTA data revealed that the two butadiene rubbers began to boil around 450 ˚C. The activation energy fixed values produced from the two isoconversional approaches, which ranged from 200 to 440 kJ/mol, were used as fixed values in a model-based kinetic process. The model-based multivariate nonlinear regression procedure's degrees of freedom were reduced as a result of the implementation. As a result, the combined model-free and model-based method accurately predicted devolatilisation of the four investigated rubbers.
Mkhize et al. (2019)	To investigate the formation of isoprene and DL-limonene during waste tyre pyrolysis in terms of the effect of the heating rate, using A Mettler Toledo TGA/DCS connected to a mass spectrometer (MS).	- Particle size: 0.6 – 0.8 mm - Argon (99.999%) as carrier gas - Sample mass: 10 mg - Temperature: up to 800 ˚C - Heating rates: 15 , 25, 50, 75 and 100 ˚C/min	They found that the increase in the heating rate up to 100 ˚C/min increased the peak temperature of both the isoprene and DL-limonene formation reactions during the waste tyre pyrolysis. The peak temperature increase being more significant in the DL-limonene than in the isoprene. Model parameters estimations through the Kissinger method provided activation energies of approximatively 133 and 115 kJ/mol for isoprene and DL-limonene formation reactions, respectively. Above α=0.5, the E_a strongly increased for both isoprene and DL-limonene formation and the Friedman method ceased to be accurate.

2.3.2. Theoretical approaches

The kinetic study of pyrolysis processes has attracted the attention of numerous researchers across the contemporary history of thermal devolatilisation for two reasons (Uzun and Yaman, 2014): i) Kinetic information are essential in the design of any device that undergoes heat decomposition, and ii) Kinetics is inextricably linked to decomposition mechanisms. Theorising mechanisms of thermal devolatilisation begins with kinetics.

Typically, kinetic information from solid-state pyrolysis processes has been gathered with discontinuous isothermal analysis approaches, which entails completing numerous investigations under isothermal environments at various temperatures. Dynamic approaches, on the other hand, have gained popularity due their capacity to quickly study a wide range of temperatures when undertaken under non-isothermal environments. Contemporary thermobalances are used in non-isothermal analytical approaches to expose materials to a controlled continuous temperature rise, guaranteeing that no temperature zones are ignored, as can happen in discontinuous isothermal analyses. Furthermore, research has revealed large differences in results obtained using dynamic approaches with a unique heating rate. Various sets of thermal data acquired by carrying out tests at varied heating rates were agreed upon as a way to increase the reliability of these procedures (White et al., 2011).

Thermal analytical approaches can be used to investigate solid-state kinetics by evaluating the properties of a sample when it is heated or kept at a specific temperature. When a response entails weight loss, the weight is tracked during the process, and the kinetics are frequently studied using thermogravimetry (TGA). Another measurable property for kinetic assessment utilising differential scanning calorimetry (DSC) or differential thermal analysis (DTA) is heat, whether it is produced or consumed. Conversion fraction (α) is used to normalise statics such as weight loss or heat flow. The conversion fraction indicates reaction progress as a function of time or temperature and varies from 0 to 1 (Khawam and Flanagan, 2006a).

2.3.3. Rate-laws

Eq. (1) depicts the rate of a solid-state reaction in its most general form (Khawam and Flanagan, 2005):

$$\frac{d\alpha}{dt} = k(T)\, f(\alpha) \qquad (1)$$

Where k represents the reaction rate constant, f(α) the reaction model, and α the conversion fraction.

The conversion percent at any particular time in isothermal thermogravimetric analysis is given by (Khawam and Flanagan, 2006a):

$$\alpha = \frac{m_0 - m_t}{m_0 - m_\infty} \quad (2)$$

With m_0 the initial sample weight, m_t the sample weight at time t, and m_∞ the final sample weight.

In non-isothermal thermogravimetric analysis, the conversion fraction at given temperature is:

$$\alpha = \frac{m_0 - m_T}{m_0 - m_\infty} \quad (3)$$

Where: m_T represents the weight of the sample at temperature T

The integral rate law is obtained by integrating the above equation,

$$g(\alpha) = kt \quad (4)$$

Where: g(t) is the integral model of degradation.

The temperature dependence of the rate constant is described by the following Arrhenius equation,

$$k = Ae^{-E_a/RT} \quad (5)$$

Where: A represents the pre-exponential factor, E_a the activation energy, T the absolute temperature, and R the gas constant.

The substitution of Eq. (5) into rate law equations gives,

$$\frac{d\alpha}{dt} = Ae^{-E_a/RT} f(\alpha) \quad (6)$$

And,

$$g(\alpha) = Ae^{-E_a/RT} t \quad (7)$$

The following equation can be used to convert Eqs. (6) and (7) into non-isothermal rate equations that express reaction rates as a function of temperature and at a fixed heating rate:

$$\frac{d\alpha}{dT} = \frac{d\alpha}{dt} \cdot \frac{dt}{dT} \quad (8)$$

Where: $d\alpha/dT$ is the non-isothermal reaction rate, $d\alpha/dt$ the isothermal reaction rate, and dT/dt the heating rate(β).

The differential formulation of the non-isothermal rate law is obtained by substituting Eq. (6) into the preceding equation.

$$\frac{d\alpha}{dT} = \frac{A}{\beta} e^{-E_a/RT} f(\alpha) \quad (9)$$

Upon integration, Eq. (9) gives,

$$g(\alpha) = \frac{A}{\beta} \int_0^T e^{-E_a/RT}\, dT$$

The integration limitations are changed when E_a/RT is substituted by "x". The preceding equation becomes,

$$g(\alpha) = \frac{AE_a}{\beta R} \int_x^{\infty} \frac{e^{-x}}{x^2}\, dx \tag{10}$$

Which is written as,

$$g(\alpha) = \frac{AE_a}{\beta R}\, p(x) \tag{11}$$

With $p(x)$, the exponential integral.

There is no analytical solution for the exponential integral ($p(x)$), however there are several approximations. As a result, understanding the various analysis approaches requires an assumption of the temperature integral (Starink, 2003). The three major ways for assessing the exponential integral are (Khawam and Flanagan, 2006a): i) numerically determining values of $p(x)$, ii) translating $p(x)$ to an approximate formulation that can be integrated and, iii) estimating $p(x)$ by a series expansion. There are three approximations that have been used frequently over the years (Flynn and Wall, 1966, Flynn, 1997): Schlömilch Expansion, Asymptotic expansion and Expansion in a series of Bernoulli Numbers.

Thus, these asymptotic expansions are generally expressed in the form (Starink, 2003):

$$p(x) = \frac{e^{-x}}{x(w+x)}(1 + g(x)) \tag{12}$$

Where w is a constant, and g(y) is an expansion whose first term is of the type y^{-1} or y^{-2}, with $g(y)$ "1", if y is greater than 10. Several other expansions can be obtained by using non-integer values of w. One of them is the approximation made by Senum and Yang described by the equation,

$$p(x) \cong \frac{e^{-x}}{x^2} h(x) \tag{13}$$

With $h(x)$ is the ratio of two polynomials and its fourth-order estimation is given by,

$$h(x) = \frac{x^4+18x^3+86x^2+96y}{x^4+20x^3+120x^2+240y+120} \tag{14}$$

For deriving $p(x)$, this expansion is usually restricted to simply the first or the first two terms. Eq. (15) gave the first term expansion and led to the Kissinger-Akira-Sunose method (Starink, 2003).

$$p(x) \cong \frac{e^{-x}}{x^2} \tag{15}$$

The two first terms approximation has been used by Coats and Redfern and is given by:

$$p(x) \cong \frac{e^{-x}}{x^2}\left(1 - \frac{2}{x}\right) \tag{16}$$

Doyle, however, proposed a linear approximation of p's logarithm.

$$\log p(x) \cong -0.4567x - 2.315 \quad (17)$$

The determination of the function $f(\alpha)$ and the constants A and E are required for a complete description of the reaction progress at all temperatures and for all temperature-time programs.

2.3.4. Models and mechanisms

A model is a conceptual and mathematical representation of experimentally obtained data. In solid-state reactions, a model defines a process that can typically be turned into a mathematical equation, such as a rate expression (Khawam and Flanagan, 2006a). The graphical structure of their isothermal profiles (α vs t or dα/dt vs α) or their mechanistic hypotheses are used to categorise models. Kinetic models are classified into acceleratory, decelerator, linear, or sigmoidal based on their profile. Models are divided into nucleation, geometrical contraction, diffusion, or reaction-order based on mechanistic considerations (Table 2.3) (Khawam and Flanagan, 2006b). However, a mathematical formulation proposed by Šesták and Berggren (1971) represents all models in a single generic expression:

$$f(\alpha) = \alpha^m(1-\alpha)^n(-\ln(1-\alpha))^p \quad (18)$$

With m, n, and p, the constant factors

Any model can be expressed by attributing values to the three variables. Perez-Maqueda et al. (2006) condensed the preceding equation into a simple formulation, which was found to be capable of describing any kinetic model by selecting the appropriate c, n and m parameters:

$$f(\alpha) = c(1-\alpha)^n\alpha^m \quad (19)$$

A modified master plot, comparing the theoretical and experimental profiles, can be used as an alternate way for developing a credible kinetic model. The master plot is a typical curve that is independent of acquisition parameters, is easily derived from experimental results, and is based on both the first and the second derivatives of α (Criado et al., 1989). The master plots are theoretical profiles that are referenced by the kinetic model but are relatively unaffected by the kinetic parameters. The correlation of the theoretical master plots created by presuming various kinetic models with the experimental master plot enables the selection of the appropriate kinetic model of the process under study or, at the very least, the kind of proper kinetic models. This approach can be used to analyse the kinetics of solid-state reactions regardless of the temperature program used to record data. In isothermal conditions, a single curve is sufficient to build the experimental master plots. To generate the master plot curves from the experimental data in non-isothermal conditions, the knowledge of α as a function of temperature and activation energy is required (Gotor et al., 2000).

Nowadays, a key stage in the pyrolysis process is the increased usage of pyrolysis reactors, which necessitates the employment of a kinetic model to accurately represent the complexities of the processes that occur during the thermal decomposition of long polymer chains (Khiari et al., 2018). A common goal of thermally activated reaction modelling is to obtain a thorough description of the development of a valid reaction for any thermal process, be it isothermal, by linear heating or any other non-isothermal process (Starink, 2003).

Because information regarding single reaction steps is typically difficult to get in solid-state kinetics, mechanistic explanations usually entail identifying a suitable reaction model. However, other complimentary techniques including microscopy, spectroscopy, and X-ray diffraction are required for the selection of reaction model (Khawam and Flanagan, 2006b). Thus, tyre pyrolysis kinetics modelling provides a description of the mechanisms accounting for the decomposition process and forecasts probable pyrolysis reactor issues (Khiari et al., 2018).

Table 2.3: Solid-state rate expressions for different reaction models (Khawam and Flanagan, 2006b)

Model	Differential form $f(\alpha) = 1/k\, d\alpha/dt$	Integral form $g(\alpha) = kt$
Nucleation models		
Power law (P2)	$2\alpha^{1/2}$	$\alpha^{1/2}$
Power law (P3)	$3\alpha^{2/3}$	$\alpha^{1/3}$
Power law (P4)	$4\alpha^{3/4}$	$\alpha^{1/4}$
Avrami – Erofeyev (A2)	$2(1-\alpha)[-\ln(1-\alpha)]^{1/2}$	$[-\ln(1-\alpha)]^{1/2}$
Avrami – Erofeyev (A3)	$3(1-\alpha)[-\ln(1-\alpha)]^{2/3}$	$[-\ln(1-\alpha)]^{1/3}$
Avrami – Erofeyev (A4)	$4(1-\alpha)[-\ln(1-\alpha)]^{3/4}$	$[-\ln(1-\alpha)]^{1/4}$
Prout – Tompkins (B1)	$\alpha(1-\alpha)$	$\ln[\alpha/(1-\alpha)]$
Geometrical contraction models		
Contracting area (R2)	$2(1-\alpha)^{1/2}$	$1-(1-\alpha)^{1/2}$
Contracting area (R3)	$3(1-\alpha)^{2/3}$	$1-(1-\alpha)^{1/3}$
Diffusion models		
1-D diffusion (D1)	$1/(2\alpha)$	α^2
2-D diffusion (D2)	$-[1/\ln(1-\alpha)]$	$((1-\alpha)\ln(1-\alpha)+\alpha$
3-D diffusion – Jander (D3)	$[3(1-\alpha)^{2/3}]/[2(1-(1-\alpha)^{1/3}]$	$(1-(1-\alpha)^{1/3})^2$
Ginstling – Brounshtein (D4)	$3/[2((1-\alpha)^{-1/3}-1)]$	$1-(2/3)\alpha-(1-\alpha)^{2/3}$
Reaction-order models		
Zero-order (F0/R1)	1	α
First-order (F1)	$(1-\alpha)$	$-\ln(1-\alpha)$
Second-order (F2)	$(1-\alpha)^2$	$[1/(1-\alpha)]-1$
Third-order (F3)	$(1-\alpha)^3$	$(1/2)[(1-\alpha)^{-2}-1]$

2.3.5. Methods for WT kinetic study

Many of the same techniques that are used to investigate solid-state kinetics are also utilised to examine WT pyrolysis kinetics. These techniques can be divided into two categories: experimental and computational (Khawam and Flanagan, 2006a).

2.3.5.1.Experimental methods

Solid-state kinetic data is obtained using both isothermal and non-isothermal approaches. Isothermal approaches perform by keeping samples at several consistent temperatures and producing a series of α – time points for each temperature. Isothermal rate equations (Eqs. (4) and (7)) are used in these approaches. Heating samples with fixed heating rates and tracking the reaction path are steps involved in non-isothermal or dynamic techniques (Khawam and Flanagan, 2006a).

Non-isothermal methods for determining kinetic parameters have several advantages, including i) the ability to establish kinetics can be established through an entire temperature range unceasingly, ii) the ability to obtain significant information such as temperature at maximum devolatilisation rate, characteristic temperatures, and kinetic parameters with a unique sample, iii) avoidance of sample-to-sample error by using a unique sample, and iv) the avoidance of some degradation that may occur during the preheating period (Carrasco, 1993).

2.3.5.2.Calculation methods

Model-fitting and model-free approaches are utilised to analyse solid-state kinetic parameters, whether it is isothermal or non-isothermal (Khawam and Flanagan, 2006a). Several researchers have regrouped these methods into several classes depending on their derivation basis. For example, Flynn and Wall (1966) classified the different methods of kinetic analysis into five categories, i.e., integral methods utilising weight loss versus temperature data directly, differential methods using the rate of weight loss, difference-differential methods involving differences in rate, methods especially applicable to initial rates and, nonlinear or cyclic rate methods. In the same way, Carrasco (1993) classified the methods into integral, differential and special methods. They defined special techniques as those that aren't integral or differential in nature. They are used based on comprehensive experimental data or require data that has already been analysed using graphical charts. However, Ortega (2002)1) stated three methods used to overcome different limitations found in fitting kinetics data: i) the empirical function which is the equation of Sestak and Beerggren, ii) the master plots and, iii) the isoconversional methods.

Both T and α change simultaneously in a non-isothermal experiment. In most cases, the model-fitting approach fails to produce a clear distinction between the temperature dependence, $k(T)$, and the reaction model, $f(\alpha)$. As a result, practically any $f(\alpha)$ can fit data satisfactorily at the cost of substantial the Arrhenius parameter variations. In addition, because isothermal and non-isothermal analyses are carried out in various temperature zones, if decomposition entails numerous stages with changing activation energies, the implications of these stages to the total decomposition rate evaluated in the thermal analysis investigation will fluctuate with temperature and conversion degree. As a result, the useful activation energy measured from thermal analysis investigations will be a function of these two factors as well. Model-fitting approaches are typically used to get a single value of activation energy for an entire process. Therefore, the value produced in this manner is an average and does not account for variations in the reaction mechanism and kinetics as a function of temperature and conversion degree (Vyazovkin and Wight, 1999).

Isoconversional approaches can be used to overcome the disadvantages of model-fitting outlined above. Firstly, these techniques enable the activation energy to be calculated in terms of the conversion extent and/or temperature. Secondly, no assumptions about the reaction model are made for determining this dependence. Hence, from both isothermal and non-isothermal tests, these approaches are expected to give consistent kinetic data.

As a result, model-free isoconversional methods arise as viable alternative to model-fitting methods because of their appealing characteristics: i) they are used to analyse both isothermal or non-isothermal data, ii) findings from both isothermal and non-isothermal analyses are logically coherent, and iii) expressive assessment of $E_a - \alpha$ dependencies can unveil challenges in reaction kinetics (Vyazovkin and Wight, 1999).

Table 2.4 presents the commonly used methods in the Kinetics study of WT pyrolysis with their characteristic equations.

Table 2.4. Kinetics methods used in WT pyrolysis mechanism's study

Method	General Equation	Description
Model-fitting methods		
Coats-Redfern Method	$\ln\frac{g(\alpha)}{T^2} = \ln\left(\frac{AR}{\beta E_a}\left[1-\left(\frac{2RT_{exp}}{E_a}\right)\right]\right) - \frac{E_a}{RT}$ (20)	Because $\ln\left(\frac{AR}{\beta E_a}\left[1-\left(\frac{2RT_{exp}}{E_a}\right)\right]\right)$ is rationally constant, a plot of $\ln\frac{g(\alpha)}{T^2}$ vs $1/T$ for low values of α, should be a straight line with a slope of $-E/R$. The activation energy and A are calculated using the slope and the y-intercept, respectively, and the model with the best linear fit is chosen.
Direct differential method	$\ln\frac{d\alpha/dT}{f(\alpha)} = \ln\frac{A}{\beta} - \frac{E_a}{RT}$ (21)	The E_a and A from the slope and y-intercept are calculated by plotting the left-hand side (containing the model) vs $1/T$. Typically, the model with the best linear fit is chosen.
Freeman-Carroll Difference-Differential	$\frac{\Delta\ln\frac{d\alpha}{dT}}{\Delta 1/T} = \frac{\Delta\ln f(\alpha)}{\Delta 1/T} - \frac{E_a}{R}$ (22) or $\frac{\Delta\ln\frac{d\alpha}{dT}}{\Delta 1/T} = -\frac{E_a}{R}\frac{\Delta 1/T}{\Delta\ln f(\alpha)}$ (23)	Plotting the left-hand side of Eq. (23) versus $\frac{\Delta\ln f(\alpha)}{\Delta 1/T}$ and evaluating the intercept for Eq. (22) and Eq. (23) or versus $\frac{\Delta 1/T}{\Delta\ln f(\alpha)}$ and evaluating the slope for (23) yields the activation energy.
Model-free methods		
Friedman's isoconversional method	$\ln\left(\beta\frac{d\alpha}{dt}\right)_\alpha = \ln A_\alpha + \ln f(\alpha) - \frac{E_{a\alpha}}{RT_\alpha}$ (24)	Plotting $\ln\left(\beta\frac{d\alpha}{dt}\right)$ vs $1/T$ for various heating rates and at a given reaction progress, α, provides a straight line with slope $-E_a/R$. Without knowing the reaction function $f(\alpha)$, the E_a can be calculated from this slope. The y-intercept of the straight line is the pre-exponential factor A.
Ozawa method	$\ln\beta = \ln\left(\frac{AE}{g(\alpha)R}\right) - 5.330 - 1.052\frac{E}{RT}$ (25)	The slope of the plots of $\ln\beta$ vs the reciprocal of the temperature for different values of α lead to the activation energy as a function of α, regardless of the kinetic model fitted by the reaction, assuming that $g(\alpha)$ is constant at a given value of α.
Kissinger method	$\ln\left(\frac{\beta}{T_m^2}\right) = \ln\left(\frac{AR}{f(\alpha)}\right) - \frac{E_a}{RT_m}$ (26)	A straight line is obtained by plotting $ln\left(\frac{\beta}{T_m^2}\right)$ vs $1/T_m$, at various heating rates, allowing the E_a to be determined from the straight line's gradient, $\frac{-E_a}{R}$. The pre-exponential reaction rate coefficient is estimated using the y-intercept.
Kissinger-Akira-Sunose (KAS) method	$\ln\left(\frac{\beta}{T^2}\right) = \ln\left(\frac{AR}{E_a}\right) - \ln g(\alpha) - \frac{E_a}{RT}$ (27)	For a constant value of α, the plot of $\ln\left(\frac{\beta}{T^2}\right)$ vs $1/T$ will form a straight line. Through multiplication with the gas constant, R, the E_a is calculated by the gradient of the curve, which is represented by $-E/R$.
Ozawa- Flynn-Wall (OFW) method	$\ln\beta = \ln\left(\frac{AE_a}{R}\right) - \ln g(\alpha) - 5.3305 - 1.052\left(\frac{E_a}{RT}\right)$ (28)	For α constant, a plot of $\ln\beta$ vs $1/T$ derived from thermal profiles taken at various heating rates should be a straight line with a slope that allows the E_a to be determined. The pre-exponential factor value is calculated from the y-intercept if the form of the integral function $g(\alpha)$ is known.
Starink Method	$\ln\left(\frac{\beta}{T^{1.8}}\right) = C_s - 1.0037\left(\frac{E_a}{RT}\right)$ (29)	The slope of $\ln\left(\frac{\beta}{T^{1.8}}\right)$ against 1/T yields Starink's activation energy whilst C_s is a constant irrespective of β and T.

It is important to note that:

- The Coats-Redfern method gives entirely satisfactory results when kinetics follow a simple order(Flynn and Wall, 1966) but presents no significant difference, at low conversion levels, between a zero and a first-order kinetic (Carrasco, 1993).
- The Freeman-Carroll Difference-Differential method shows some imprecisions due to the determination of the first and second conversion derivatives from differences between two discontinuous experimental points ($\Delta f/\Delta T$). Moreover, due to the approximation $\frac{d^2f}{dT^2} \approx \frac{\Delta^2 f}{\Delta T^2}$, this method is, therefore, of low accuracy (Flynn and Wall, 1966).
- Friedman's method applies to sets of data obtained at various heating rates β_i and/or various temperatures T_i (Venkatesh et al., 2013). It does, however, necessitate numerical differentiation of the empirical α versus T curves, which often results in noisy rate data, as a result, unstable E_a values. Using the integral isoconversional methods, this drawback is overcome (Vyazovkin and Sbirrazzuoli, 2006).
- When compared to isoconversional approaches, the Kissinger method has a drawback in that it only generates a unique value of activation energy for the entire process. As a result, the computed value is valid only if E_a remains constant during the process. Regrettably, such differences are rather common, and the Kissinger approach is incapable of detecting them. As result, until an isoconversional approach has proved that E_a is independent of α, the E_a values derived by this technique should be considered with caution (Vyazovkin and Sbirrazzuoli, 2006).
- Starink's method combines the Flynn-Wall-Ozawa (FWO) and Kissinger-Akira-Sunose (KAS) isoconversional approaches into a single equation. This method, applied in several kinetic studies, emerges as more precise than the FWO and KAS approaches (Starink, 1996, Starink, 2003).

2.4. Conclusion

This chapter reviewed the progress in understanding mechanisms underlying the WT pyrolysis process. Based on various data from the literature, the WT pyrolysis is dependent on its operating parameters, primarily the temperature. A full assessment of the influence of numerous variables on products yields and properties was included in the review. Several authors have initiated kinetics studies to understand the reactions pathways to design the process reactors better and increase the process's economic viability. The study presented and discussed solid-state kinetics models and methods for determining kinetic parameters. The literature has revealed that selecting the correct form of the model function and choosing the proper determination method would result in a more accurate prediction of WT pyrolysis mechanisms. Due to the average values of kinetic parameters obtained, model-fitting approaches cannot disclose the complexity of reactions in solid-state thermal analysis. On the other hand, model-free isoconversional approaches enable unambiguously identifying multi-step kinetics dependency of the activation energy on the conversion degree. Still, they are also subject to some uncertainties, owing to the approximations necessary for their applicability. As a result, a trend has arisen to combine the two approaches to predict mechanisms better.

Recent studies have also shown that combining TGA, Py-GC/MS and modelling permits a deeper comprehension of the reaction routes that control WTs pyrolysis, providing a groundwork to future research in this field (Ding et al., 2015, Menares et al., 2020). According to the literature, devolatilisation and condensation processes followed by a conversion of radicals, monomers and dimers to char, volatiles, and gas characterise the thermal devolatilisation of WTs. Furthermore, depending on temperatures and bond energies, the process balances endothermic and exothermic reactions.

However, the kinetic mechanism studies on the thermochemical treatment of waste tyres are inadequate and restricted due to an emphasis on profiling/tracking devolatilisation of the feedstock's main components rather than tracking the chemicals' formation such as limonene, terpinolene, indene and p-cymene. The limited information available in the literature focuses primarily on increasing DL-limonene in TDO and estimating kinetic parameters related to the formation of isoprene and DL-limonene. As a result, further research is needed to correlate the yields of significant chemicals to kinetic data and reach general agreements on the reaction pathways, thereby increasing the process's economic viability. Moreover, since the reaction pathways for waste tyre pyrolysis are susceptible to the material characteristics, particle diameter, thermal regime and, therefore, to the experimental setup, more research into the influence of these parameters on the kinetics and selectivity to attractive fractions or chemicals will aid process design and scaling up.

3. Materials and methods

3.1. Feedstock

Truck Tyre crumbs samples of particle size < 1 mm, were used for all experiments conducted in this study. Samples were obtained from a local tyre recycler and stored in airtight plastic bags.

3.2. Compositional analysis

Because tyres include over a hundred constituents, it becomes indispensable to conduct a detailed characterisation evaluation to help identify components and forecast devolatilisation mechanisms. The empirical approach consists of proximate and ultimate analysis.

The proximate analysis estimates the volatile matter, the fixed carbon, the inherent moisture and ash contents from waste tyres. Several methods of proximate analysis of tyres can be utilised, including a series of American Society for Testing and Materials standard methods (ASTM), the International Organisation for Standardisation (ISO), the South African National Standards (SANS) and the South African Bureau of Standard (SABS).

The proximate analysis in this work was carried out using a thermogravimetric analyser (TA 60WS, Shimadzu, Japan), which consists of an analytical balance with a sample holder and a configurable temperature sensor housed within the oven.

The maximum temperature was set to 800 ^{o}C to determine the mass loss as temperature increases. Nitrogen was used as an inert medium to purge hot volatiles at a low heating rate (10 ^{o}C/min) before switching to oxygen, the combusting/oxidising medium. The moisture content is evaporated at around 110 ^{o}C, while the volatile matter is formed between 110 – 550 ^{o}C under nitrogen. The sample is maintained at 800 ^{o}C, and the atmosphere shifted from N_2 to O_2 to allow the combustion of fixed carbon. The ash content is the material left after the tyre has lost its moisture, volatile materials, and fixed carbon as a result of O_2 combustion.

The computations were carried out using a slightly modified ASTM E 1131-08 (2008), which is the Standard Test Method for Compositional Analysis by Thermogravimetry.

The ultimate analysis evaluates the C, H, N, and S quantities in the analytical WT. The Leco SC 632 analyser was used to conduct this analysis. For CO_2 and SO_2 formation, a sample of 0.5 mm was combusted into pure O_2, followed by detection and quantification by infrared detection.

For the compositional analysis completion, the higher heating value of the sample (HHV) was calculated using the Boiés correlation (Han et al., 2017) for polymeric materials and biomass.

3.3. Fourier transformed infra-red (FT-IR) spectroscopy

The organic compounds in WT crumbs were investigated using an FT-IR spectrometer (Prestige-21, Shimadzu, Japan) integrated with a platinum attenuated total reflection (ATR) single-reflection module, which provided a spectrum at ambient pressure and room temperature. The samples' spectra were aggregated from 32 scans with a resolution of 4 cm^{-1} in the 400 – 4000 cm^{-1} range. Data were analysed using LabSolutions IR software.

3.4. Thermogravimetric analysis and kinetics

From 30 °C to 800 °C, a thermobalance (TA 60WS, Shimadzu, Japan) was used to record weight loss as a function of temperature. Kinetic experiments were conducted at several heating rates (10, 20, 30, 40 and 50 °C/min) and making use of the same carrier gas N_2 at the rate of 100 mL/min to support the WTs pyrolysis understanding. (10±1) mg was used as sample weight in all tests repeated twice.

The linear mathematical analysis methods approached the kinetics for the decomposition of WTs. Using mass loss determination information collected at multiple devolatilisation rates, these approaches allow for the establishment of a linear relationship between the kinetic parameters.

This research considered two calculation approaches: model-fitting and model-free. Among the model-fitting approaches, we selected the direct differential and Coats-Redfern methods. From the isoconversional Friedman method, the Kissinger and Starink methods have been chosen as model-free methods.

By numerically computing the differential ($\frac{d\alpha}{dT} \approx \frac{\Delta\alpha}{\Delta T}$), the direct differential technique employs the differential formulation of the non-isothermal rate law. By considering the logarithm form of the non-isothermal rate law, the general expression of this method is given by Eq. (21) presented in the previous chapter, $\ln\frac{d\alpha/dT}{f(\alpha)} = \ln\frac{k_0}{\beta} - \frac{E_a}{RT}$. With f(α) the reaction model, α the conversion fraction, T the temperature, $\Delta\alpha$ and ΔT their respective incremental differences, $d\alpha/dT$ the non-isothermal reaction rate, R the gas constant and β the heating rate. The activation energy (E_a) and pre-exponential factor (k_0) are obtained from the slope of $\ln\frac{d\alpha/dT}{f(\alpha)}$ versus 1/T (Khawam and Flanagan, 2006a).

The Coats-Redfern method uses the integral form of the non-isothermal rate law and its approximation. The mathematical assumption of this method corresponds to a zero-order reaction, and its general equation is given by Eq. (20) in chapter 2, $\ln\frac{g(\alpha)}{T^2} = \ln\left(\frac{k_0 R}{\beta E_a}\left[1 - \left(\frac{2RT_{exp}}{E_a}\right)\right]\right) - \frac{E_a}{RT}$ (Coats and Redfern, 1965, Khawam and Flanagan, 2006a).

The E_a and k_0 are obtained from the slop of $\ln\frac{g(\alpha)}{T^2}$ versus 1/T. Where g(t) represents the integral decomposition model and T_{exp} the mean experimental temperature.

Friedman's isoconversional approach is based on a comparison of tests conducted at various linear heating rates. It works with varying conversion degrees by using the logarithm of conversion rate as a function of inverse temperature (Friedman, 1964, Venkatesh et al., 2013). The mathematical form of this method given by Eq. (24) in chapter 2 is, $\ln\left(\beta\frac{d\alpha}{dt}\right)_\alpha = \ln k_{0\alpha} + \ln f(\alpha) - \frac{E_{a\alpha}}{RT_\alpha}$. The Kinetic parameters are obtained from the plot of $\ln\left(\beta\frac{d\alpha}{dt}\right)$ against 1/T, with $\frac{d\alpha}{dt}$ the isothermal reaction rate.

The Kissinger method is based on determining the temperature at the highest devolatilisation rate at different heating rates (Kissinger, 1957). Eq. (26) in chapter 2, given by $\ln\left(\frac{\beta}{T_m^2}\right) = \ln\left(\frac{k_0 R}{f(\alpha)}\right) - \frac{E_a}{RT_m}$, represents its mathematical form. In this method, E_a and k_0 are obtained from the slop of $ln\left(\frac{\beta}{T_m^2}\right)$ versus 1/T, T_m is the temperature at which the maximum rate occurs.

Starink's method combines the FWO and KAS isoconversional methods into a single expression (Starink, 2003) given by Eq. (29) in chapter 2, $\ln\left(\frac{\beta}{T^{1.8}}\right) = C_s - 1.0037\left(\frac{E_a}{RT}\right)$. In this expression, C_s is a constant factor that is irrespective of β and T. Starink's activation energy and pre-exponential factor are calculated from the slop of $\ln\left(\frac{\beta}{T^{1.8}}\right)$ against 1/T.

3.5. Pyrolysis in conjunction with Mass Spectrometry (Py-GC/MS)

3.5.1. Description

The pyrolysis was performed in a multi-shot pyrolyser (EGA/PY-3030D, Frontier Laboratories Ltd., Japan) based on a proprietary, high-temperature-resistant ceramic heater with low heat capacity. The system consists of the pyrolyser furnace, which also serves as a thermal desorption unit, and temperature controller. In this technique, the sample contained in a cup free-falls into a micro furnace. The sample temperature goes from ambient (+10 °C) to the pyrolysis or furnace temperature (up to 1050 °C) in several tens of milliseconds due to the high-temperature ceramic heater which rapidly heats and cools. This system has very fine temperature control and very little pyrolysate condensation. A schematic of the multi-shot pyrolyser is presented in Figure 3.1 (https://manualzz.com/doc/22427966/multi-shot-pyrolyzer-model-ega-py-3030d-operation).

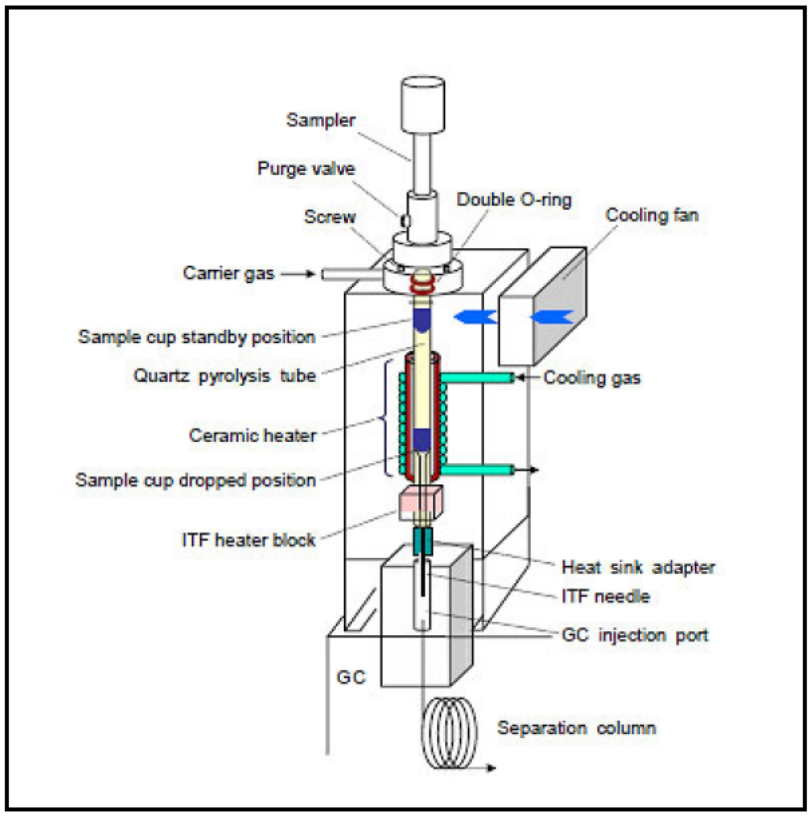

Figure 3.1: Schematic of the multi-shot pyrolyser (https://manualzz.com/doc/22427966/multi-shot-pyrolyzer-model-ega-py-3030d-operation).

The EGA/PY-3030D system allows four analytical methods, i.e., Single-shot gas chromatography GC, Double-Shot GC, Evolved gas analysis - Mass spectrometry EGA-MS and Heart-Curt EGA-GC/MS with five samplers (Double-Shot sampler, Liquid sampler, Online-micro reaction sampler, Micro thermal desorption sampler and Online micro UV sampler).

The analytical capability of the EGA/PY-3030D is expanded by adding peripheral devices such as the selective sampler, the auto-shot sampler, the microjet cryo-trap, etc. In addition, MS search software has been developed to facilitate the rapid and in-depth characterisation of polymeric materials, and the manufacturer has offered a host of polymeric/additives libraries.

The multi-shot pyrolyser is associated with the GC/MS equipment, which comprises of a gas chromatographic combined with a mass spectrometer to separate, categorise and measure sophisticated polymeric materials.

The multi-shot pyrolyser EGA/PY-3030D used in this study was interfaced with a gas chromatograph (GC-2010 Plus, Shimadzu, Japan) with the AOC-20I auto-injector, fitted with a MS detector (QP 2010 Ultra, Shimadzu, Japan). In all the tests, the interface line remained fixed at 250 °C, and the volatile compounds were carried out of the pyrolysis reactor using a regular air flow of 54.1 mL/min.

The products of pyrolysis (1:50 split ratio) were isolated in a zebron capillary GC column (ZB-5MS) of 30 m length, 0.25 mm internal diameter and 0.25 µm film thickness, and were analysed in an mass spectrometer sensor (70 eV ionisation) in the *m/z* range of 30-800. The carrier gas was made up of 99.99 % pure helium.

For all the experiments, 1±02 mg of WTs sample were loaded into a sample holder (Frontier Laboratories Eco-cup SF, 50 µL) and inserted into the oven using an auto-shot sampler.

In this work, two separate analytical procedures were applied, namely single-shot and evolved gas analysis, which are detailed in the subsequent sections.

3.5.2. Single-shot experiments

These experiments have been conducted to investigate the effect of temperature on the chemicals production and, therefore, determine the optimal pyrolysis temperature. Based on data from the thermogravimetric analysis, tests were carried out at various temperatures (400, 500, 600, and 700 °C) using the EGA/PY-3030D equipment and its accessories. Chromatograms were analysed regarding the Area % of two marketable chemicals, i.e., Limonene and Indene.

3.5.2.1.Method description

In this method, also called flash pyrolysis, the sample is placed in a cup which is then attached to the sampler. The sampler is attached to the multi-shot pyrolyser. Pyrolysis starts when the cup is released and free-falls into the pyrolyser furnace at a pre-defined temperature. The carrier gas sweeps the gases generated into the furnace. The sample hot volatiles is split, a portion going to the analytical column and a part exiting via the split vent. Figure 3.22 presents a typical instrument configuration for this method (https://manualzz.com/doc/22427966/multi-shot-pyrolyzer-model-ega-py-3030d-operation).

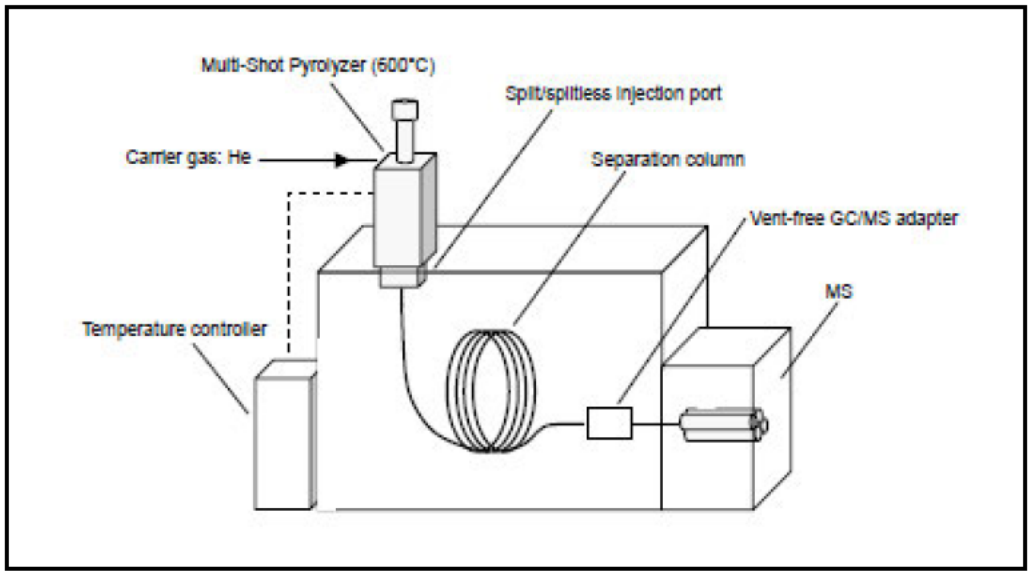

Figure 3.2: Single shot system configuration
(https://manualzz.com/doc/22427966/multi-shot-pyrolyzer-model-ega-py-3030d-

This method has been realised into four steps:

1. Install the 30 mm ZB-5MS capillary column,
2. Set the pyrolysis and GC/MS conditions as presented in Table 3.1: set the interface temperature (ITF TEMP) to auto mode and set the pyrolysis temperature in single-shot analysis screen,
3. Prepare the sample: place 10±1 mg of the WT sample in an Eco cup SF (Frontier Laboratories Eco-cup SF, 50 µL), attach a stick to the sample cup and fi the assembly to the sampler. Attach the sampler to the pyrolyser and wait for 1 min so to purge the residual air,
4. Click the start button when the temperature and pressure stabilise: press the sample drop button located at the top of the sampler, which releases the cup and drops it into the furnace. Then click the start button for GC analysis.

3.5.2.2.Parameters setting

Table 3.1 present the different parameters set for the pyrolysis and GC/MS analysis.

Table 3.1: Single Shot Pyrolysis and GC/MS parameters

Parameters	
Pyrolysis	
Initial temperature	40 °C
Final temperature	400, 500, 600, 700 °C
GC	
Column oven temperature	40 °C
Injection temperature	250 °C
Injection mode	Split
Pressure	49.7 kPa
Total flow	100 mL/min
Column flow	1.0 mL/min
Linear velocity	36.1 cm/s
Purge flow	3.0 mL/min
Split ratio	96
Oven temperature program	40 °C to 200 °C (2 min) at a rate of 3 °C/min, 200 °C to 280 °C (17 min) at a rate of 5 °C/min
MS	
MS temperature	200 °C (Ion source) 230 °C (Interface)
Solvent cut time	1.00 min
Time	1.00 to 88.33 min
Scan speed	3333
m/z	30 - 800

3.5.3. Direct Evolved Gas Analysis (EGA)

EGA experiments have been conducted at various heating rates considered in the kinetics study (10, 20, 30, 40 and 50 °C/min) to investigate the effect of heating rate at the optimal temperature.

3.5.3.1.Method description

An EGA capillary tube is used in this analysis mode to connect the GC injector to the detector with the GC oven temperature set between 250 and 300 °C. The thermally desorbed components and gases resulting from the WT sample are released and detected when the sample is heated. Figure 3.3 shows a typical instrument configuration for EGA (https://manualzz.com/doc/22427966/multi-shot-pyrolyzer-model-ega-py-3030d-operation).

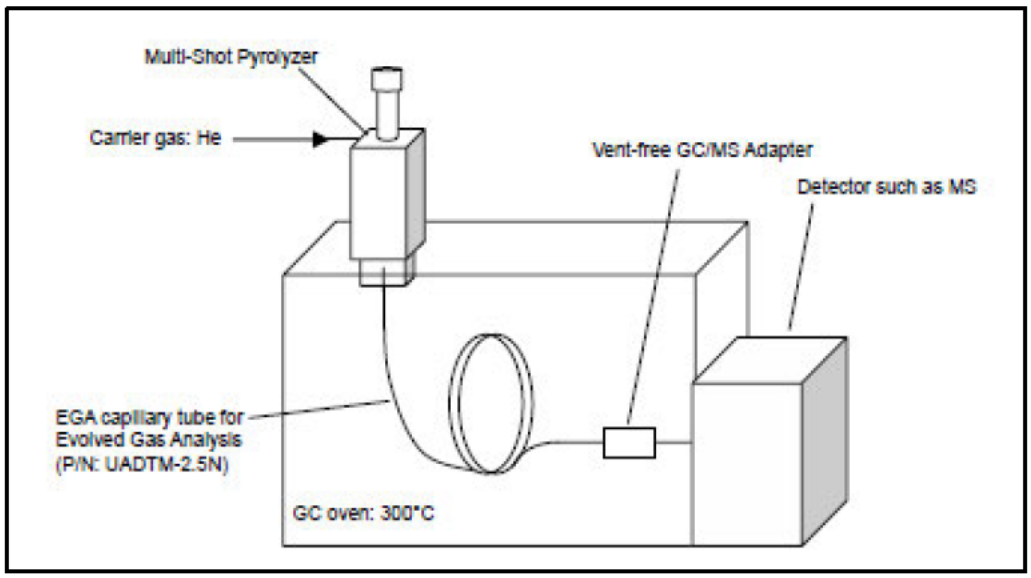

Figure 3.3: Evolved gas analysis system configuration (https://manualzz.com/doc/22427966/multi-shot-pyrolyzer-model-ega-py-3030d-operation).

1. Install the 30 mm ZB-5MS capillary column;
2. Set the analytical conditions for pyrolyser and GC/MS (Table 3.2): set the interface temperature to auto mode and set the furnace in the direct EGA analysis screen.
3. Load the sample: place 10±1 mg of the WT sample into an Eco cup SF, attach an Eco stick SF to the sample cup and fix it to the sampler. Push the slider of the sampler down, attach the sampler to the pyrolyser and wait for 1 min.
4. When temperatures and pressures stabilise, click the start button: press the sample drop button located at the top of the sampler that drops the sample cup into the furnace. Then click the start button for GC analysis.

3.5.3.2.Parameters setting

Table 3.2 presents the different parameters used in this analysis mode.

Table 3.2: EGA analysis parameters

Parameters	
Pyrolysis	
Initial temperature	40 °C
Final temperature	500 °C
Heating rates	10, 20, 30, 40 and 50 °C/min
GC	
Column oven temperature	40 °C
Injection temperature	300 °C
Injection mode	Split
Pressure	49.7 kPa
Total flow	54.1 mL/min
Column flow	1.0 mL/min
Linear velocity	36.1 cm/s
Purge flow	3.0 mL/min
Split ratio	50
Oven temperature program	40 °C to 200 °C (for 2 min) at a rate of 5 °C/min, 200 °C to 300 °C (for 15 min) at a rate of 3 °C/min
MS	
MS temperature	230 °C (Ion source) 250 °C (Interface)
Solvent cut time	0.00 min
Time	0.00 to 82.33 min
Scan speed	1250
m/z	50 - 400

3.5.4. Data processing

The data from the Py-GC/MS analysis were analysed using the selectivity to a specific specie S_i, defined as the proportion of an ith- chromatographic compound's peak (PArea$_i$) to the aggregate of all detected peak areas ($\sum PArea_i$) Eq. (30). Furthermore, the factor ξ_{a-b} was employed to assess the relative production of relevant compounds, Eq. (31) (Menares et al., 2020).

$$S_i = 100\ x\ (PArea_i\ /\ \sum_{i=1}^{n} PArea_i) \quad (30)$$

$$\xi_{a-b} = (S_a/S_b) \quad (31)$$

With:

- S_i, the selectivity to a specific specie or compound i,
- $PArea_i$, the chromatographic peak of an ith compound,
- $\sum_{i=1}^{n} PArea_i$, the aggregate of all detected peak areas,
- ξ_{a-b}, a quantifier of a and b compounds relative formation
- a, b, the produced compounds such as limonene, etc.

4. Results and discussion

4.1. Compositional characterisation

The process of tyre decomposition and the final composition of the volatile products from tyre pyrolysis are affected by waste tyre properties or composition. These components are identified via proximate and ultimate investigations that allow for the estimation of the pyrolysis opportunities of WTs. The maximal pyrolysable content of the waste tyre is its volatile matter. Polymeric substances produced from natural and styrene rubbers were used in this tyre component. The char left after pyrolysis should logically match the fixed carbon (non-volatile) and ash fractions of WTs, deriving from the carbon black used in the tyres construction and inorganics (different from steel), respectively.

Summarised in Table 4.1 are the proximate and ultimate analysis data of the studied WT and the calculated calorific value.

The reported high content of volatile matter (60.8%) indicates that this material is pyrolysable. The results in Table 4.1 are consistent with many of those previously published on WTs, which range from 58 to 66% for the volatile matter, 27.5 to 32% for the fixed carbon and 4.2 to 5.4% for the ash content (Roy and Unsworth, 1989, Li et al., 2004, Iwarere and Mkhize, 2019, Menares et al., 2020).

Table 4.1: Waste truck tyre compositional analysis

Proximate analysis (wt.%)	
Moisture	3.4
Volatile Matter	60.8
Fixed Carbon	30.4
Ash	5.3
HHV (MJ/kg)	34.12
Ultimate Analysis (wt.%)	
C	77.9
H	6.6
N	0.5
S	2.8
O	6.8

The high carbon content of the investigated material, as demonstrated by the ultimate analysis, indicates that it is a promising source of energy, whether through direct combustion or as a raw material for the generation of liquid fuels. The estimated higher heating value (HHV) matched that reported by previous researches (Li et al., 2004, Menares et al., 2020).

Figure 4.1 shows the FTIR spectrum of the sample used to identify the possible rubbers of the truck tyre. From the spectrum, characteristic bands can be observed at 2915 and 2846 $cm^{-1,}$ which are commonly linked to $-CH-$ asymmetric stretching vibrations of $-CH_3$ and $-CH_2-$ chemical groups and, to the $-C-H$ symmetric stretching vibrations of the same chemical groups. These two bands are characteristic of the spectrum of natural rubber NR (Nunes et al., 2018).

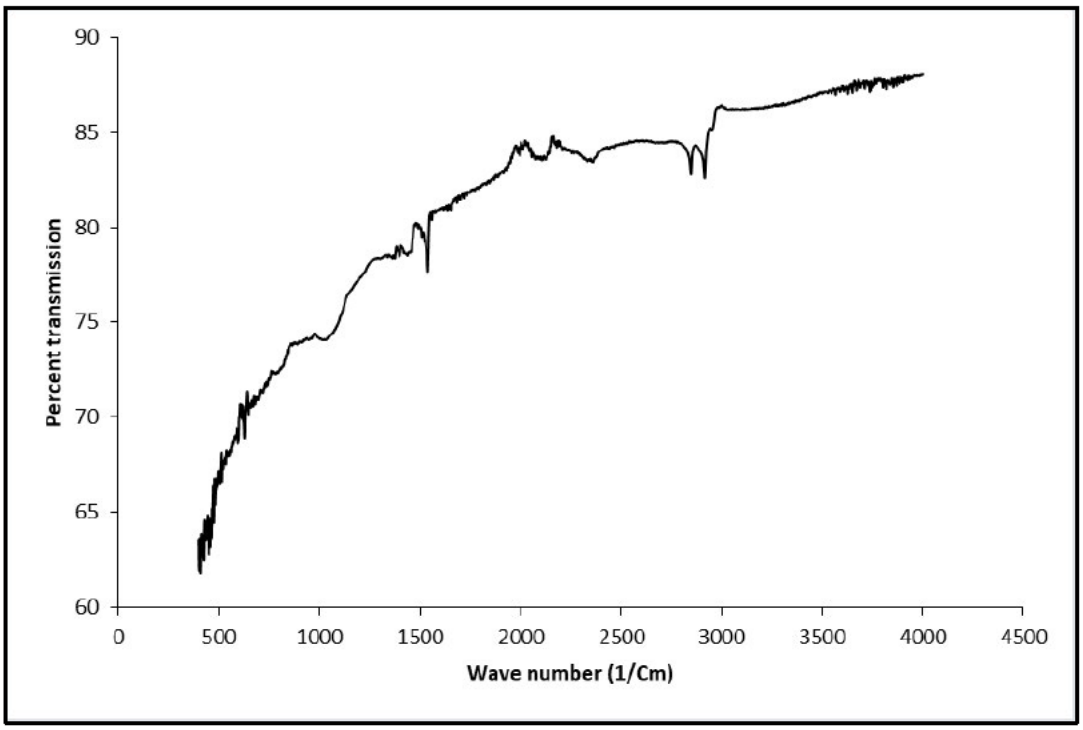

Figure 4.1: Waste truck tyre FTIR spectrum

Besides the two bands, the other three characteristic vibrational signals were observed at around 1537, 1438 and 1373 cm^{-1}. These absorbance peaks respectively showed the stretching of $C-H$, $C-C$ and $C-N$ functional groups, related to the Synthetic rubber (SBR and BR) (Khan et al., 2017, Nunes et al., 2018). The elemental analysis verified that the moderate vibrations between 626 and 513 cm^{-1} were connected with $C-S$ bonds. Some infra-red (IR) vibrations, on the other hand, can be linked to tyre additives (Menares et al., 2020).

As a consequence of the aforesaid compositional analyses and FTIR results, the truck tyre contains natural, butadiene and styrene-butadiene rubbers.

4.2. Thermogravimetric analysis

The experimental WT's thermal devolatilisation was examined in this part. Comparison of the thermal degradation behaviour to some compositional characteristics of the tyre has been performed, and therefore, required data for the kinetic study were gathered.

4.2.1. Thermogravimetric analysis (TGA)

The profiles of the thermogravimetric analysis (TGA) based on the pyrolysis temperature at five heating rates are illustrated in Figure 4.2. From Figure 4.2, we observe that the mass loss of the tyre at different heating rates is modest before 200 °C. Although the mass loss of WT appears to begin at about 200 °C, the rate of mass loss stays modest until 300 °C, when the WT devolatilisation becomes considerably more rapid until the final temperatures are reached. The terminal pyrolysis temperature of the experimental tyre ranges from 500 – 600 °C, according to the heating rate, and is more precisely established by analysing the derivative thermogravimetric profile. The final temperature is defined as the temperature at which mass loss remains constant and no significant changes occur when the temperature rises. Figure 4.2 depicts this behaviour, with graphs at various heating rates appearing to reach a plateau.

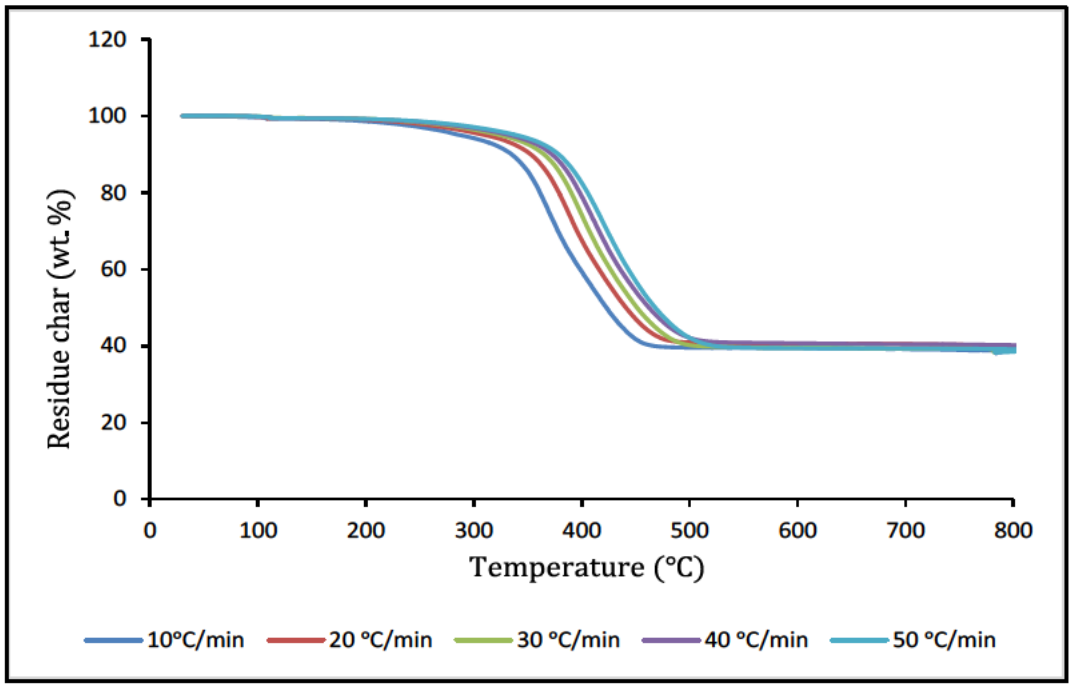

Figure 4.2: Truck tyre TGA profiles

The thermogravimetric profiles reveal that irrespective of the heating rate, the shapes converge to the same solid residual value at the end of pyrolysis. The stated char values are the aggregate of the fixed carbon and ash contents observed during proximate analysis and are based on an average all the heating rates (10 to 50 °C/min). The observed char residual, 38.7 wt.%, is comparable to the previously reported work (Menares et al., 2020). It is important to note that when investigating the slope, this approximation is totally dependent on the user's discretion.

4.2.2. Derivative thermogravimetric (DTG) and reaction progress

Figure 4.3 and Figure 4.4, respectively, illustrate the profiles of the first derivative (DTG) and reaction progress based on the pyrolysis temperature at different heating rates. The pattern of the curves exhibited in Figure 4.3 indicates two peaks at a lower heating rate, namely a significant devolatilisation peak at low temperature (378.9 °C at 20 °C/min) and a tiny peak or shoulder at elevated temperature (433.7 °C at 20 °C/min) as reported by previous researchers (Mkhize et al., 2019). We observed that the prominent peak increases while the shoulder disappears by increasing the heating rate. Previous research has linked the phenomenon to the reduction of second reactions at higher heating rates while promoting the devolatilisation of rubbers (Danon et al., 2015).

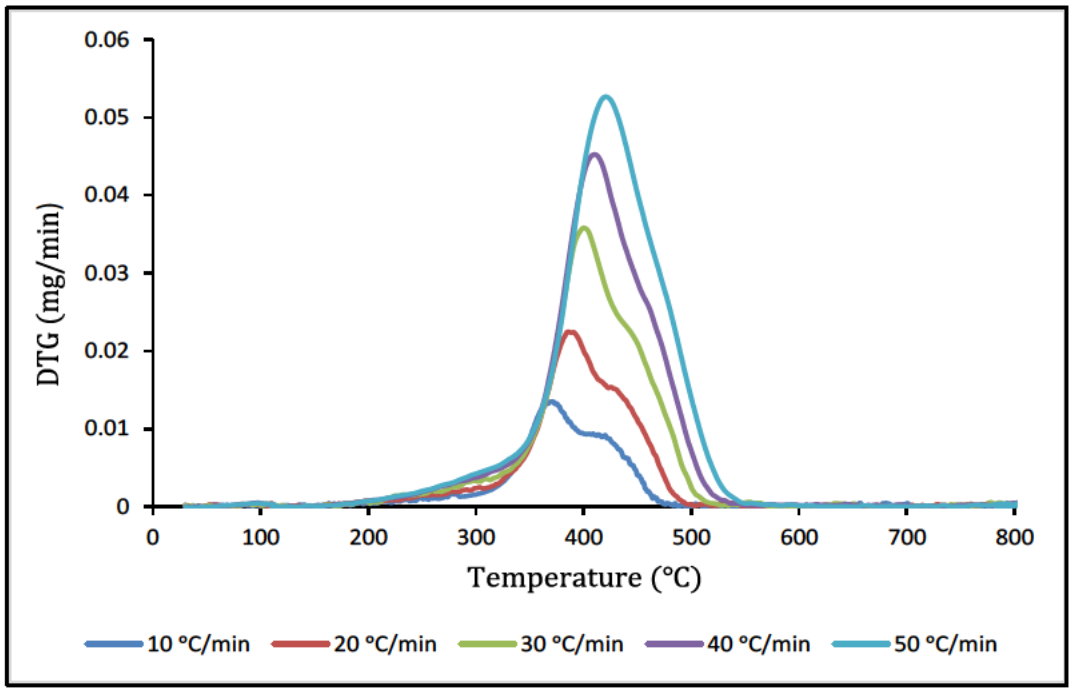

Figure 4.3: Waste truck tyre DTG profiles

The DTG profile at heating rate $\beta = 20$ °C/min presented a prominent devolatilisation peak around 378,9 °C with a shoulder at 433,7 °C; which are comparable to those reported in previous work at the similar heating rate (Menares et al., 2020). These two peaks have long been thought to be characteristic of polyisoprene rubbers (Danon and Görgens, 2015). Devolatilisation/condensation reactions at moderate temperatures are more likely to produce condensation compounds, which then fragment and reorganise to produce pyrolysis products, according to several studies (Mkhize et al., 2016, Xu et al., 2018). Furthermore, at lower temperatures, the primary devolatilisation peak has been linked to the decomposition of polyisoprene and, to less extent, styrene-butadiene rubber. Hence, some alkenes such as limonene are abundant in the pyrolysis of hot volatiles at these lower temperatures (363.35 °C at 10 °C/min to 424.6 °C at 50 °C/min) (Danon et al., 2015, Mkhize et al., 2016).

The final temperature is obtained using tyre differential thermogravimetric profiles, as earlier discussed in this section. When the differential thermogravimetric profiles revert to zero after the final loss peak, the temperature may be read off from the graph. Knowing when to end the temperature ramp-up in pyrolysis is crucial for producing commercial products from the WT while minimising costs, and will specify the intervals of investigation for process optimisation.

Figure depicts the relationship between heating rate and devolatilisation reaction progress. Table 4.2 shows different temperatures at maximum conversion rate (considered to be 90%) for various heating rates.

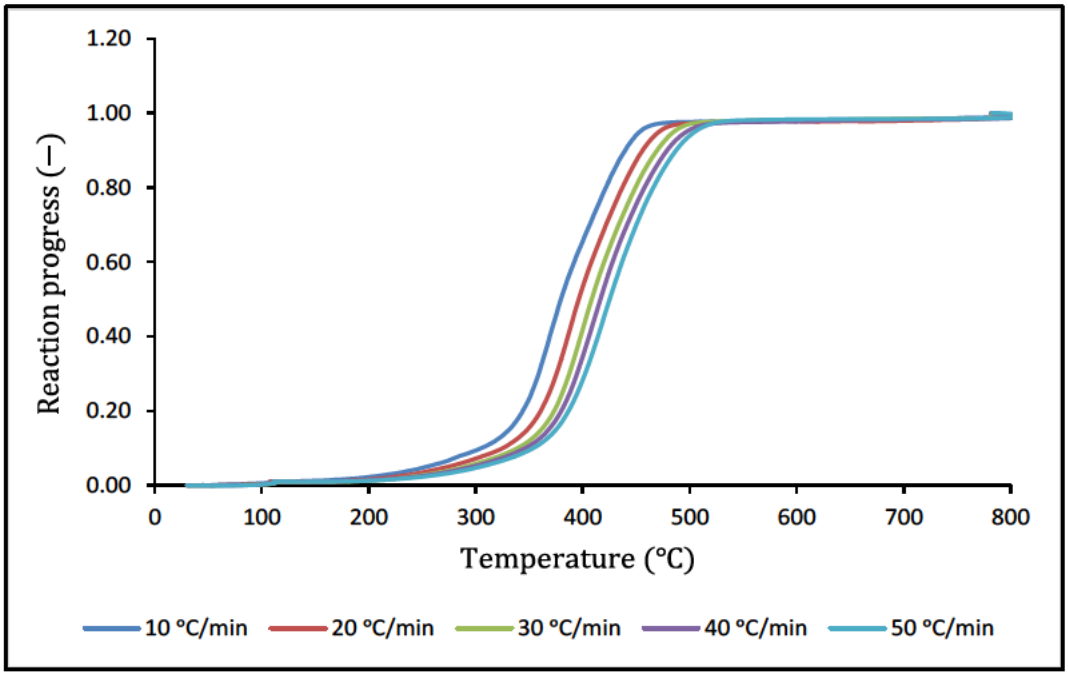

Figure 4.4: Reaction progress of the waste truck tyre

As shown in Figure and Table 4.2, the influence of the heating rate on the devolatilisation peak temperature is evidenced by a rise of temperature linked with the maximum devolatilisation rate as the heating rate rises.

Table 4.2: Maximum pyrolysis temperature

β (°C/min)	10	20	30	40	50
T_{max} (°C)	438.72	454.93	468.49	478.29	486.14

T_{max} is the temperature at the estimated maximum conversion rate and β, the heating rate.

From the above information gathered to perform kinetic analysis, the WT thermal devolatilisation is explained by devolatilisation/condensation reactions followed by fragmentation/rearrangement of radicals, mono and dimers to form char, volatiles compounds and gas.

4.3. Kinetic analysis

4.3.1. Model-free methods

4.3.1.1.Friedman method

Figure 4.5 illustrates the isoconversional Friedman method's experimental tyre linear plots as a function of reaction conversion. These linear plots, generated from the plotting of $\ln\left(\beta\frac{d\alpha}{dT}\right)$ versus $\frac{1}{T}$ (Eq. (24)), have an identical gradient, and therefore, the estimated activation energy E_a is irrespective of the reaction progress.

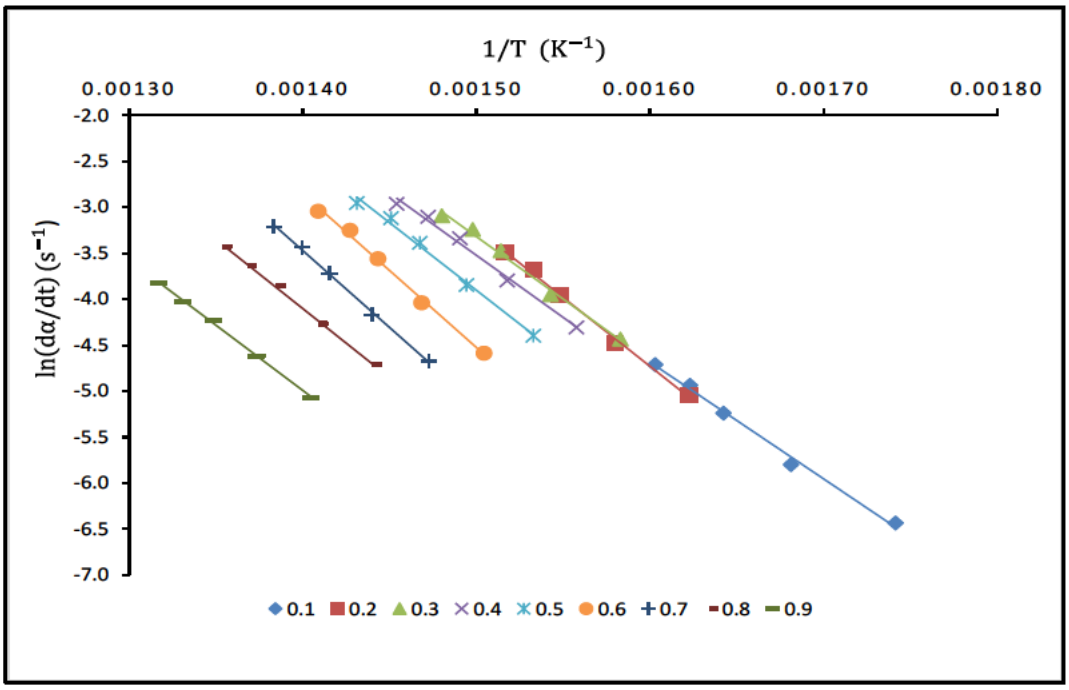

Figure 4.5: Friedman method linear plots

Table 4.3 and Figure 4.6 and Figure 4.7 present the activation energies and pre-exponential factors at various conversion rates, calculated from the gradient and intercept of different plots.

Table 4.3: Friedman calculated activation energies

α	$-E_a/R$	$\ln k_0$	E_a (kJ. mol^{-1})	k_0 (s^{-1})
0.1	12691	15.619	105.5	6E+06
0.2	14983	19.241	124.6	2E+08
0.3	13577	17.047	112.9	3E+07
0.4	13490	16.713	112.2	2E+07
0.5	14711	18.163	122.3	8E+07
0.6	16713	20.546	138.97	8E+08
0.7	16722	19.939	139.04	5E+08
0.8	15026	16.933	124.9	2E+07
0.9	14190	14.873	118.0	3E+06
Average			122.0	2E+08

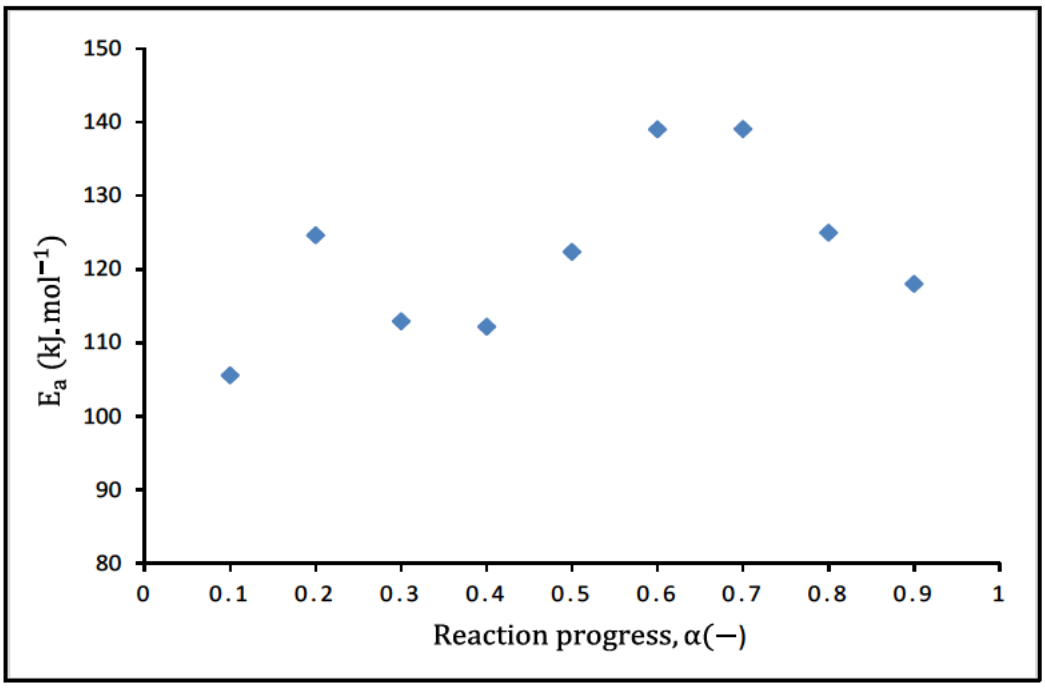

Figure 4.6: Friedman activation energy vs reaction progress

Figure 4.6 shows two sets of linear plots for the experimental tyre, i.e., the first set from reaction progress of 0.1 to 0.4 with a maximum peak at reaction progress of 0.2 and the second set from reaction progress of 0.4 to 0.9 with the maximum peak at reaction progress of 0.7.

As a result, the activation energy (E_a) as a measure of the reaction progress (α) reaches a maximum value of 139.04 kJ. mol^{-1} at reaction progress of 0.7. Iwarere and Mkhize (2019) also reported a maximum peak at reaction progress of 0.7 for truck tyres, with a similar estimation approach. Values of E_a obtained in the present study by the isoconversional Friedman method ranged from 105.5 to 139.04 kJ. mol^{-1} with an average estimated at 122.0 kJ. mol^{-1}.

Alternatively, the pre-exponential factor (k_0) reported in Figure 4.7 presents a similar trend as in the E_a, with an average k_0 estimated at 2E+08 s^{-1}.

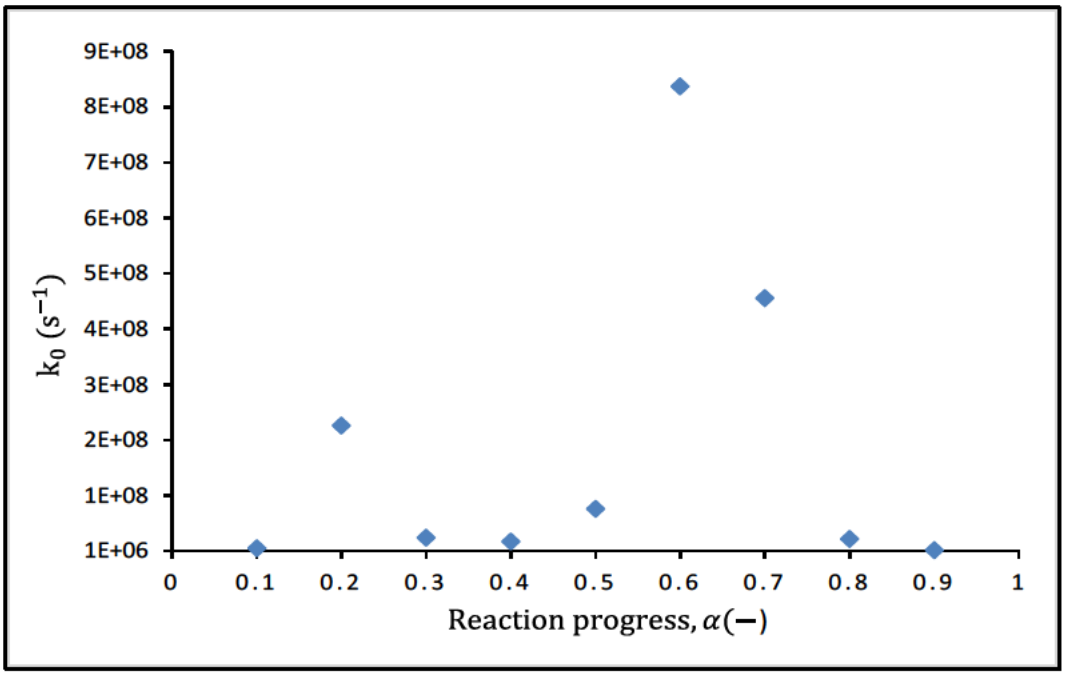

Figure 4.7: Friedman pre-exponential factor vs reaction progress

Two significant regions corresponding to the two peaks are identified from the E_a vs α profile presented in Figure 4.6. Between 343 °C and 386 °C, the first region is associated with the devolatilisation/condensation of NR and SBR. The allylic poly-isoprene molecules undergo depropagation and intramolecular cyclisation-scission in this zone, generating isoprene and limonene as hinted by Mkhize et al. (2016). The scission and dehydrogenation of the SBR, which results in the synthesis of styrene and butadiene monomers, could be linked to second zone, between 392 and 437 °C. Menares et al. (2020) also reported the presence of two significant regions at 358 – 382 °C and 387 – 433 °C, respectively.

4.3.1.2.Kissinger method

Figure 4.8 presents the Kissinger plot for the experimental truck tyre. The isoconversional Kissinger method provides an alternative to the Friedman method. This method uses an integrated approach also utilised to determine activation energy (E_a) and pre-exponential factor (k_0).

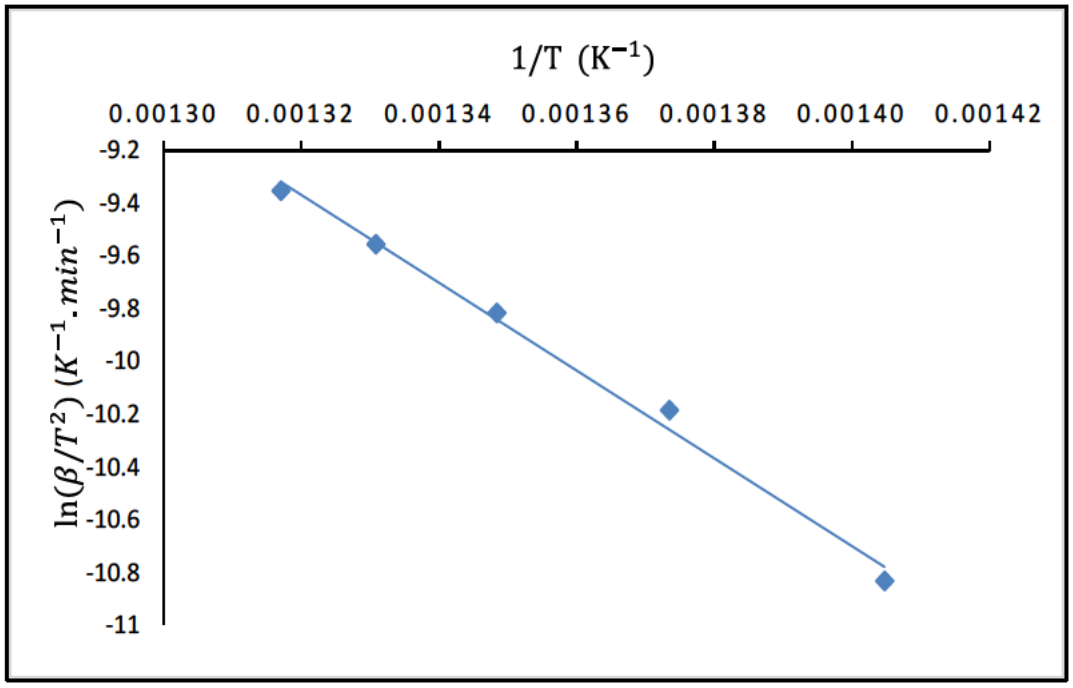

Figure 4.8: Kissinger method linear plot

The E_a estimated using the Kissinger plots was 138.5 kJ. mol^{-1} with a pre-exponential factor of 3E+05 s^{-1}. A difference between the E_a calculated from the Friedman method (average), and the Kissinger method is around 16.5 kJ. mol^{-1}. However, the value of E_a obtained with the present method is comparable to the maximum value of E_a estimated with the Friedman method at around 0.5 units of difference. The appearance of the shoulder on the profiles of the first derivative, which disappears as the heating rate rises, could explain the disparity in activation energy values. The absorption of the shoulder to the prominent peak affects the estimation of the E_a. In addition, the pre-exponential coefficient in the Friedman approach was shown to be greater than in the Kissinger approach.

4.3.1.3.Starink's method

Similar to the Kissinger method, Starink's method integrates into a single equation two iso-conversional techniques, i.e., the FWO and the KAS techniques. Figure 4.9 illustrates the plot obtained from Starink's approach.

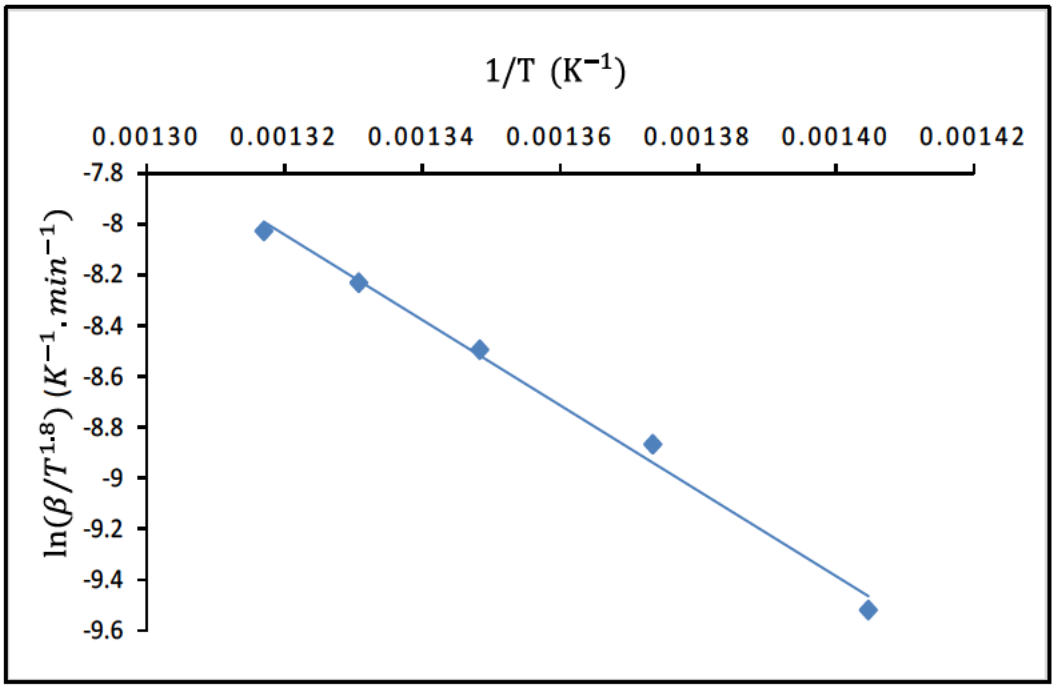

Figure 4.9: Starink's method linear plot

The estimated values of E_a and k_0 using this method, were 139.7 kJ.mol^{-1} and 1E+06 s^{-1}, respectively. The obtained E_a value falls in the range of those obtained by Menares et al. (2020) using a similar method. They reported values of E_a ranging from 101.5±2 to 176.7±2 kJ.mol^{-1}.

The maximum values of E_a estimated with the model-free methods have slight differences, with the highest value obtained with Starink's approach. The same technique presented the highest pre-exponential factor.

4.3.2. Model-based methods

For five distinct heating rates (10, 20, 30, 40 and 50 °C/min), two conventional methods, the direct differential and the Coats-Redfern methods, were used.

For E_a and k_0 estimation, we fitted ten models in the two calculations methods. The used models were the first order (F1), the second-order (F2), the first diffusion (D1), the second diffusion (D2), the power low (P2), the power low (P3), the Avrami-Erofyev (A2) and (A3), the Prout-Tompkins (B1) and the contracting area (R2) models. For each method, the best-fitting model used to evaluate the kinetic parameters has a greater coefficient of determination R^2.

Figure 4.10 and Figure 4.11 show the linear plots of considered models for the two methods at 20 °C/min. Appendix B presents the linear profiles obtained at other heating rates.

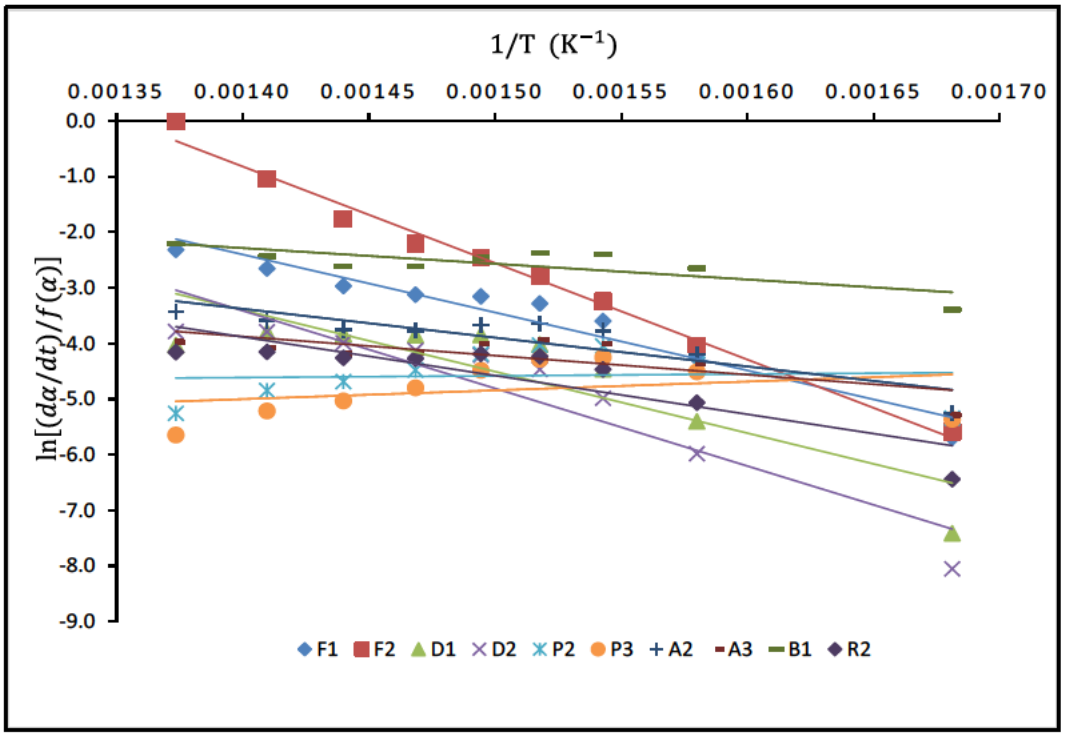

Figure 4.10: Differential method linear plots

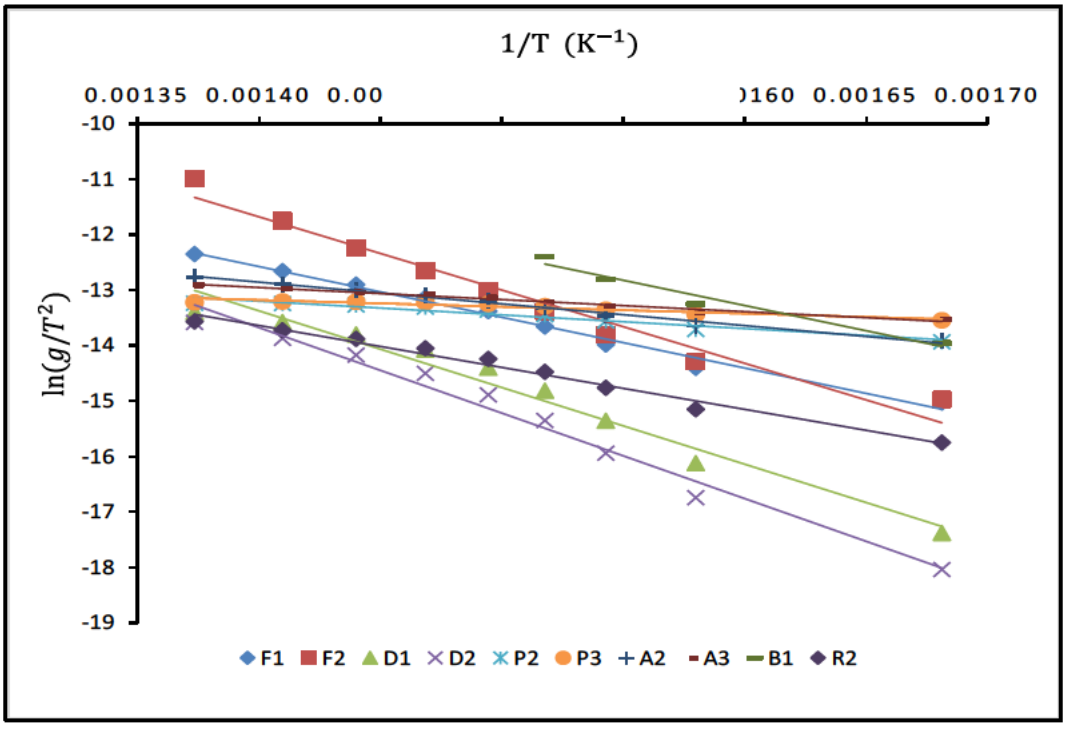

Figure 4.11: Coats-Redfern method linear plots

From Figure 4.10 and Figure 4.11, E_a and k_0 were estimated for each considered model and are presented in Table 4.4.

Among all considered models, the second-order and first diffusion models have been considered the best fitting for the Coats-Redfern (C&R) and differential method (Diff.), respectively.

Using the differential method, E_a was estimated at 144.4 $kJ.mol^{-1}$ While 128.3 $kJ.mol^{-1}$ was found for Coats-Redfern approach. The pre-exponential factor k_0 was 1.6E+10 s^{-1} and 2.8E+03s^{-1}.

A comparison of different activation energies estimated at various heating rates and shown in Table 4.5 reveals an increase in activation energy as the heating rate rises. A similar trend was observed for the pre-exponential factor k_0 that tended to rise with the rise in the heating rate. These results are in good correlation with those reported by Leung and Wang (1998) while conducting a kinetic analysis of WT pyrolysis. Chen et al. (2014) discovered a similar pattern when investigating the effect heating rate on the kinetic parameters and product characteristics of Moso-bamboo slow pyrolysis. When evaluating the influence of demineralisation and heating rate on the pyrolysis kinetics of Jordanian oil shales, Al-Harahsheh et al. (2011) also reported increased values of E_a and k_0 with an increased heating.

Table 4.4: Activation energies and pre-exponential coefficient estimated with the model-fitting methods at 20 °C/min

Method	Models	$-E_a/R$	$\ln k_0$	E_a $(kJ.mol^{-1})$	k_0 (s^{-1})	R^2
C&R	F1	9156.7	0.2453	76.1	1.3E+00	0.99
	F2	13211	6.8196	109.8	9.2E+02	0.97
	D1	13850	6.0184	115.2	4.1E+02	0.97
	D2	15431	7.928	128.3	2.8E+03	0.98
	P2	2476	-9.731	20.6	5.9E-05	0.94
	P3	1212.2	-11.481	10.1	1.0E-05	0.88
	A2	3920.7	-7.3678	32.6	6.3E-04	0.98
	A3	2175.4	-9.9055	18.1	5.0E-05	0.97
	B1	9098	1.2788	75.6	3.6E+00	0.96
	R2	7570.1	-30363	62.9	0.0E+00	0.98
Diff.	F1	10421	12.189	86.6	2.0E+05	0.94
	F2	17364	23.49	144.4	1.6E+10	0.99
	D1	11060	12.081	92.0	1.8E+05	0.75
	D2	13949	16.115	116.0	1.0E+07	0.87
	P2	313	-5.0546	2.6	6.4E-03	0.00
	P3	-1577.5	-7.21	-13.1	7.4E-04	0.08
	A2	5184.9	3.383	43.1	2.9E+01	0.77
	A3	3439.6	0.9398	28.6	2.6E+00	0.57
	B1	2838.4	1.6895	23.6	5.4E+00	0.61
	R2	6949.2	5.8456	57.8	3.5E+02	0.74

Table 4.5: Activation energies obtained at five considered heating rates

Method	β (°C/min)	10	20	30	40	50
C&R	E_a $(kJ.mol^{-1})$	116.9	128.3	134.6	135.2	137.99
	k_0 (s^{-1})	6.5E+02	2.8E+03	5.3E+03	4.4E+03	5.2E+03
Diff.	E_a $(kJ.mol^{-1})$	136.1	144.4	146.9	146.0	148.69
	k_0 (s^{-1})	4.1E+09	1.6E+10	2.4E+10	2.0E+10	2.9E+10

From Table 4.5, the average E_a has been estimated at 144.4 kJ. mol^{-1} and 130.6 kJ. mol^{-1} with the Differential method and the Coats-Redfern method, respectively. The obtained pre-exponential factor is 1.9E+10 s^{-1} and 3.7E+03 s^{-1}, respectively.

4.3.3. Conclusion on kinetics modelling

Table 4.6 summarises different activation energies and pre-exponential factors estimated with the five considered approaches.

Table 4.6: Kinetic parameters obtained with different methods

Methods	E_a (kJ. mol^{-1})	k_0 (s^{-1})
Friedman	122.0	1.9E+08
Kissinger	138.5	3.0E+05
Starink	139.7	1.4E+06
Differential	144.4	1.90E+10
Coats-Redfern	130.6	3.70E+03

It may be observed from Table 4.6 some differences in the activation energy estimated from considered approaches. The differential method provided the highest activation energy with a difference of about five units with the two model-free approaches of Kissinger and Starink. The Friedman's and Coats-Redfern methods present the lower activation energy values with a significant difference of about 22 and 16 with the differential method.

The estimated values of E_a are in the range of 122 and 145 kJ.mol^{-1}. These results for the combined model-free and model-fitting methods agree with those obtained by Menares et al. (2020), who found values of E_a in the range of 101.5±2 and 176.7±2 kJ.mol^{-1} for WT pyrolysis using the combined method. The obtained values of the present study also agree with the observations made by Williams and Besler (1995). The authors proved that the E_a present higher values for the individual component conversion, in the range of 195 to 223 kJ.mol^{-1} at 20 ℃/min than those obtained for waste tyres. Danon et al. (2015) also confirmed this observation when conducting a cumulative model-based and model-free kinetics research on rubber and tyres devolatilisation.

These lower activation energies obtained in this study indicate that the process requires less energy and, therefore, does not necessarily require a catalyst for its completion.

4.4. Py-GC/MS

To match the TGA data and kinetic observations with the potential reaction pathways happening in truck tyre pyrolysis, various Py-GC/MS tests were conducted. As previously stated, the truck tyre is converted by devolatilisation/condensation processes, which are followed by a sequence of reactions resulting in monomeric chemicals (isoprene) formation and their derived products such as limonene and indene. However, WTs pyrolysis is a technique with unique characteristics in terms of products distribution. Some variables, such as the heating rate and, most significantly, the reaction temperature, are critical in determining transport restrictions and reaction kinetics. To improve the selectivity of specific marketable chemicals, a detailed evaluation of WT pyrolysis variables is necessary.

4.4.1. Compounds identification

Appendix Table C.1**:** presents a detailed list of identified chemicals. Gases (alkanes, alkenes, CO_x and H_2), cyclic hydrocarbons (Cyclo-butene, cyclo-propane, limonene, isoprene and indene) and aromatics (xylene, benzene, and styrene) are the most abundant compounds identified. Aromatics are generated after a significant conversion cyclic compounds through aromatisation and hydrogenation, as observed by Ding et al. (2016).

Two intense peaks were identified from all the experiments conducted at different temperatures (400 – 700 ℃). The two peaks correspond to isoprene and limonene. These two chemicals have a cumulative peak-based selectivity of about 40 % below 600 ℃, which declines at temperatures 600 ℃ and above. The significant cumulative selectivity below 600 ℃ indicates that only minor cyclisation and aromatisation reactions occur in condensed molecules, as observed by Menares et al. (2020). The increase in temperature to 500 ℃ and above led the peak-based selectivity of benzene, toluene, xylene, styrene, and indene to increase from about 6 % to 12 % at 700 ℃.

According to the findings, temperature is the most important factor in the pyrolysis of truck tyres. As a result, temperature dictates the kinetics and product distribution.

4.4.2. Temperature influence on chemicals production

As observed in previous research, temperature is a major operating parameter in WT pyrolysis (Ding et al., 2015, Xu et al., 2018, Menares et al., 2020). This research examines two chemicals derived from WTs during Py-GC/MS experiments and involves tests conducted at various temperatures. Figure 4.1212, Figure 4.133, Figure 4.144 and Figure 4.155 depict chromatograms obtained at various considered temperatures.

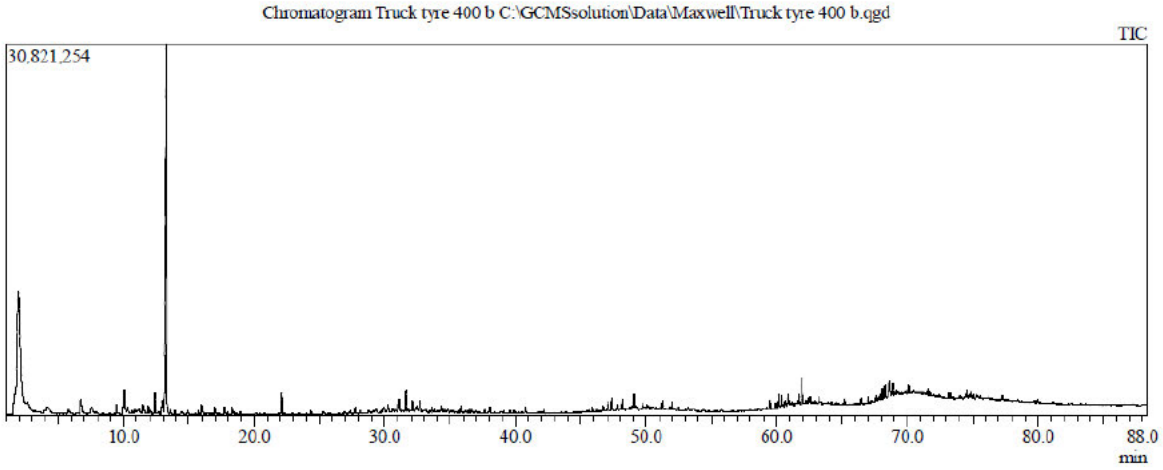

Figure 4.12: Chromatogram for TT obtained at 400 °C

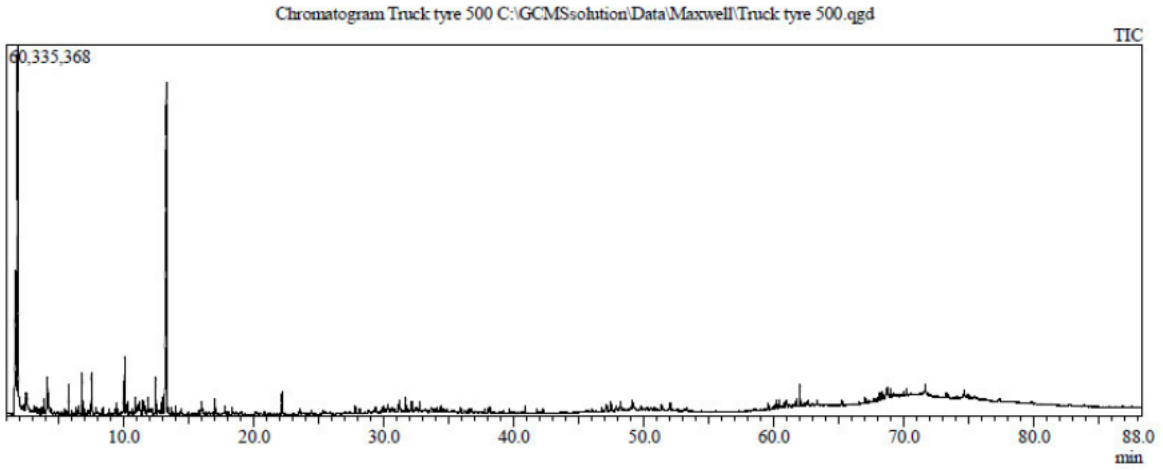

Figure 4.13: Chromatogram for TT obtained at 500 °C

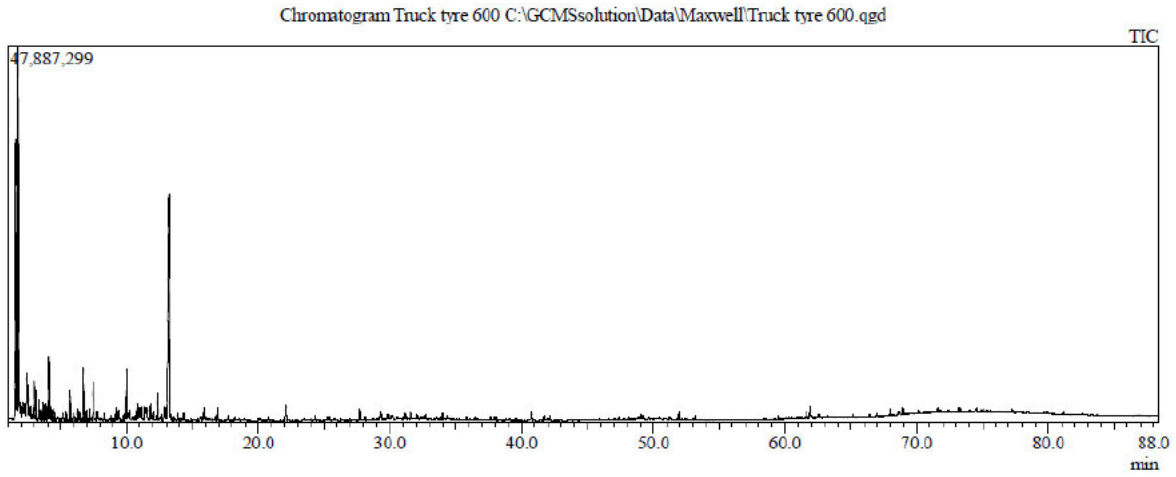

Figure 4.14: Chromatogram for TT obtained at 600 °C

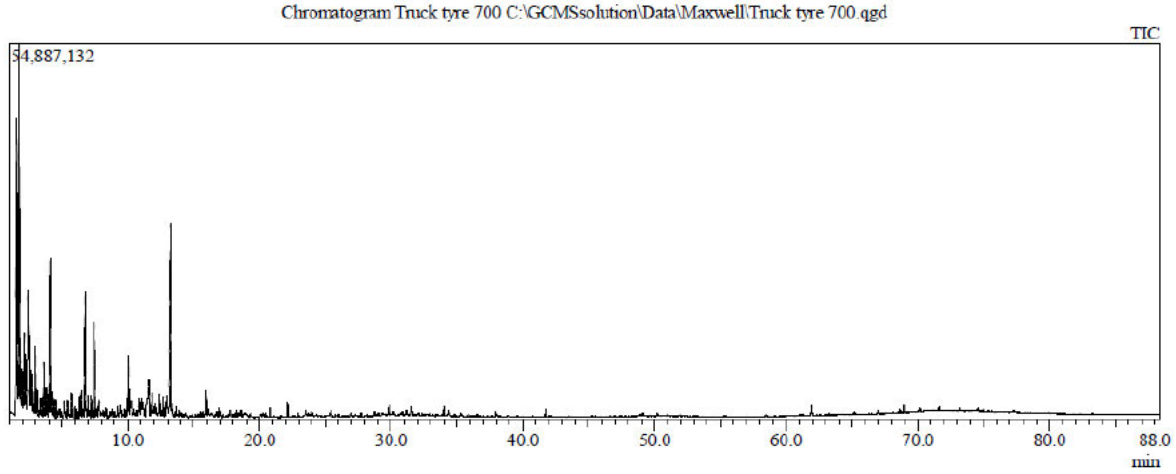

Figure 4.15: Chromatogram for TT obtained at 700 °C

Table 4.7 lists the significant compounds detected from the chromatograms for analysis purposes, and Figure 4.16 presents their respective selectivity calculated based on the total peak areas.

Table 4.7: Selectivity of important compounds

Compounds	Peak areas (%)				Selectivity (%)			
Temp. (°C)	400	500	600	700	400	500	600	700
Isoprene	10.21	16.81	13.52	11.67	27.1	37.6	35.2	36.6
Limonene	24.17	22.28	16.75	9.13	64.2	49.9	43.6	28.6
Styrene	1.17	1.86	1.89	2.97	3.1	4.2	4.9	9.3
Benzene	0.1	0.28	0.49	1.09	0.3	0.6	1.3	3.4
Toluene	0.97	1.35	2.85	3.06	2.6	3.0	7.4	9.6
Xylene	1.03	2.01	2.81	3.97	2.7	4.5	7.3	12.4
Indene		0.08	0.09		0.0	0.2	0.2	0.0
Total	37.65	44.67	38.4	31.89	100	100	100	100

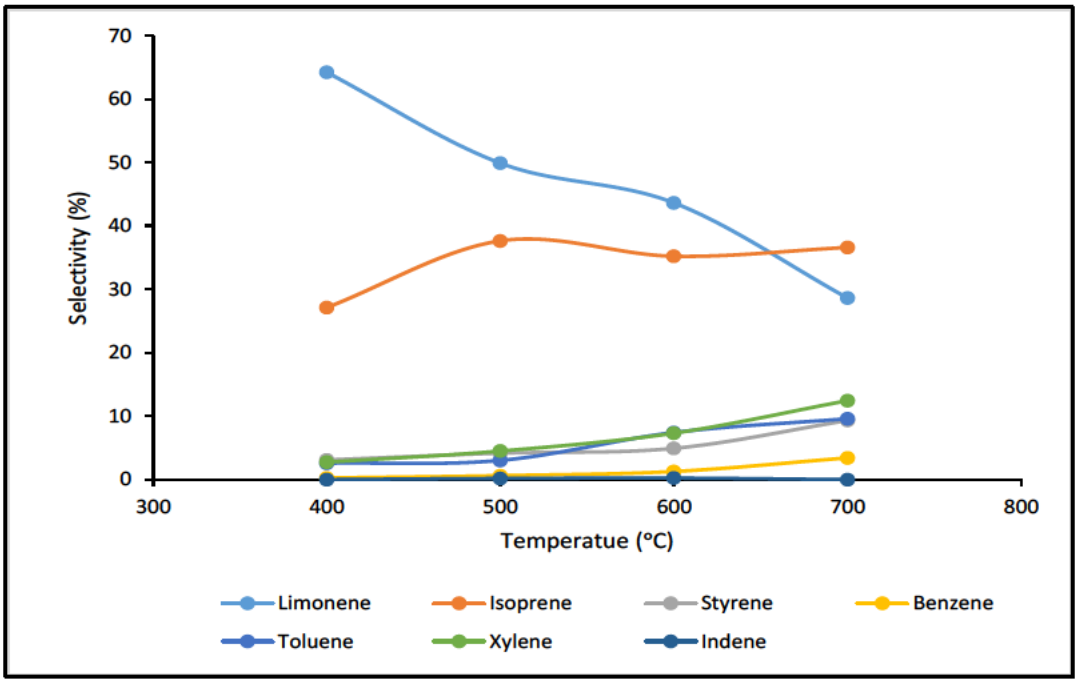

Figure 4.16: Selectivity to important compounds

Figure 4.16 shows the temperature effect on the selectivity of significant chemicals. The selectivity to limonene appeared to continuously decay with the increase in temperature up to a minimum selectivity of 28.5% at 700 °C. In contrast, the selectivity to indene tends to be constant at 500 and 600 °C. The latter has been only detected at temperatures of 500 and 600 °C, and the temperature has no major influence on the productivity of this compound in the considered range of temperatures. These results on indene productivity agree with those obtained by Li et al. (2004), who observed an increase in indene productivity at around 500 before it tends to decrease at higher temperatures. However, the transition of limonene to alkenes under 600 °C and the conversion of a fraction of limonene into monocyclic aromatics such as benzene, toluene and xylene can justify the drop in selectivity to limonene (Menares et al., 2020). Isoprene, one of the significant compounds detected, shows a maximum at around 500 °C. Therefore, 500 °C emerged as optimal temperature.

Several researchers have evidenced that isoprene and limonene are synthesised from natural rubber, via a sequence of β-scission and depropagation processes of NR and intramolecular cyclisation and scission of monomeric isoprene, respectively. Limonene is also synthesised from isoprene at higher temperatures through Diels-Alder reactions (Mkhize et al., 2016, Xu et al., 2018). On another side, Doddipatla et al. (2021) proved that indene is formed via a bimolecular reaction involving the simplest organic radical methylidyne (CH) and styrene ($C_6H_5C_2H_5$) through the hitherto elusive methylidyne addition, cyclisation and aromatisation.

From Table 4.7, the relative formation of limonene to isoprene (ξ_{l-i} or S_l/S_i) and indene to styrene (ξ_{i-s} or S_i/S_s) have been calculated and presented in Figure 4.17. It can be observed that the selectivity ratios of indene to styrene and of limonene to isoprene show a plateau (0.4 – 0.5) and (1.3 – 1.2), respectively, between 500 and 600 °C. This observation suggests that several equilibrated reactions steps could be taking place between styrene and indene, and isoprene and limonene between 400 and 600 °C. Over 600 °C, the selectivity ratio of limonene to isoprene decays up to 0.7 at 700 °C. This could be attributed to cyclisation, hydrogenation and aromatisation reactions, as also reported by Mkhize et al. (2016) and Menares et al. (2020).

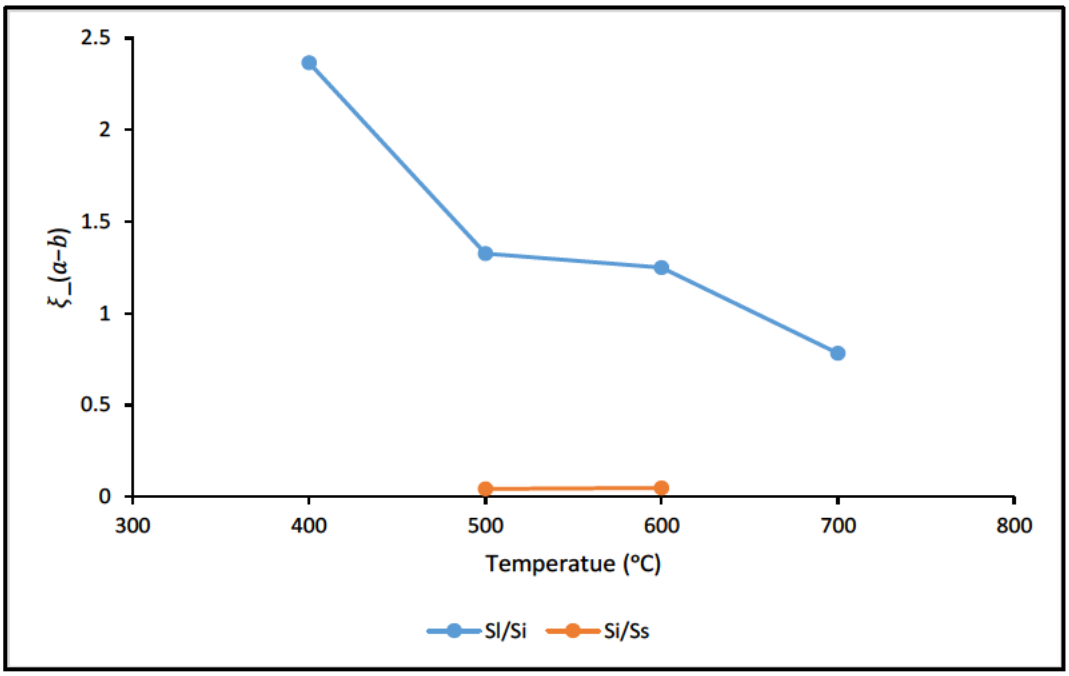

Figure 4.17: Relative formation of important compounds

4.4.3. Effect of heating rate

In a series of Evolved Gas Analysis experiments, the heating rate was varied from 20 to 50 °C/min, and chromatograms are presented in Figure 4.18. All the experiments were conducted at optimal temperature obtained of 500 °C.

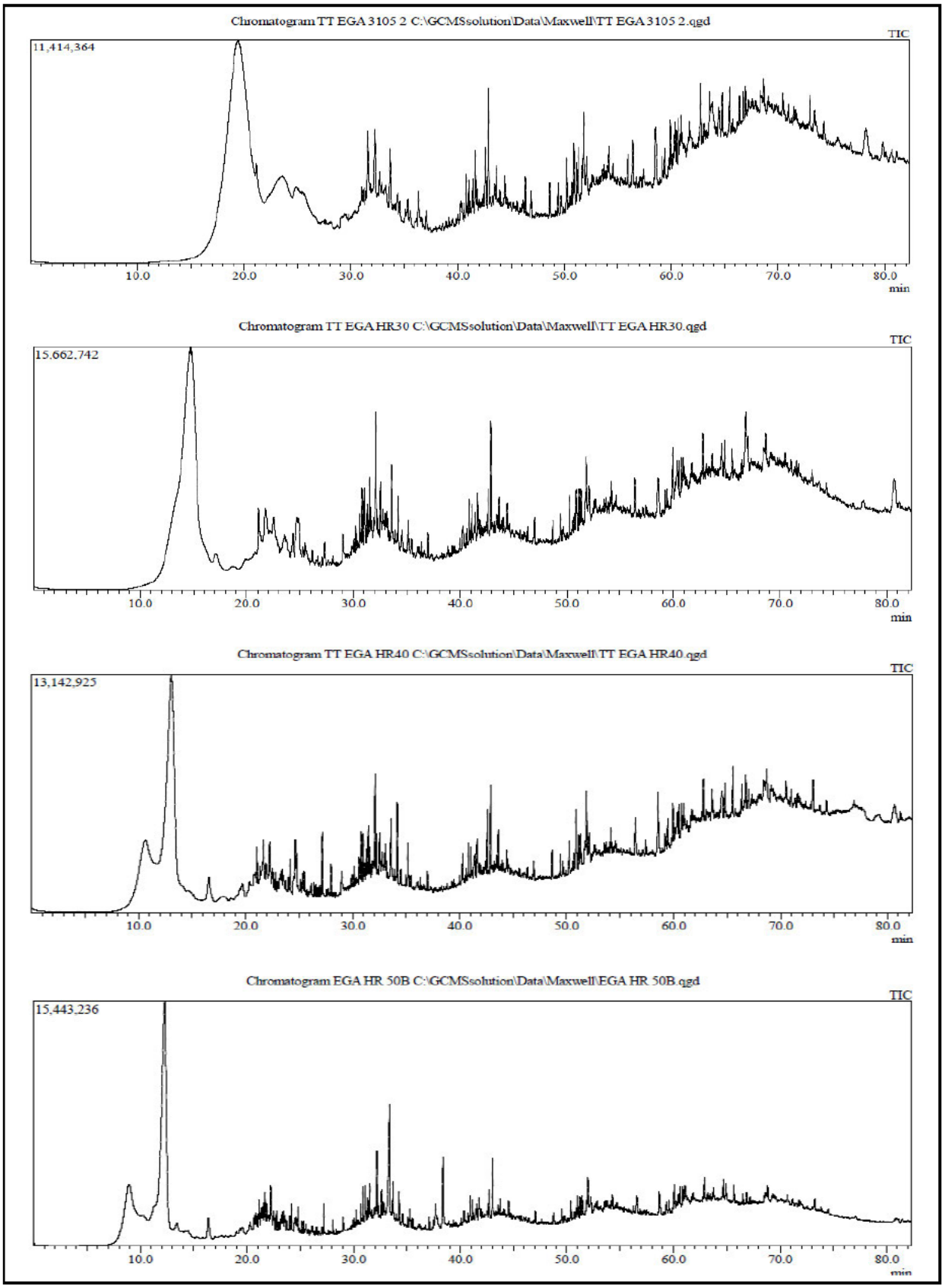

Figure 4.18: EGA chromatograms obtained at 20, 30, 40 and 50 °C /min

The heating rate was found to have an influence on WTs pyrolysis kinetic parameters by increasing the activation energy and pre-exponential coefficient with an increase in the heating rate (Leung and Wang, 1998). Moreover, Mkhize et al. (2019) evidenced the effect of heating rate on isoprene and dl-limonene production. They reported that the reaction progress at peak dl-limonene increased as the heating rate was raised to higher values, up to 100 °C/min. In this study, the heating rate has been increased varied from 20 to 50 °C/min, then 100 °C/min for trend verification and confirmation. Figure 4.19 presents the selectivity to limonene formation at various heating rates.

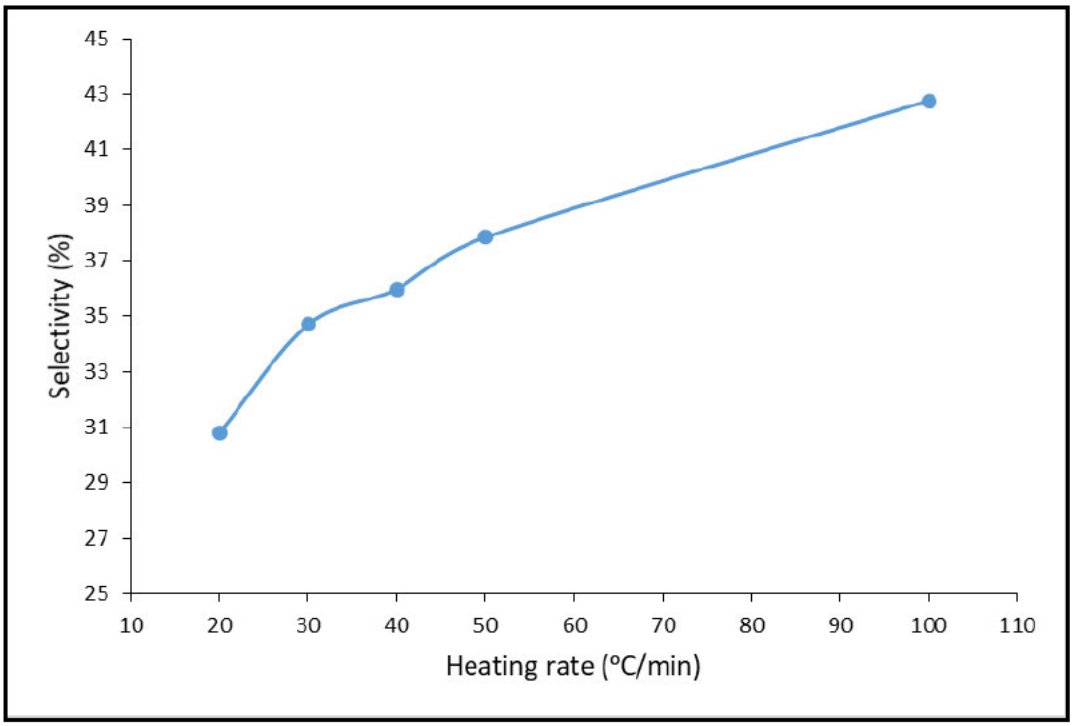

Figure 4.19: Selectivity to limonene formation

Figure 4.19 shows an increase in selectivity to limonene with the rise of heating rate, from around 30.8 % at 20 °C/min to 37.8 % at 50 °C/min. To confirm the observed trend, an experiment at a greater heating rate, i.e., 100 °C/min, has been conducted. Figure 4.19 shows that the selectivity to limonene rises with the rise of heating rate values. Therefore, the heating rate plays a major role in the WTs pyrolysis for valuable products formation. From the above observations, limonene formation is favoured by high heating rates, as stated by Mkhize et al. (2019).

4.4.4. Description of the truck tyre pyrolysis mechanisms

The reaction pathways for WTs are susceptible to the experimental system, including the pyrolysis parameters and the thermal regime. Thus, there is no agreement on a general rule of the WTs pyrolysis mechanisms.

However, from the kinetics and Py-GC/MS observations, and on the basis of recent studies of Mkhize et al. (2016), Menares et al. (2020), Figure 4.20 presents a suggested simplified reaction map. Equilibrated reactions involved in the synthesis of limonene-isoprene and styrene-indene are included in the reaction map, as stated in section 4.4.2 of the present study.

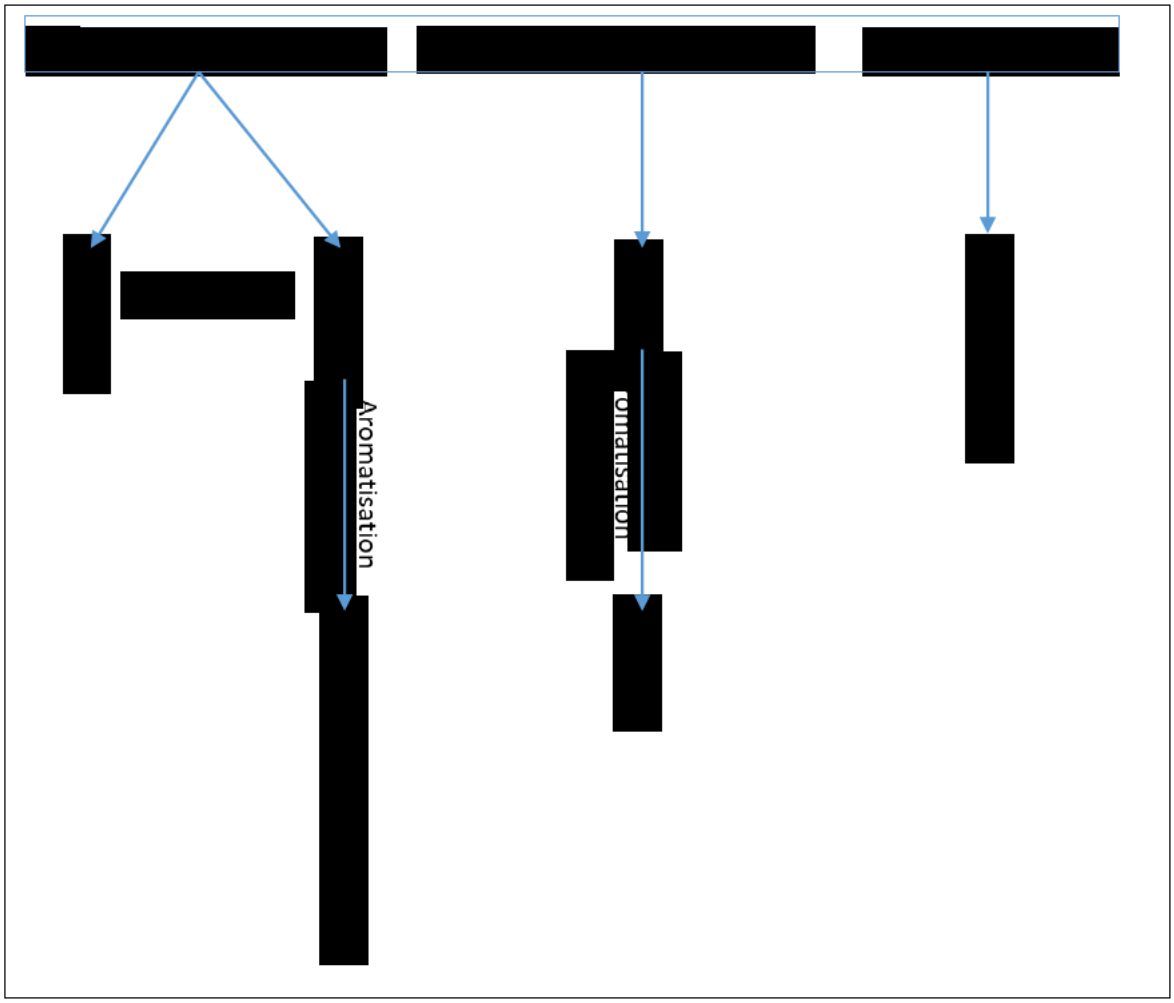

Figure 4.20: Simplified truck tyre reaction map

5. Conclusion and recommendations

Truck tyre crumbs of about 60.8 % volatile matter content were used in the present study on the pyrolysis kinetics and mechanisms for valuable and marketable products formation, such as limonene and indene. The samples were constituted of NR, the principal source of beneficial chemicals but also of BR and SBR as evidenced by the FTIR analysis.

The thermogravimetric analysis conducted at five different heating rates evidenced an average char value of 38.7 wt.% regardless of the heating rate, which matches the aggregate of the fixed carbon and ash content estimated in proximate analysis on the studied samples. The profiles of the DTG curves at various heating rates (10, 20, 30, 40 and 50 °C/min) evidenced the presence of a prominent devolatilisation peak at lower temperature and a tiny peak at elevated temperature. Due to the second orders reactions elimination at elevated heating rates with the promotion of rubber devolatilisation, the small peak or shoulder tends to disappear as the prominent peak becomes higher. The first peak has been associated with the decomposition into polyisoprene with the formation of some alkenes such as limonene in the pyrolysis hot volatiles.

The kinetic study, conducted through combined model-free and model-based methods, considered five different approaches, i.e., three model-free methods (Friedman's, Kissinger and Starink's methods) and two model-based methods (differential and Coats-Redfern methods). From the model-free methods, two major regions (peaks) could be identified from the activation energy vs reaction progress profiles. The first is between 343 °C and 386 °C and associated with the devolatilisation/condensation of NR and SBR with the synthesis of isoprene and limonene from the degradation and intramolecular cyclisation-scission of allylic poly-isoprene radicals. The second region, between 392 and 437 °C, has been associated with the scission and dehydrogenation of SBR, resulting in the synthesis of styrene and butadiene monomers. The model-based methods show that the process reaction can be described by a first diffusion model (D2) or a second-order reaction model (F2). The estimated values of E_a are in the range of 122 and 145 kJ.mol^{-1} as obtained in previous research (Menares et al., 2020).

The Py-GC/MS experiments carried out at several temperatures (400 – 700 °C) in single-shot mode and heating rates (20, 30, 40, 50 and 100 °C/min) in direct EGA mode have led to the identification of multiple compounds during the TT pyrolysis. The most abundant compounds identified are cyclic hydrocarbons (i.e., limonene, isoprene, cyclo-butene), the aromatics (i.e., Xylenem benzene, styrene) from the intensive conversion of cyclic products, and gases (i.e., alkanes, alkenes, CO_x and H_2). Experiments conducted in single-shot have evidenced the presence of two intense peaks corresponding to isoprene and limonene, respectively, with high combined selectivity (over 80 % under 600 °C), showing that cyclisation and aromatisation reactions of

condensed compounds happen to a lesser extent. The selectivity to limonene decreased with the increase in temperature from 64.2 % at 400 °C to 28.6 % at 700 °C, while no significant change in the selectivity to indene could be observed in the considered range of temperature. On the contrary, increasing the heating rate results in the selectivity to limonene increase, as evidenced by experiments conducted in EGA mode. The selectivity to limonene varied from 30.8 % at 20 °C/min to 37.8 % at 50 °C/min and 42.7 % at 100 °C/min, which confirms that high heating rates favour the synthesis of limonene.

Waste tyres pyrolysis reactions pathways are susceptible to the material characteristics and dimensions, the thermal environment and thus, to the experimental system. Therefore, this study should be in future extended to the influence of other parameters such as feedstock characteristics, dwelling time of hot volatiles in the reactor and the influence of catalyst on the pyrolysis mechanisms for marketable products maximisation to further the current contribution to the understanding of TT pyrolysis kinetic and mechanisms.

References

ACEA 2019. The automobile industry Pocket Guide 2019/2020.

ACEVEDO, B. & BARRIOCANAL, C. 2014. Fuel-oils from co-pyrolysis of scrap tyres with coal and a bituminous waste. Influence of oven configuration. *Fuel,* 125**,** 155-163.

ACEVEDO, B. & BARRIOCANAL, C. 2015. The influence of the pyrolysis conditions in a rotary oven on the characteristics of the products. *Fuel processing technology,* 131**,** 109-116.

AL-HARAHSHEH, M., AL-AYED, O., ROBINSON, J., KINGMAN, S., AL-HARAHSHEH, A., TARAWNEH, K., SAEID, A. & BARRANCO, R. 2011. Effect of demineralization and heating rate on the pyrolysis kinetics of Jordanian oil shales. *Fuel Processing Technology,* 92**,** 1805-1811.

AL-SALEM, S., LETTIERI, P. & BAEYENS, J. 2009. Kinetics and product distribution of end of life tyres (ELTs) pyrolysis: A novel approach in polyisoprene and SBR thermal cracking. *Journal of hazardous materials,* 172**,** 1690-1694.

ALVAREZ, J., LOPEZ, G., AMUTIO, M., MKHIZE, N., DANON, B., VAN DER GRYP, P., GÖRGENS, J., BILBAO, J. & OLAZAR, M. 2017. Evaluation of the properties of tyre pyrolysis oils obtained in a conical spouted bed reactor. *Energy,* 128**,** 463-474.

ANTONIOU, N. & ZABANIOTOU, A. 2013. Features of an efficient and environmentally attractive used tyres pyrolysis with energy and material recovery. *Renewable and Sustainable Energy Reviews,* 20**,** 539-558.

ARABIOURRUTIA, M., LOPEZ, G., ELORDI, G., OLAZAR, M., AGUADO, R. & BILBAO, J. 2007. Product distribution obtained in the pyrolysis of tyres in a conical spouted bed reactor. *Chemical Engineering Science,* 62**,** 5271-5275.

ASLAN, D. I., PARTHASARATHY, P., GOLDFARB, J. L. & CEYLAN, S. 2017. Pyrolysis reaction models of waste tires: Application of Master-Plots method for energy conversion via devolatilization. *Waste Management,* 68**,** 405-411.

AYLÓN, E., CALLÉN, M., LÓPEZ, J., MASTRAL, A. M., MURILLO, R., NAVARRO, M. & STELMACH, S. 2005. Assessment of tire devolatilization kinetics. *Journal of analytical and applied pyrolysis,* 74**,** 259-264.

BAJUS, M. & OLAHOVÁ, N. 2011. THERMAL CONVERSION OF SCRAP TYRES. *Petroleum & Coal,* 53.

BANAR, M., AKYıLDıZ, V., ÖZKAN, A., ÇOKAYGIL, Z. & ONAY, Ö. 2012. Characterization of pyrolytic oil obtained from pyrolysis of TDF (Tire Derived Fuel). *Energy Conversion and Management,* 62**,** 22-30.

BETANCUR, M., MARTÍNEZ, J. D. & MURILLO, R. 2009. Production of activated carbon by waste tire thermochemical degradation with CO2. *Journal of Hazardous Materials,* 168**,** 882-887.

CARRASCO, F. 1993. The evaluation of kinetic parameters from thermogravimetric data: comparison between established methods and the general analytical equation. *Thermochimica Acta,* 213**,** 115-134.

CHEN, D., ZHOU, J. & ZHANG, Q. 2014. Effects of heating rate on slow pyrolysis behavior, kinetic parameters and products properties of moso bamboo. *Bioresource Technology,* 169**,** 313-319.

CHEN, J., CHEN, K. & TONG, L. 2001. On the pyrolysis kinetics of scrap automotive tires. *Journal of hazardous materials,* 84**,** 43-55.

CHEUNG, K.-Y., LEE, K.-L., LAM, K.-L., LEE, C.-W. & HUI, C.-W. 2011. Integrated kinetics and heat flow modelling to optimise waste tyre pyrolysis at different heating rates. *Fuel processing technology,* 92**,** 856-863.

CHOI, G.-G., OH, S.-J. & KIM, J.-S. 2016. Non-catalytic pyrolysis of scrap tires using a newly developed two-stage pyrolyzer for the production of a pyrolysis oil with a low sulfur content. *Applied Energy,* 170**,** 140-147.

COATS, A. & REDFERN, J.-P. 1965. Kinetic parameters from thermogravimetric data. II. *Journal of Polymer Science Part B: Polymer Letters,* 3**,** 917-920.

CONESA, J., FONT, R. & MARCILLA, A. 1997. Mass spectrometry validation of a kinetic model for the thermal decomposition of tyre wastes. *Journal of analytical and applied pyrolysis,* 43**,** 83-96.

CONESA, J. A., MARTIN-GULLON, I., FONT, R. & JAUHIAINEN, J. 2004. Complete study of the pyrolysis and gasification of scrap tires in a pilot plant reactor. *Environmental science & technology,* 38**,** 3189-3194.

CRIADO, J., MALEK, J. & ORTEGA, A. 1989. Applicability of the master plots in kinetic analysis of non-isothermal data. *Thermochimica Acta,* 147**,** 377-385.

CUNLIFFE, A. M. & WILLIAMS, P. T. 1998. Composition of oils derived from the batch pyrolysis of tyres. *Journal of Analytical and applied Pyrolysis,* 44**,** 131-152.

DAI, X., YIN, X., WU, C., ZHANG, W. & CHEN, Y. 2001. Pyrolysis of waste tires in a circulating fluidized-bed reactor. *Energy,* 26**,** 385-399.

DANON, B. & GÖRGENS, J. 2015. Determining rubber composition of waste tyres using devolatilisation kinetics. *Thermochimica Acta,* 621**,** 56-60.

DANON, B., MKHIZE, N., VAN DER GRYP, P. & GÖRGENS, J. 2015. Combined model-free and model-based devolatilisation kinetics of tyre rubbers. *Thermochimica Acta,* 601**,** 45-53.

DING, K., ZHONG, Z., ZHANG, B., SONG, Z. & QIAN, X. 2015. Pyrolysis characteristics of waste tire in an analytical pyrolyzer coupled with gas chromatography/mass spectrometry. *Energy & Fuels,* 29**,** 3181-3187.

DING, K., ZHONG, Z., ZHANG, B., WANG, J., MIN, A. & RUAN, R. 2016. Catalytic pyrolysis of waste tire to produce valuable aromatic hydrocarbons: an analytical Py-GC/MS study. *Journal of Analytical and Applied Pyrolysis,* 122**,** 55-63.

DODDIPATLA, S., GALIMOVA, G. R., WEI, H., THOMAS, A. M., HE, C., YANG, Z., MOROZOV, A. N., SHINGLEDECKER, C. N., MEBEL, A. M. & KAISER, R. I. 2021. Low-temperature gas-phase formation of indene in the interstellar medium. *Science advances,* 7**,** eabd4044.

FLYNN, J. H. 1997. The 'temperature integral'—its use and abuse. *Thermochimica Acta,* 300**,** 83-92.

FLYNN, J. H. & WALL, L. A. 1966. General treatment of the thermogravimetry of polymers. *Journal of Research of the National Bureau of Standards. Section A, Physics and Chemistry,* 70**,** 487.

FRIEDMAN, H. L. Kinetics of thermal degradation of char-forming plastics from thermogravimetry. Application to a phenolic plastic. Journal of polymer science part C: polymer symposia, 1964. Wiley Online Library, 183-195.

GAUTHIER-MARADEI, P., VALDERRAMA, Y. C. & NABARLATZ, D. 2019. Mathematical model of scrap tire rubber pyrolysis in a non-isothermal fixed bed reactor: Definition of a chemical mechanism and determination of kinetic parameters. *Waste and Biomass Valorization,* 10**,** 561-573.

GONZÁLEZ, J. F., ENCINAR, J. M., CANITO, J. L. & RODRíGUEZ, J. J. 2001. Pyrolysis of automobile tyre waste. Influence of operating variables and kinetics study. *Journal of Analytical and Applied Pyrolysis,* 58**,** 667-683.

GOTOR, F. J., CRIADO, J. M., MALEK, J. & KOGA, N. 2000. Kinetic analysis of solid-state reactions: the universality of master plots for analyzing isothermal and nonisothermal experiments. *The journal of physical chemistry A,* 104**,** 10777-10782.

HAN, J., LI, W., LIU, D., QIN, L., CHEN, W. & XING, F. 2018. Pyrolysis characteristic and mechanism of waste tyre: A thermogravimetry-mass spectrometry analysis. *Journal of Analytical and Applied Pyrolysis,* 129**,** 1-5.

HAN, J., YAO, X., ZHAN, Y., OH, S.-Y., KIM, L.-H. & KIM, H.-J. 2017. A method for estimating higher heating value of biomass-plastic fuel. *Journal of the Energy Institute,* 90**,** 331-335.

HAYDARY, J., JELEMENSKÝ, Ľ., GAŠPAROVIČ, L. & MARKOŠ, J. 2012. Influence of particle size and kinetic parameters on tire pyrolysis. *Journal of Analytical and Applied Pyrolysis,* 97**,** 73-79.

HITA, I., ARABIOURRUTIA, M., OLAZAR, M., BILBAO, J., ARANDES, J. M. & CASTAÑO, P. 2016. Opportunities and barriers for producing high quality fuels from the pyrolysis of scrap tires. *Renewable and Sustainable Energy Reviews,* 56**,** 745-759.

ISAYEV, A. I. 2005. Recycling of rubbers. *Science and technology of rubber.* Elsevier.

ISHOLA FELIX, A., AJAYI OLUSEYI, O., OYAWALE, F. & AKINLABI, S. A. Sustainable End-of-Life Tyre (EOLT) Management for Developing Countries–A Review. Proceedings of the International Conference on Industrial Engineering and Operations Management, Pretoria/Johannesburg, South Africa, 2018.

ISLAM, M. R., JOARDDER, M. U. H., KADER, M. & SARKER, M. 2011. Valorization of solid tire wastes available in Bangladesh by thermal treatment.

IWARERE, S. A. & MKHIZE, N. M. 2019. PYROLYSIS OF VARIOUS TYRE TYPES: CHARACTERISTICS AND KINETIC STUDIES USING THERMOGRAVIMETRIC ANALYSIS. *Detritus***,** 0.

KHAN, A., AKHTAR, J., SHAHZAD, K., SHEIKH, N. & MUNIR, S. 2017. Co-pyrolysis and hyrdogenation of waste tires and thar coal blends. *Energy Sources, Part A: Recovery, Utilization, and Environmental Effects,* 39**,** 1664-1670.

KHAWAM, A. & FLANAGAN, D. R. 2005. Complementary use of model-free and modelistic methods in the analysis of solid-state kinetics. *The Journal of Physical Chemistry B,* 109**,** 10073-10080.

KHAWAM, A. & FLANAGAN, D. R. 2006a. Basics and applications of solid-state kinetics: a pharmaceutical perspective. *Journal of pharmaceutical sciences,* 95**,** 472-498.

KHAWAM, A. & FLANAGAN, D. R. 2006b. Solid-state kinetic models: basics and mathematical fundamentals. *The journal of physical chemistry B,* 110**,** 17315-17328.

KHIARI, B., KORDOGHLI, S., MIHOUBI, D., ZAGROUBA, F. & TAZEROUT, M. 2018. Modeling kinetics and transport phenomena during multi-stage tire wastes pyrolysis using Comsol®. *Waste Management,* 78**,** 337-345.

KISSINGER, H. E. 1957. Reaction kinetics in differential thermal analysis. *Analytical chemistry,* 29**,** 1702-1706.

LANTEIGNE, J.-R., LAVIOLETTE, J.-P., TREMBLAY, G. & CHAOUKI, J. 2013. Predictive kinetics model for an industrial waste tire pyrolysis process. *Energy & fuels,* 27**,** 1040-1049.

LARESGOITI, M., CABALLERO, B., DE MARCO, I., TORRES, A., CABRERO, M. & CHOMÓN, M. 2004. Characterization of the liquid products obtained in tyre pyrolysis. *Journal of Analytical and Applied Pyrolysis,* 71**,** 917-934.

LARESGOITI, M. F., DE MARCO, I., TORRES, A., CABALLERO, B., CABRERO, M. A. & CHOMÓN, M. J. 2000. Chromatographic analysis of the gases obtained in tyre pyrolysis. *Journal of Analytical and Applied Pyrolysis,* 55**,** 43-54.

LEUNG, D. & WANG, C. 1998. Kinetic study of scrap tyre pyrolysis and combustion. *Journal of Analytical and Applied Pyrolysis,* 45**,** 153-169.

LI, S.-Q., YAO, Q., CHI, Y., YAN, J.-H. & CEN, K.-F. 2004. Pilot-scale pyrolysis of scrap tires in a continuous rotary kiln reactor. *Industrial & engineering chemistry research,* 43**,** 5133-5145.

LOPEZ, F. A., EL HADAD, A. A., ALGUACIL, F. J., CENTENO, T. A. & LOBATO, B. 2013. Kinetics of the thermal degradation of granulated scrap tyres: a model-free analysis. *Materials Science,* 19**,** 403-408.

LOPEZ, G., AMUTIO, M., ELORDI, G., ARTETXE, M., ALTZIBAR, H. & OLAZAR, M. 2010. A conical spouted bed reactor for the valorisation of waste tires.

MARTÍNEZ, J. D., PUY, N., MURILLO, R., GARCÍA, T., NAVARRO, M. V. & MASTRAL, A. M. 2013. Waste tyre pyrolysis–A review. *Renewable and Sustainable Energy Reviews,* 23**,** 179-213.

MCCULLOUGH, D. P., VAN EYK, P. J., ASHMAN, P. J. & MULLINGER, P. J. 2015. Impact of sodium and sulfur species on agglomeration and defluidization during spouted bed gasification of south Australian lignite. *Energy & Fuels,* 29**,** 3922-3932.

MENARES, T., HERRERA, J., ROMERO, R., OSORIO, P. & ARTEAGA-PÉREZ, L. E. 2020. Waste tires pyrolysis kinetics and reaction mechanisms explained by TGA and Py-GC/MS under kinetically-controlled regime. *Waste Management,* 102**,** 21-29.

MIRANDA, M., PINTO, F., GULYURTLU, I. & CABRITA, I. 2013. Pyrolysis of rubber tyre wastes: A kinetic study. *Fuel,* 103**,** 542-552.

MKHIZE, N., DANON, B., VAN DER GRYP, P. & GÖRGENS, J. 2019. Kinetic study of the effect of the heating rate on the waste tyre pyrolysis to maximise limonene production. *Chemical Engineering Research and Design,* 152**,** 363-371.

MKHIZE, N., VAN DER GRYP, P., DANON, B. & GÖRGENS, J. 2016. Effect of temperature and heating rate on limonene production from waste tyre pyrolysis. *Journal of analytical and applied pyrolysis,* 120**,** 314-320.

MKHIZE, N. M. 2018. *Pyrolysis process optimisation to maximise limonene production from waste tyres.* Stellenbosch: Stellenbosch University.

NGXANGXA, S. 2016. *Development of GC-MS methods for the analysis of tyre pyrolysis oils.* Stellenbosch: Stellenbosch University.

NKOSI, N. & MUZENDA, E. 2014. A review and discussion of waste tyre pyrolysis and derived products.

NUNES, A. T., SANTOS, R. E. D., PEREIRA, J. S., BARBOSA, R. & AMBRÓSIO, J. D. 2018. Characterization of waste tire rubber devulcanized in twin-screw extruder with thermoplastics. *Progress in Rubber, Plastics and Recycling Technology,* 34**,** 143-157.

ORTEGA, A. 2002. The kinetics of solid-state reactions toward consensus, Part 2: Fitting kinetics data in dynamic conventional thermal analysis. *International Journal of Chemical Kinetics,* 34**,** 193-208.

PARTHASARATHY, P., CHOI, H. S., PARK, H. C., HWANG, J. G., YOO, H. S., LEE, B.-K. & UPADHYAY, M. 2016. Influence of process conditions on product yield of waste tyre pyrolysis-A review. *Korean Journal of Chemical Engineering,* 33**,** 2268-2286.

PEREZ-MAQUEDA, L., CRIADO, J. & SANCHEZ-JIMENEZ, P. 2006. Combined kinetic analysis of solid-state reactions: a powerful tool for the simultaneous determination of kinetic parameters and the kinetic model without previous assumptions on the reaction mechanism. *The Journal of Physical Chemistry A,* 110**,** 12456-12462.

QUEK, A. & BALASUBRAMANIAN, R. 2009. An algorithm for the kinetics of tire pyrolysis under different heating rates. *Journal of hazardous materials,* 166**,** 126-132.

QUEK, A. & BALASUBRAMANIAN, R. 2012. Mathematical modeling of rubber tire pyrolysis. *Journal of Analytical and Applied Pyrolysis,* 95**,** 1-13.

QUEK, A. & BALASUBRAMANIAN, R. 2013. Liquefaction of waste tires by pyrolysis for oil and chemicals—a review. *Journal of Analytical and Applied Pyrolysis,* 101**,** 1-16.

RAMIREZ-CANON, A., MUÑOZ-CAMELO, Y. F. & SINGH, P. 2018. Decomposition of used Tyre Rubber by pyrolysis: enhancement of the physical properties of the liquid fraction using a hydrogen stream. *Environments,* 5**,** 72.

ROFIQUL, I. M., HANIU, H. & RAFIQUL, A. B. M. 2007. Limonene-rich liquids from pyrolysis of heavy automotive tire wastes. *Journal of Environment and Engineering,* 2**,** 681-695.

ROWHANI, A. & RAINEY, T. J. 2016. Scrap tyre management pathways and their use as a fuel—a review. *Energies,* 9**,** 888.

ROY, C., DARMSTADT, H., BENALLAL, B. & AMEN-CHEN, C. 1997. Characterization of naphtha and carbon black obtained by vacuum pyrolysis of polyisoprene rubber. *Fuel processing technology,* 50**,** 87-103.

ROY, C. & UNSWORTH, J. 1989. Pilot plant demonstration of used tyres vacuum pyrolysis. *Pyrolysis and gasification***,** 180-189.

SEIDELT, S., MÜLLER-HAGEDORN, M. & BOCKHORN, H. 2006. Description of tire pyrolysis by thermal degradation behaviour of main components. *Journal of Analytical and Applied Pyrolysis,* 75**,** 11-18.

ŠESTÁK, J. & BERGGREN, G. 1971. Study of the kinetics of the mechanism of solid-state reactions at increasing temperatures. *Thermochimica Acta,* 3**,** 1-12.

SINGH, J. 2015. A review paper on pyrolysis process of waste tyre. *International journal of applied research,* 1**,** 258-262.

SINGH, R. K., RUJ, B., JANA, A., MONDAL, S., JANA, B., SADHUKHAN, A. K. & GUPTA, P. 2018. Pyrolysis of three different categories of automotive tyre wastes: Product yield analysis and characterization. *Journal of Analytical and Applied Pyrolysis,* 135**,** 379-389.

SONG, Z., YANG, Y., ZHAO, X., SUN, J., WANG, W., MAO, Y. & MA, C. 2017. Microwave pyrolysis of tire powders: evolution of yields and composition of products. *Journal of Analytical and Applied Pyrolysis,* 123**,** 152-159.

STARINK, M. 1996. A new method for the derivation of activation energies from experiments performed at constant heating rate. *Thermochimica Acta,* 288**,** 97-104.

STARINK, M. 2003. The determination of activation energy from linear heating rate experiments: a comparison of the accuracy of isoconversion methods. *Thermochimica Acta,* 404**,** 163-176.

UZUN, B. B. & YAMAN, E. 2014. Thermogravimetric characteristics and kinetics of scrap tyre and Juglans regia shell co-pyrolysis. *Waste Management & Research,* 32**,** 961-970.

VENKATESH, M., RAVI, P. & TEWARI, S. P. 2013. Isoconversional kinetic analysis of decomposition of nitroimidazoles: Friedman method vs Flynn–Wall–Ozawa method. *The Journal of Physical Chemistry A,* 117**,** 10162-10169.

VIGLASKY, J., KLUKAN, J. & JEZO, M. 2017. SCRAP TYRES AND EXPLOITATION OPTIONS FOR TYRE RUBBER MIX.

VYAZOVKIN, S. & SBIRRAZZUOLI, N. 2006. Isoconversional kinetic analysis of thermally stimulated processes in polymers. *Macromolecular Rapid Communications,* 27**,** 1515-1532.

VYAZOVKIN, S. & WIGHT, C. A. 1999. Model-free and model-fitting approaches to kinetic analysis of isothermal and nonisothermal data. *Thermochimica acta,* 340**,** 53-68.

WHITE, J. E., CATALLO, W. J. & LEGENDRE, B. L. 2011. Biomass pyrolysis kinetics: a comparative critical review with relevant agricultural residue case studies. *Journal of analytical and applied pyrolysis,* 91**,** 1-33.

WILLIAMS, P. T. 2013. Pyrolysis of waste tyres: a review. *Waste management,* 33**,** 1714-1728.

WILLIAMS, P. T. & BESLER, S. 1995. Pyrolysis-thermogravimetric analysis of tyres and tyre components. *Fuel,* 74**,** 1277-1283.

XU, F., WANG, B., YANG, D., MING, X., JIANG, Y., HAO, J., QIAO, Y. & TIAN, Y. 2018. TG-FTIR and Py-GC/MS study on pyrolysis mechanism and products distribution of waste bicycle tire. *Energy Conversion and Management,* 175**,** 288-297.

ZABANIOTOU, A. A. & STAVROPOULOS, G. 2003. Pyrolysis of used automobile tires and residual char utilization. *Journal of Analytical and Applied Pyrolysis,* 70**,** 711-722.

ZHANG, X., WANG, T., MA, L. & CHANG, J. 2008. Vacuum pyrolysis of waste tires with basic additives. *Waste Management,* 28**,** 2301-2310.

Appendix

A. Proximate analysis

✓ Moisture content

The following equation determined the high volatile matter content:

$$V = \frac{W - R}{W} \times 100$$

Where:

V = Moisture content or high volatile matter content (%),

W = original specimen mass (mg), and

R = mass measured at temperature x (mg).

W = 15.55 mg, R = 15.02 mg, T_x = 110 ℃ and V = 3.4 %

✓ Volatile matter

The volatile matter or medium volatile mater content was determined using the following equation:

$$O = \frac{R - S}{W} \times 100$$

Where:

O = volatile matter content (%),

R = mass measured at temperature x (mg),

S = mass measured at temperature y (mg), and

W = original specimen mass (mg).

R = 15.02 mg, S = 5.57 mg, W= 15.55 mg, T_y = 560 ℃ and O = 60.8 %

✓ Fixed carbon or combustible material content

The following equation served to estimate the fixed carbon:

$$C = \frac{S - T}{W} \times 100$$

Where:

C = Carbon content (%),

S = mass measured at temperature y (mg),

T = mass measured at temperature z (mg), and

W = original specimen mass (mg).

S = 5.57 mg, T = 0.83 mg, W= 15.55 mg, T_z = 772℃, and C= 30.4 %

✓ Ash content

The ash content was determined using the below equation:

$$A = \frac{T}{W} \times 100$$

Where:

A = Ash content (%)

T = mass measured at temperature z (mg), and

W = original specimen mass (mg).

T = 0.83 mg, W = 15.55 mg, and A = 5.3 %

B. Model-based methods Kinetic analysis

B.1. Differential method profiles

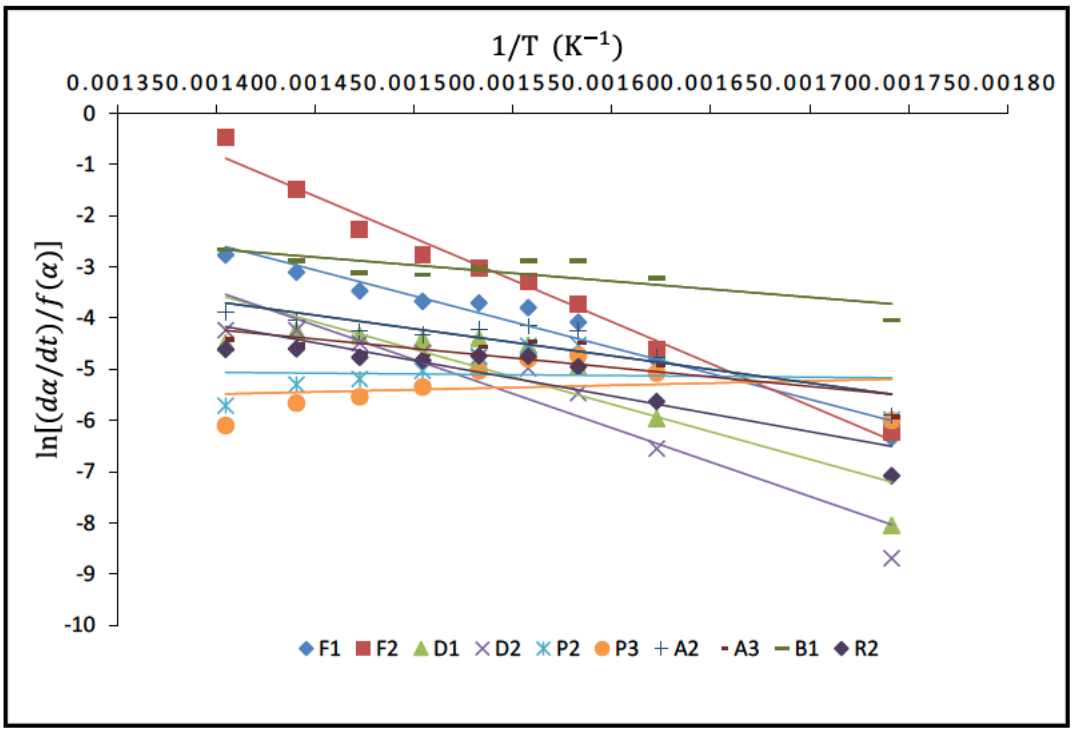

Figure B.1: Differential method linear plots at β=10 °C/min

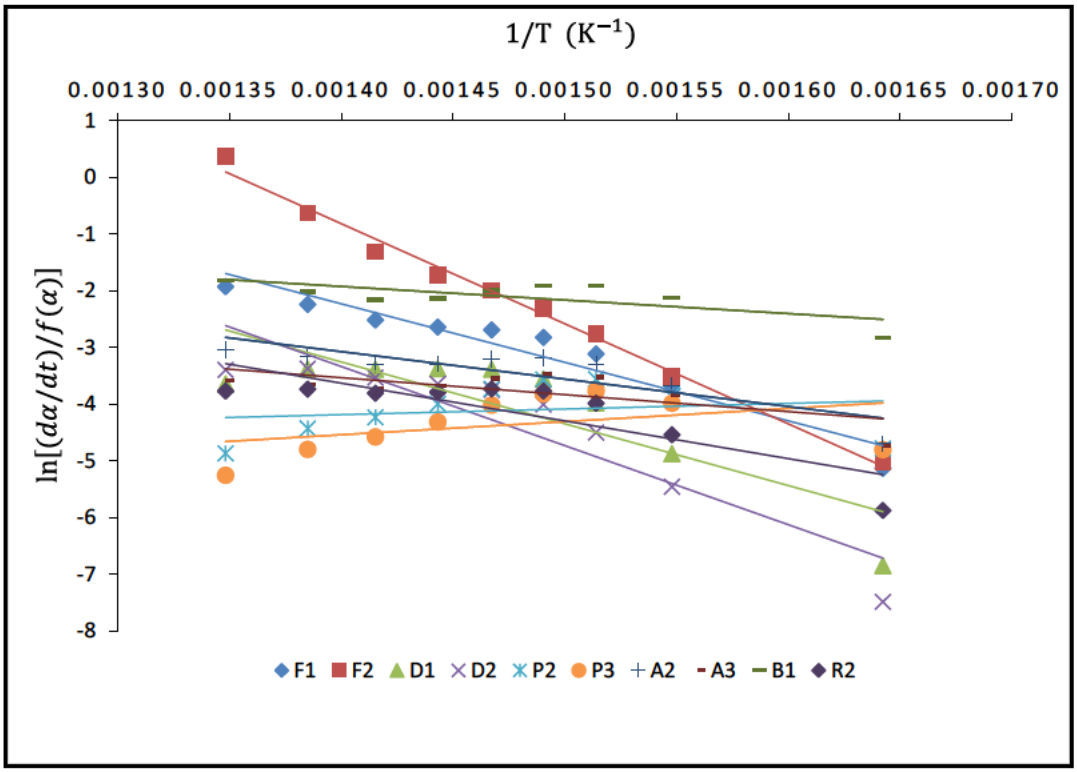

Figure B.2: Differential method linear plots at β=30 °C/min

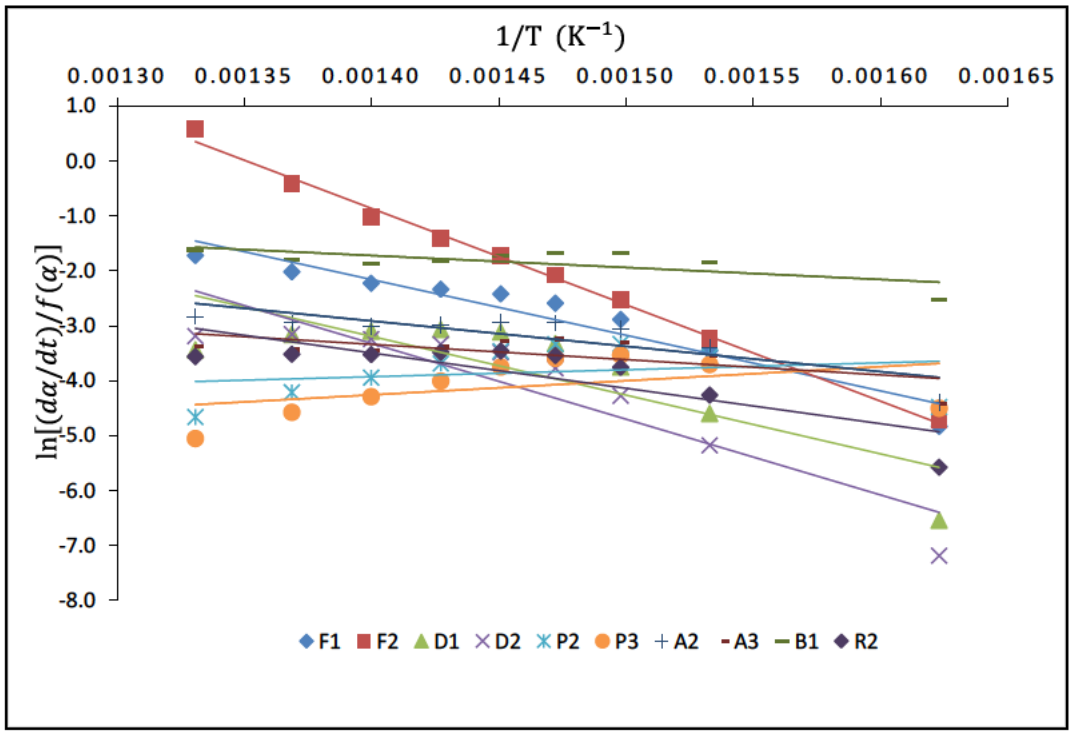

Figure B.3: Differential method linear plots at β=40 °C/min

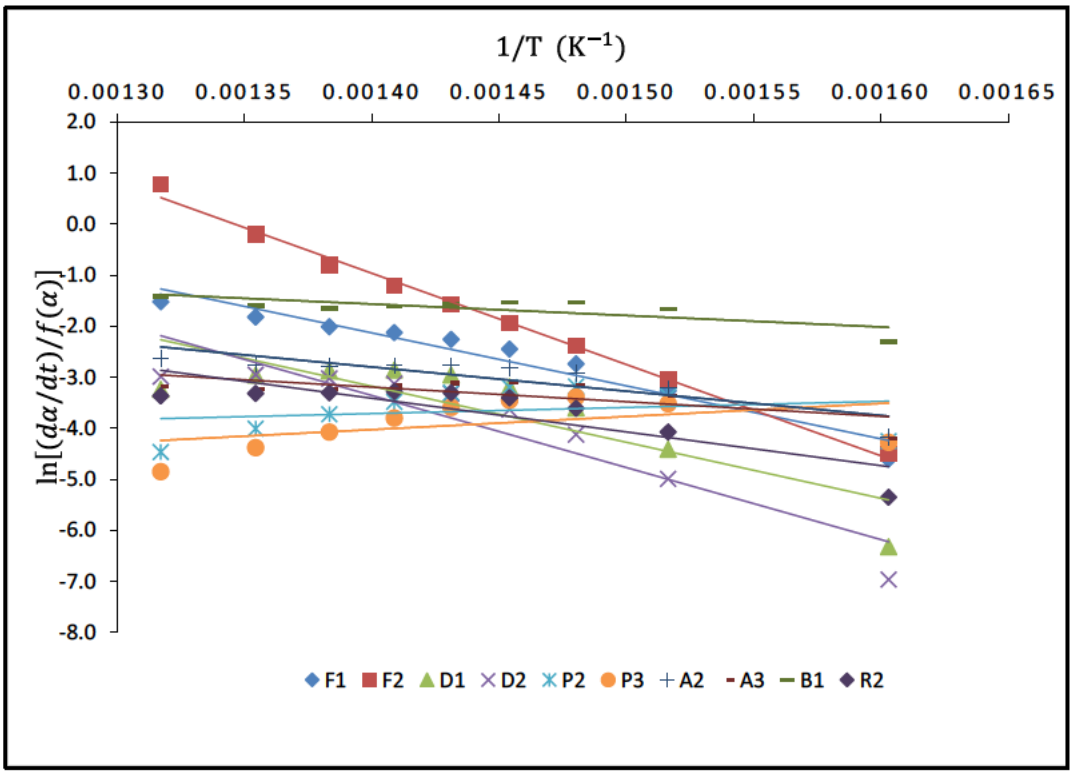

Figure B.4: Differential method linear plots at β=50 °C/min

B.2. Coats-Redfern method

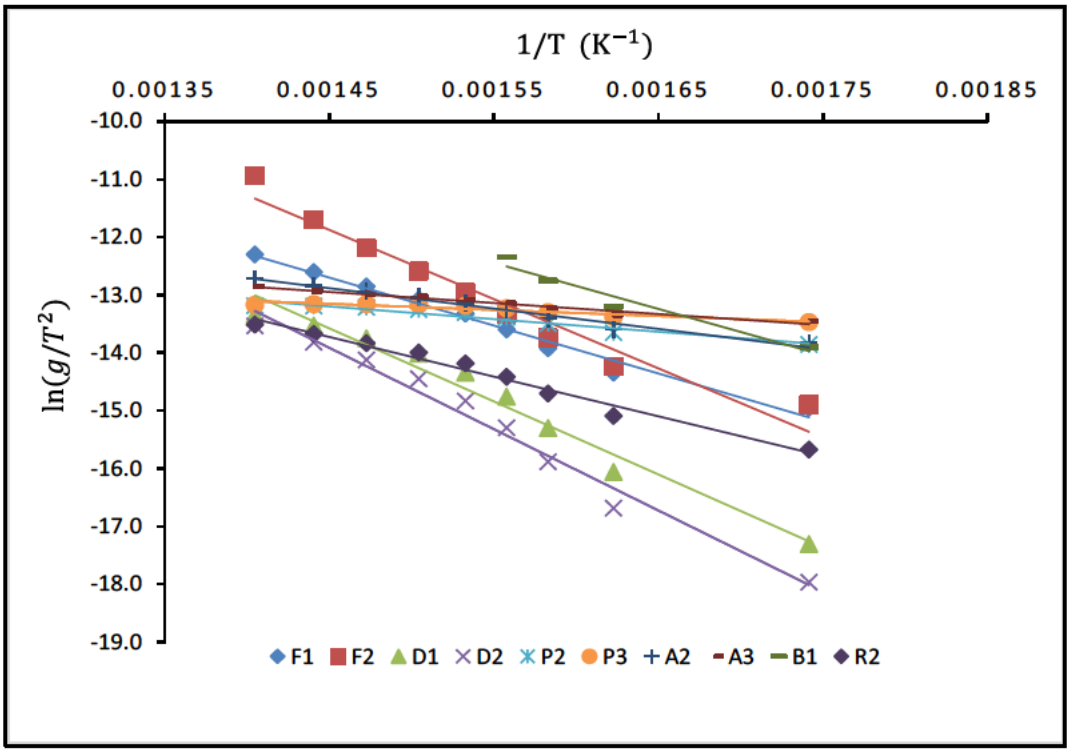

Figure B.5: Coats-Redfern method linear plots at β=10 °C/min

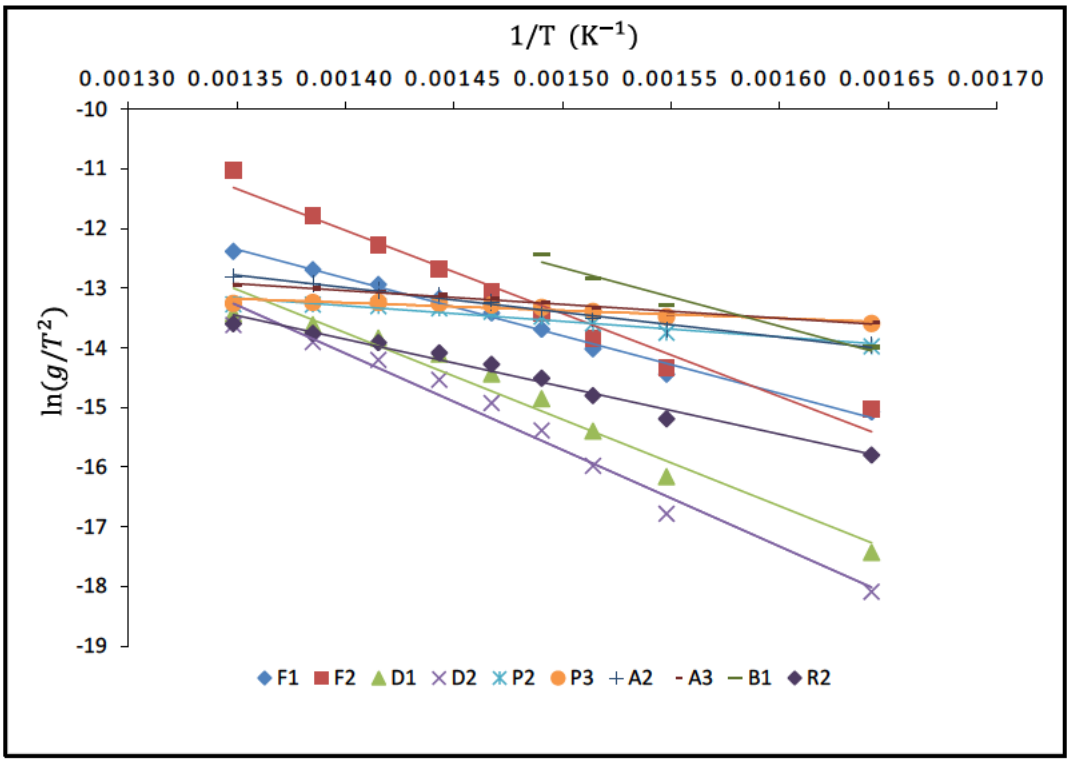

Figure B.6: Coats-Redfern method linear plots at β=30 °C/min

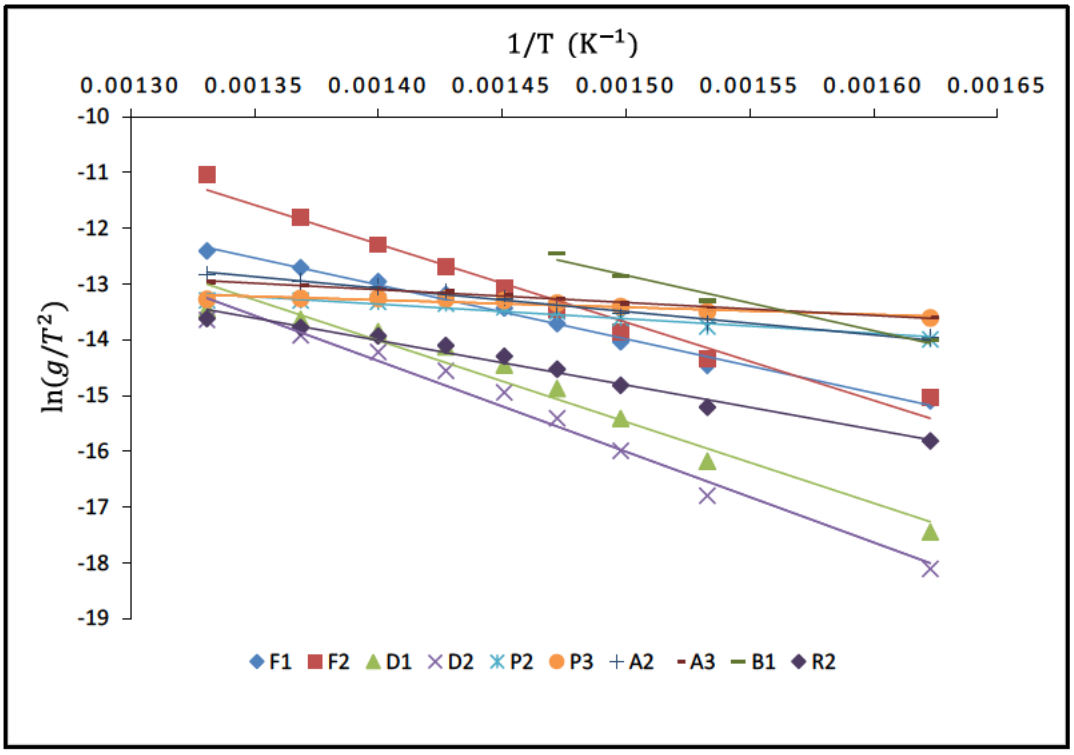

Figure B.7: Coats-Redfern method linear plots at β=40 °C/min

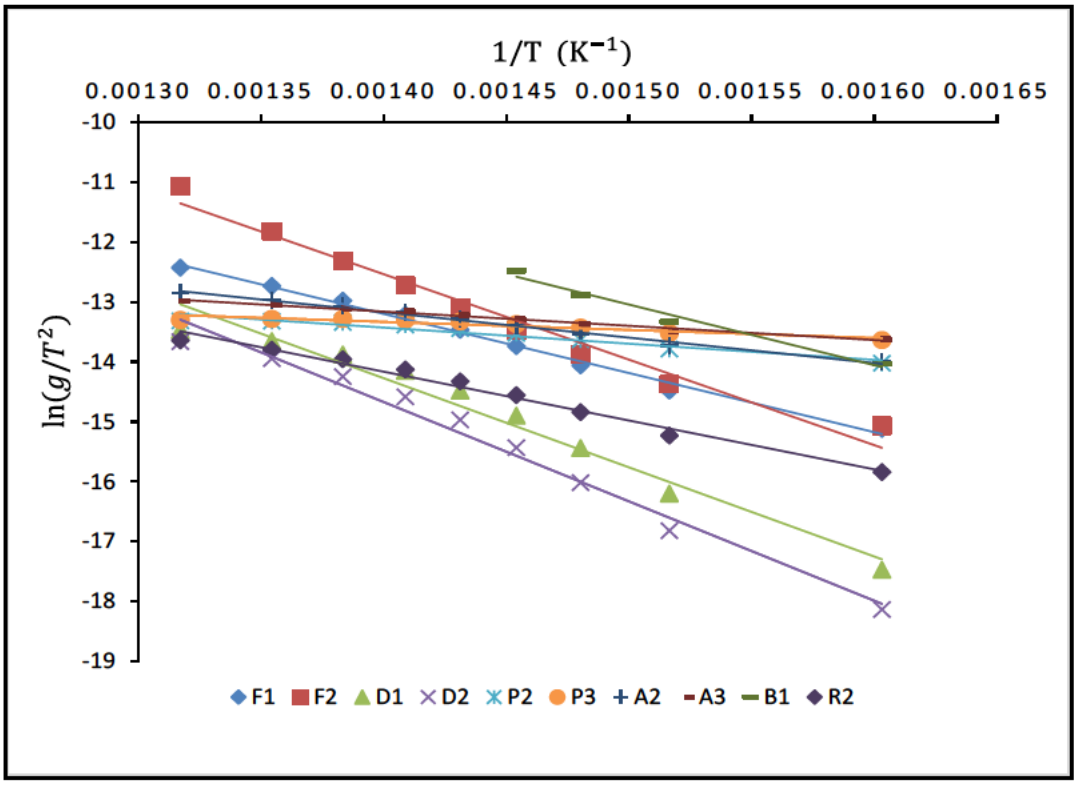

Figure B.8: Coats-Redfern method linear plots at β=50 °C/min

Table B.1: Activation energies and pre-exponential factors obtained at β=10 °C/min

Meth	Models	E_a/R	ln k_0	E_a	k_0	R^2
C&R	F1	8294.7	-0.672	69.0	5.1E-01	0.98
	F2	11965	5.4707	99.5	2.4E+02	0.95
	D1	12625	4.7272	105.0	1.1E+02	0.97
	D2	14061	6.475	116.9	6.5E+02	0.98
	P2	2198	-10.011	18.3	4.5E-05	0.94
	P3	1038.4	-11.648	8.6	8.7E-06	0.88
	A2	3508.4	-7.7978	29.2	4.1E-04	0.98
	A3	1913	-10.173	15.9	3.8E-05	0.97
	B1	7965.4	-0.1005	66.2	9.0E-01	0.95
	R2	6856.3	-3.7875	57.0	2.3E-02	0.98
DIFF	F1	10081	11.555	83.8	1.0E+05	0.95
	F2	16373	22.124	136.1	4.1E+09	0.98
	D1	10742	11.504	89.3	9.9E+04	0.78
	D2	13363	15.237	111.1	4.1E+06	0.89
	P2	314.29	-4.6201	2.6	9.9E-03	0.00
	P3	-844.31	-6.6631	-7.0	1.3E-03	0.03
	A2	5295.2	3.7357	44.0	4.2E+01	0.80
	A3	3439.6	0.955	28.6	2.6E+00	0.64
	B1	3129.8	1.7293	26.0	5.6E+00	0.67
	R2	6935.7	5.5771	57.7	2.6E+02	0.78

Table B.2: Activation energies and pre-exponential factors obtained at β=30 °C/min

Meth	Models	E_a/R	ln k_0	E_a	k_0	R^2
C&R	F1	9638.6	0.6601	80.1	1.9E+00	0.99
	F2	13929	7.4681	115.8	1.8E+03	0.97
	D1	14517	6.5741	120.7	7.2E+02	0.96
	D2	16184	8.5666	134.6	5.3E+03	0.98
	P2	2621.9	-9.6234	21.8	6.6E-05	0.93
	P3	1300.2	-11.423	10.8	1.1E-05	0.87
	A2	4147.7	-7.1812	34.5	7.6E-04	0.98
	A3	2317.5	-9.795	19.3	5.6E-05	0.98
	B1	9783.7	2.0177	81.4	7.5E+00	0.96
	R2	7961.9	-2.7096	66.2	6.7E-02	0.98
DIFF	F1	10321	12.218	85.8	2.0E+05	0.93
	F2	17663	23.91	146.9	2.4E+10	0.99
	D1	10910	12.017	90.7	1.7E+05	0.71
	D2	13961	16.208	116.1	1.1E+07	0.85
	P2	985.25	-5.5665	8.2	3.8E-03	0.03
	P3	-2306.9	-7.7716	-19.2	4.2E-04	0.16
	A2	4830.6	3.6837	40.2	4.0E+01	0.72
	A3	3000.3	0.6644	24.9	1.9E+00	0.49
	B1	2391.4	1.4198	19.9	4.1E+00	0.52
	R2	6650.6	5.6788	55.3	2.9E+02	0.70

Table B.3: Activation energies and pre-exponential factors obtained at β=40 °C/min

Meth	Models	E_a/R	ln k_0	E_a	k_0	R^2
C&R	F1	9689.6	0.5495	80.6	1.7E+00	0.99
	F2	14022	7.3468	116.6	1.6E+03	0.97
	D1	14581	6.4001	121.2	6.0E+02	0.96
	D2	16262	8.385	135.2	4.4E+03	0.98
	P2	2625.4	-9.6853	21.8	6.2E-05	0.92
	P3	1297	-11.473	10.8	1.0E-05	0.86
	A2	4165	-7.2488	34.6	7.1E-04	0.98
	A3	2323.4	-9.483	19.3	7.6E-05	0.98
	B1	9939.9	2.0643	82.6	7.9E+00	0.97
	R2	7997.4	-2.8146	66.5	6.0E-02	0.98
DIFF	F1	10147	12.051	84.4	1.7E+05	0.93
	F2	17558	23.721	146.0	2.0E+10	0.99
	D1	10706	11.797	89.0	1.3E+05	0.69
	D2	13785	15.977	114.6	8.7E+06	0.84
	P2	-1249.3	-5.6746	-10.4	3.4E-03	0.05
	P3	-2577.7	-7.8674	-21.4	3.8E-04	0.19
	A2	4622.4	3.5591	38.4	3.5E+01	0.71
	A3	2780.8	0.5542	23.1	1.7E+00	0.46
	B1	2176.9	1.3269	18.1	3.8E+00	0.50
	R2	6441.4	5.5223	53.6	2.5E+02	0.68

Table B.4: Activation energies and pre-exponential factors obtained at β=50 °C/min

Meth	Models	E_a/R	ln k_0	E_a	k_0	R^2
C&R	F1	9880.7	0.6334	82.2	1.9E+00	0.99
	F2	14270	7.4388	118.7	1.7E+03	0.97
	D1	14888	6.5671	123.8	7.1E+02	0.97
	D2	16596	8.5606	138.0	5.2E+03	0.98
	P2	2690.8	-9.6603	22.4	6.4E-05	0.94
	P3	1335.5	-11.463	11.1	1.1E-05	0.88
	A2	4252.8	-7.218	35.4	7.3E-04	0.99
	A3	2376.9	-9.8351	19.8	5.4E-05	0.98
	B1	10139	2.1623	84.3	8.7E+00	0.98
	R2	8164.4	-2.7361	67.9	6.5E-02	0.98
DIFF	F1	10369	12.385	86.2	2.4E+05	0.94
	F2	17882	24.075	148.7	2.9E+10	0.99
	D1	10986	12.206	91.3	2.0E+05	0.72
	D2	14110	16.398	117.3	1.3E+07	0.86
	P2	-1211	-5.4075	-10.1	4.5E-03	0.05
	P3	-2566.2	-7.616	-21.3	4.9E-04	0.75
	A2	4740.8	3.8402	39.4	4.7E+01	0.76
	A3	2864.8	0.8176	23.8	2.3E+00	0.52
	B1	2237.1	1.5665	18.6	4.8E+00	0.58
	R2	6611.7	5.8466	55.0	3.5E+02	0.72

A. Py-GCMS

C.1. EGA Chromatograms and compounds obtained at β= 100 °C/min

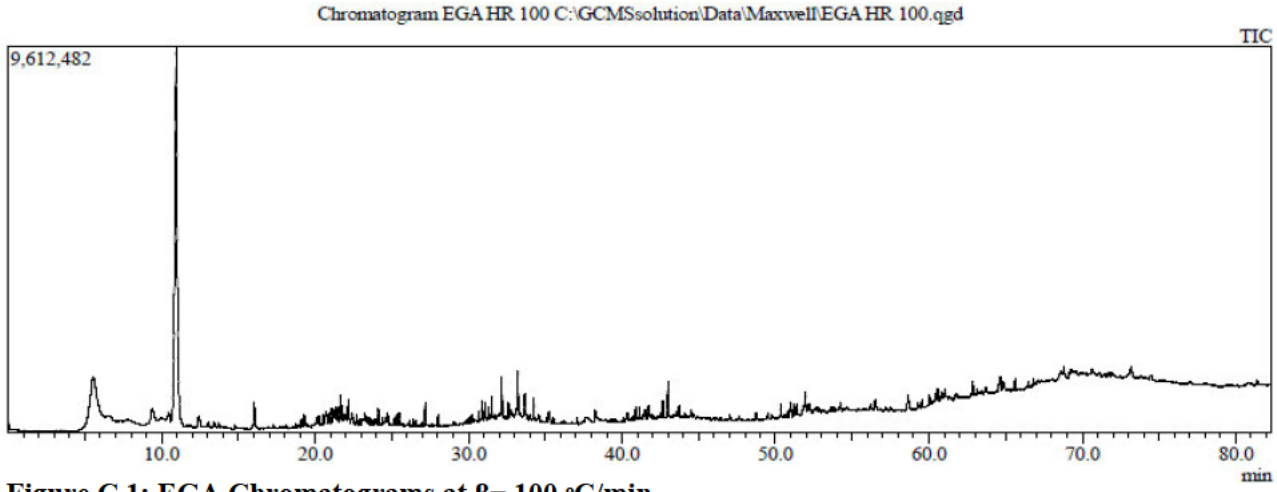

Figure C.1: EGA Chromatograms at β= 100 °C/min

Table C.1: Compounds obtained at β= 100 °C/min

Peak Report TIC

Peak#	R.Time	Area%	Name	Similarity	Base m/z
1	0.019	0.06	Ethyl iso-allocholate	83	55.05
2	10.937	42.76	D-Limonene	97	68.05
3	12.435	0.97	2,5-Dimethylphenyl methyl carbinol	86	107.10
4	13.385	0.60	2,4,6-Octatriene, 2,6-dimethyl-, (E,Z)-	91	121.10
5	16.038	1.18	Benzothiazole	96	135.00
6	19.118	0.28	1,4-Methanocyclooct[d]pyridazine, 1,4,4a,5,(	81	107.10
7	19.295	0.54	2,4,4,6,6,8,8-Heptamethyl-2-nonene	89	97.10
8	20.240	0.30	2,4,4,6,6,8,8-Heptamethyl-1-nonene	88	57.05
9	20.545	0.48	(1R,4R,5S)-1,8-Dimethyl-4-(prop-1-en-2-yl)sp	86	119.10
10	20.691	0.93	Azulene, 1,2,3,5,6,7,8,8a-octahydro-1,4-dimet	88	107.10
11	20.919	0.49	3,7,11,Trimethyl-8,10- dodecedienylacetate	83	81.10
12	21.084	0.66	Cyclohexanamine, N-cyclohexyl-	89	138.15
13	21.235	1.15	3,7,11,Trimethyl-8,10- dodecedienylacetate	86	81.10
14	21.375	0.88	(1S,2E,6E,10R)-3,7,11,11-Tetramethylbicyclo[	89	121.10
15	21.500	0.60	Squalene	90	69.10
16	21.639	1.30	Quinoline, 1,2-dihydro-2,2,4-trimethyl-	91	158.10
17	21.792	0.80	2,6,9,11-Dodecatetraenal, 2,6,10-trimethyl-, (E	88	93.05
18	22.021	0.82	1,5,9-Cyclododecatriene, 1,5,9-trimethyl-	81	107.10
19	22.159	1.66	(Z)-1-Methyl-4-(6-methylhept-5-en-2-ylidene))	89	93.10
20	22.425	1.01	Azulene, 1,2,3,5,6,7,8,8a-octahydro-1,4-dimet	87	93.10
21	22.712	0.55	.alpha.-Farnesene	89	93.10
22	22.918	0.34	Bicyclo[7.2.0]undec-4-ene, 4,11,11-trimethyl-(	81	93.10
23	23.035	0.56	1-Naphthalenol, 1,2,3,4-tetrahydro-2,5,8-trime	68	157.10
24	23.221	0.43	(3S,4R,5R,6R)-4,5-Bis(hydroxymethyl)-3,6-di	80	121.10
25	23.334	0.54	cis-.alpha.-Bisabolene	85	93.10
26	23.515	0.47	trans-8-Isopropylbicyclo[4.3.0]non-3-ene	77	121.10
27	23.690	0.33	1,4-Methanocyclooct[d]pyridazine, 1,4,4a,5,(	82	107.10
28	23.952	0.45	(Z)-1-Methyl-4-(6-methylhept-5-en-2-ylidene))	74	119.10
29	24.118	0.71	Cyclohexane, 1-ethenyl-1-methyl-2,4-bis(1-me	89	81.10
30	24.414	0.43	cis-.alpha.-Bisabolene	82	109.10
31	24.572	0.44	.alpha.-Bisabolol	81	109.10
32	24.742	0.71	1H-Benzocycloheptene, 2,4a,5,6,7,8,9,9a-octa	85	109.15
33	25.134	0.20	(Z)-1-Methyl-4-(6-methylhept-5-en-2-ylidene))	85	119.10
34	25.275	0.33	Bis(2-ethylhexyl) methylphosphonate	85	97.10
35	25.498	0.35	Phenol, 4-(1,1,3,3-tetramethylbutyl)-	96	135.10
36	26.416	0.21	Phenol, 2-methyl-4-(1,1,3,3-tetramethylbutyl)-	89	149.10
37	26.581	0.21	(1S,7S,8aR)-1,8a-Dimethyl-7-(prop-1-en-2-yl)	83	119.10
38	26.978	0.19	Acenaphthylene, dodecahydro-3-pentadecyl-	81	121.10
39	27.174	0.68	Bis(2-ethylhexyl) methylphosphonate	88	97.10
40	28.021	0.29	2,4,4,6,6,8,8-Heptamethyl-1-nonene	88	57.05
41	30.208	0.20	1,3,6,10-Cyclotetradecatetraene, 3,7,11-trimeth	88	81.05
42	30.654	0.29	Squalene	83	81.10
43	30.863	0.86	6,10,14,18,22-Tetracosapentaen-2-ol, 3-bromo	87	81.10
44	31.065	0.64	2,6,10,14,18-Pentamethyl-2,6,10,14,18-eicosa	92	69.10
45	31.322	0.40	Bicyclo[5.2.0]nonane, 4-methylene-2,8,8-trime	85	134.10
46	31.523	0.70	1,3,6,10-Cyclotetradecatetraene, 3,7,11-trimeth	86	134.10
47	32.165	1.47	Cyclohexane, 1-ethenyl-1-methyl-2-(1-methyle	87	121.10
48	32.264	0.32	Bis(2-ethylhexyl) methylphosphonate	87	97.10
49	32.587	0.74	1,5-Cycloundecadiene, 8,8-dimethyl-9-methyle	86	93.10
50	32.805	0.45	(1S,2E,6E,10R)-3,7,11,11-Tetramethylbicyclo[	84	121.10
51	33.209	2.14	n-Hexadecanoic acid	95	73.05

Peak#	R.Time	Area%	Name	Similarity	Base m/z
52	33.657	1.08	1,3,6,10-Cyclotetradecatetraene, 3,7,11-trimeti	85	93.05
53	34.246	0.85	Bis(2-ethylhexyl) methylphosphonate	86	97.10
54	34.583	0.28	1,3,6,10-Cyclotetradecatetraene, 3,7,11-trimeti	83	93.05
55	35.078	0.21	.gamma.-Elemene	86	121.10
56	35.235	0.67	2,4,4,6,6,8,8-Heptamethyl-1-nonene	79	57.10
57	35.533	0.29	(R,1E,5E,9E)-1,5,9-Trimethyl-12-(prop-1-en-2	81	121.10
58	37.084	0.33	.alpha.-Santalol	72	107.10
59	38.263	0.42	Octadecanoic acid	93	73.05
60	40.376	0.48	Bis(2-ethylhexyl) methylphosphonate	85	97.10
61	40.909	0.59	6,10,14,18,22-Tetracosapentaen-2-ol, 3-bromo	88	81.10
62	41.133	0.56	2,6,10,14,18-Pentamethyl-2,6,10,14,18-eicosa	91	69.10
63	41.509	0.38	1,3,6,10-Cyclotetradecatetraene, 3,7,11-trimeti	86	134.10
64	41.721	0.73	Cycloheptane, 4-methylene-1-methyl-2-(2-met	87	81.10
65	42.680	0.77	Sulfurous acid, cyclohexylmethyl heptyl ester	84	97.10
66	42.990	1.48	1,4-Benzenediamine, N-(1,3-dimethylbutyl)-N	95	211.10
67	43.529	0.28	Cyclohexane, 1-ethenyl-1-methyl-2,4-bis(1-me	85	81.10
68	43.714	0.55	2,4,4,6,6,8,8-Heptamethyl-1-nonene	76	57.05
69	44.507	0.35	Octadecane, 1-chloro-	78	57.10
70	48.744	0.37	Sulfurous acid, cyclohexylmethyl pentadecyl e	85	97.10
71	49.510	0.28	Hexatriacontane	90	57.05
72	50.355	0.58	4,4'-((p-Phenylene)diisopropylidene)diphenol	75	331.20
73	50.823	0.25	Thunbergol	86	81.05
74	50.968	0.63	Bis(2-ethylhexyl) methylphosphonate	84	97.10
75	51.055	0.21	Squalene	85	81.10
76	51.229	0.59	Squalene	89	81.10
77	51.415	0.40	1,6,10,14,18,22-Tetracosahexaen-3-ol, 2,6,10,	91	69.10
78	51.801	0.43	9,19-Cycloergost-24(28)-en-3-ol, 4,14-dimeth	84	81.10
79	51.952	1.40	Tricyclo[20.8.0.0(7,16)]triacontane, 1(22),7(1	75	57.05
80	52.212	0.81	5-Phenyl-2,4-pyrimidinediamine, 2TMS deriva	59	315.15
81	54.244	0.28	Nonacosane	86	57.10
82	56.185	0.38	Piperine	90	201.05
83	56.543	0.82	Sulfurous acid, cyclohexylmethyl octadecyl est	84	97.10
84	58.633	0.99	Sulfurous acid, cyclohexylmethyl octadecyl est	85	97.10
85	59.549	0.25	Heptyl triacontyl ether	75	113.15
86	60.035	0.50	Stigmast-5-en-3-ol, oleate	87	147.15
87	60.431	0.44	Squalene	88	81.10
88	60.581	0.50	Squalene	89	69.10
89	60.817	0.40	Hexatriacontane	95	57.10
90	60.935	0.22	Cyclohexane, 1-ethenyl-1-methyl-2,4-bis(1-me	81	81.10
91	61.051	0.36	Thunbergol	82	81.10
92	61.822	0.40	(R)-2,7,8-Trimethyl-2-((3E,7E)-4,8,12-trimeth	84	151.10
93	62.867	0.55	2-Methylhexacosane	80	57.10
94	63.694	0.23	2-Thiopheneacetic acid, butyl ester	81	97.10
95	64.629	1.10	.gamma.-Sitosterol	82	97.10
96	64.875	0.58	Tetrapentacontane	93	57.05
97	65.621	0.46	Sulfurous acid, cyclohexylmethyl octadecyl est	83	97.10
98	66.474	0.29	Borinic acid, diethyl-, (2-ethyl-1,3,2-dioxaboro	75	113.15
99	68.792	0.42	2,2,4-Trimethyl-3-(3,8,12,16-tetramethyl-hept	79	69.10
100	73.175	0.48	2-Thiopheneacetic acid, butyl ester	80	97.10
		100.00			

Table C.1: Detected compounds from Py-GCMS analysis

Peak Nº	R. Time	Area %	Name
1	1.021	0.03	R-(-)-Cyclohexylethylamine
2	1.657	9.5	2-Butene
3	1.827	16.81	Isoprene
4	1.994	0.09	2-Pentene, 2-methyl-
5	2.272	0.3	1,3-Pentadiene, 3-methyl-, (Z)-
6	2.47	1.02	1,3,5-Hexatriene, (Z)-
7	2.565	0.46	1,4-Pentadiene, 3-methyl-
8	2.66	0.09	Benzene
9	2.741	0.08	1,3-Cyclopentadiene, 1-methyl-
10	2.944	0.07	Cyclohexane, 1-(1,1-dimethylethyl)-4-methyl-
11	3.094	0.33	1,3-Pentadiene, 2,4-dimethyl-
12	3.239	0.29	1-Pentene, 2,4,4-trimethyl-
13	3.43	0.33	Cyclohexane, 1,4-dimethyl-, cis-
14	3.67	0.29	3-Methylenecyclohexene
15	3.842	0.69	Cyclobutane, (1-methylethylidene)-
16	3.94	0.12	1,3,5-Hexatriene, 3-methyl-, (Z)-
17	4.048	0.24	Cyclopentane, 1,3-bis(methylene)-
18	4.126	1.41	1,3,5-Cycloheptatriene
19	4.208	0.62	Formic acid, 2,4,4-trimethylpentyl ester
20	4.355	0.1	Thiophene, 3-methyl-
21	4.425	0.21	2-Cyclohexen-1-ol, 3-methyl-
22	4.656	0.17	Cyclopentanone
23	4.867	0.11	1,3,5-Hexatriene, 3-methyl-, (Z)-
24	5.027	0.05	Cyclohexane, 1,4-dimethyl-
25	5.206	0.25	Cyclopentadiene, 2,5,5-trimethyl-
26	5.456	0.21	1,3-Dimethyl-1-cyclohexene
27	5.51	0.1	Cyclopentane, 1,2-dimethyl-3-methylene-, cis-
28	5.748	1	Cyclohexene, 4-ethenyl-
29	5.986	0.23	3,5-Heptadien-2-ol, 2,6-dimethyl-
30	6.23	0.09	3-Oxatricyclo [3.2.1.0] octane, (1alph.,2beta,4.8beta.,5alpha..1)-
31	6.359	0.22	Cyclopentadiene, 2,5,5-trimethyl-
32	6.511	0.34	o-Xylene
33	6.776	1.67	o-Xylene
34	7.004	0.17	Cyclopentene, 3-ethylidene-1-methyl-
35	7.243	0.15	L-Fenchone
36	7.33	0.14	(3aR,4R,8R,8aS)-3a,4,8a-Trimethyl-7-methylenedeca 7h4y dro-4,8 -9m3.e1t0ha noazulene-rel-
37	7.507	1.86	Styrene
38	7.84	0.13	3,3-Dimethyl-6-methylenecyclohexene
39	8.379	0.19	2,4,6-Octatriene, 2,6-dimethyl-, (E,Z)-
40	8.875	0.18	Tricyclo[5.2.1.0(1,5)]decane

Table C.1 continued

Peak Nº	R. Time	Area %	Name
41	8.945	0.04	1,7-Octadiene, 2,7-dimethyl-
42	9.318	0.25	1,5-Heptadiene, 3,3,5-trimethyl-
43	9.451	0.44	Cyclohexene, 1,5,5-trimethyl-3-methylene-
44	9.517	0.19	Cyclohexanethiol
45	9.81	0.09	1,3-Cyclopentadiene, 5,5-dimethyl-1-propyl-
46	9.96	0.6	1,7-Octadien-3-ol, 3,7-dimethyl-
47	10.059	1.91	D-Limonene
48	10.16	0.19	Benzene, 1-ethyl-2-methyl-
49	10.282	0.65	Carveol
50	10.415	0.07	1,3,7-Octatriene, 2,7-dimethyl-
51	10.474	0.12	Bicyclo[3.1.0]hexan-3-ol,4-methylene-1-(1-methylet h7y8l)-, [1S- 9(11..a1l0p ha.,3.beta.,5.alpha.)]
52	10.624	0.24	Tricyclo[5.2.1.0(1,5)]decane
53	10.754	0.15	Aniline
54	10.908	0.65	9-Dodecyn-1-ol
55	11.076	0.57	1,3-Cyclohexadiene, 1,3,5,5-tetramethyl-
56	11.155	0.12	Chloroacetic acid, dodec-9-ynyl ester
57	11.221	0.41	1,5-Heptadiene, 3,3,5-trimethyl-
58	11.458	0.77	1,6-Octadiene, 2,6-dimethyl-, (Z)-
59	11.614	0.37	1-(2-Methylphenyl)ethanol
60	11.842	0.63	cis-2,6-Dimethyl-2,6-octadiene
61	12.037	0.32	Spiro[4.5]dec-1-ene
62	12.132	0.26	p-Menth-4(8)-en-9-ol
63	12.455	1.26	1,3,6-Heptatriene, 2,5,6-trimethyl-
64	12.621	0.21	(+)-4-Carene
65	12.738	0.15	Mesitylene
66	12.952	0.89	Carveol
67	13.277	20.37	D-Limonene
68	13.335	0.12	Mesitylene
69	13.433	0.21	Cyclohexane, 1-methylene-4-(1-methylethenyl)-
70	13.64	0.21	Cyclohexane, 1-methylene-4-(1-methylethenyl)-
71	13.742	0.08	Indene
72	13.984	0.25	1,3,6-Octatriene, 3,7-dimethyl-, (Z)-
73	14.399	0.19	Disulfide, bis(1,1,3,3-tetramethylbutyl)
74	14.971	0.12	1,3-Cyclopentadiene, 5,5-dimethyl-2-propyl-
75	15.66	0.08	1,6-Octadiene, 5,7-dimethyl-, (R)- 7
76	15.74	0.14	Cyclohexene, 1-methyl-4-(1-methylethylidene)-
77	15.957	0.49	Benzene, 2-ethenyl-1,3-dimethyl-
78	16.035	0.15	1,3-Cyclopentadiene, 5,5-dimethyl-1-propyl-
79	16.126	0.09	1-Undecene
80	16.292	0.07	Cyclopentanone, 2-(2-methylpropylidene)-

Table C.1 continued

Peak Nº	R. Time	Area %	Name
81	16.541	0.09	Undecane, 2,6-dimethyl-
82	16.843	0.06	Benzene, 1-methyl-4-(1-methylpropyl)-
83	17.014	0.59	1,3,8-p-Menthatriene
84	17.784	0.29	2,4,6-Octatriene, 2,6-dimethyl-, (E,Z)-
85	18.024	0.06	Adamantane-1-carboxamide, N-(4-isopropylphenyl)-
86	18.338	0.23	2,4,6-Octatriene, 2,6-dimethyl-, (E,Z)-
87	19.023	0.11	Cyclohexane, 1,2,4-triethenyl-
88	20.095	0.07	Benzene, (2-methyl-1-butenyl)-
89	20.85	0.17	Cyclododecane
90	22.162	1.05	Benzothiazole
91	23.551	0.18	Caprolactam
92	24.428	0.13	Bis(2-ethylhexyl) methylphosphonate
93	25.335	0.17	Phenol, m-tert-butyl-
94	25.467	0.11	1-Pentadecene
95	25.855	0.11	Tridecane
96	27.782	0.29	Bis(2-ethylhexyl) methylphosphonate
97	28.149	0.17	Phenol, 4-(1,1-dimethylethyl)-2-methyl-
98	28.818	0.09	1H-Indene, 1,1,3-trimethyl-
99	29.3	0.11	(Z)-1-Methyl-4-(6-methylhept-5-en-2-ylidene)cyclohe-1-ene
100	29.375	0.18	Disulfide, bis(1,1,3,3-tetramethylbutyl)
101	29.875	0.13	1-Tetradecanol
102	29.986	0.32	(Z)-1-Methyl-4-(6-methylhept-5-en-2-ylidene)cyclohe 8x8-1 -ene
103	30.299	0.58	Bicyclo[5.2.0]nonane, 4-methylene-2,8,8-trimethyl-2 -8v7in yl-
104	30.599	0.28	1-Cycloheptene, 1,4-dimethyl-3-(2-methyl-1-propene -818- yl)-4-v1i0ny7l.-1
105	30.815	0.08	Cycloheptane, 4-methylene-1-methyl-2-(2-methyl-1-prpen-1-yl)3-1.1-vinyl-
106	31.105	0.26	trans-Geranylgeraniol
107	31.198	0.53	Bicyclo[5.2.0]nonane, 4-methylene-2,8,8-trimethyl-2 -8v2in yl-
108	31.33	0.06	Bicyclo[4.4.0]dec-6-en-9.beta.-ol, 1,7-dimethyl-4.alp h6a2. -isopro p5e7n.1yl
109	31.661	0.61	2-(3-Chloro-propyl)-1,1-dimethyl-3-methylene-cycloh 7e4x ane
110	31.833	0.15	Azulene, 1,2,3,4,5,6,7-octahydro-1,4-dimethyl-7-(17-5methyl ethenyl)-,
111	32.128	0.44	Bicyclo[7.2.0]undec-4-ene, 4,11,11-trimethyl-8-methylene-
112	32.382	0.19	Tricyclo[7.2.0.0]undec-4-ene, 4,8,11,11-tetramethyl-
113	32.455	0.12	(1R,4R,4aS,8aR)-4,7-Dimethyl-1-(prop-1-en-2-yl)-1, 28,13 ,4,4a, 51,169,8.1a0-octa hydronaphtalene
114	32.551	0.19	(1R,4R,4aS,8aR)-4,7-Dimethyl-1-(prop-1-en-2-yl)-1, 28,73 ,4,4a, 51,169,8.1a0-octa hydronaphtalene
115	32.615	0.1	Supraene
116	32.76	0.49	(Z)-1-Methyl-4-(6-methylhept-5-en-2-ylidene)cyclohe 8x7-1 -ene
117	33.46	0.13	Benzene, 1-(1,5-dimethyl-4-hexenyl)-4-methyl-
118	33.66	0.3	.alpha.-Farnesene
119	33.891	0.16	(1S,2E,6E,10R)-3,7,11,11-Tetramethylbicyclo[8.1.0] u7n5d eca-2,6 9-3d.i1en0e
120	34.05	0.17	Trifluoroacetic acid,n-tridecyl ester

Table C.1 continued

Peak Nº	R. Time	Area %	Name
121	34.385	0.28	7-Hexadecenal, (Z)-
122	34.607	0.13	(2S,4R)-p-Mentha-[1(7),8]-diene 2-hydroperoxide
123	34.856	0.13	(3S,4R,5R,6R)-4,5-Bis(hydroxymethyl)-3,6-dimethyl cyclohex
124	35.337	0.1	Naphthalene, 2,3,6-trimethyl-
125	35.885	0.3	Cyclohexane, 1-ethenyl-1-methyl-2,4-bis(1-methylethenyl)-
126	36.438	0.07	Cyclohexene, 4-[(1E)-1,5-dimethyl-1,4-hexadien-1-yl]--meth 1yl-
127	36.599	0.2	1,5-Cyclodecadiene, 1,5-dimethyl-8-
128	36.748	0.17	Cyclohexene, 4-[(1E)-1,5-dimethyl-1,4-hexadien-1-yl]-1 -methyl
129	37.741	0.14	Bis(2-ethylhexyl) methylphosphonate
130	38.006	0.16	1-Heptadecene
131	38.138	0.33	Phenol, 4-(1,1,3,3-tetramethylbutyl)-
132	39.203	0.09	Sulfurous acid, cyclohexylmethyl octadecyl ester
133	39.655	0.16	Phenol, 2-methyl-4-(1,1,3,3-tetramethylbutyl)-
134	40.854	0.29	Bis(2-ethylhexyl) methylphosphonate
135	41.765	0.15	1-Nonadecene
136	42.039	0.06	Heptadecane
137	42.245	0.16	2,4,4,6,6,8,8-Heptamethyl-1-nonene
138	45.98	0.13	1,3,6,10-Cyclotetradecatetraene, 3,7,11-trimethyl-14-(1-methylethyl)-,
139	46.752	0.19	Squalene
140	47.113	0.38	1,6,10,18,22-Tetracosahexaen-3-ol, 2,6,10,15,2 837- hexame ethyl-
141	47.453	0.36	trans-Geranylgeraniol
142	47.877	0.18	(Z)-1-Methyl-4-(6-methylhept-5-en-2-ylidene)cyclohe-1-ene
143	48.215	0.38	Bicyclo[5.2.0]nonane, 4-methylene-2,8,8-trimethyl-2-vinyl-
144	48.833	0.16	Caryophyllene oxide
145	48.981	0.16	Nerolidyl propionate
146	49.123	0.57	Cyclohexane, 1-ethenyl-1-methyl-2-(1-methylethenyl)
147	49.251	0.1	1-(Trimethylsilyl)-1-propyne
148	49.778	0.19	Cycloheptane, 4-methylene-1-methyl-2-(2-methyl-1-propenyl)
149	50.161	0.15	Cyclohexane, 1-ethenyl-1-methyl-2,4-bis(1-methylethenyl)-
150	50.834	0.17	Ethyl iso-allocholate
151	51.364	0.27	1,3,6,10-Cyclotetradecatetraene, 3,7,11-trimethyl-14-(1-methylethyl)-
152	51.864	0.08	Cyclohexane, 1-ethenyl-1-methyl-2,4-bis(1-methylethenyl)-
153	52.027	0.37	Sulfurous acid, cyclohexylmethyl pentadecyl ester
154	53.259	0.19	2,4,4,6,6,8,8-Heptamethyl-1-nonene
155	59.566	0.27	14Z-Eeicosatetraenoic acid, 3-ethenylmethyl ester
156	59.952	0.1	Squalene
157	60.172	0.37	Squalene
158	60.392	0.33	1,6,10,14,18-Tetracosahexaen-3-ol, 2,6,10,15,19,2 838- hexamethyl-
159	60.49	0.08	.beta.-Humulene
160	60.583	0.09	Sulfurous acid, cyclohexylmethyl pentadecyl ester

Table C.1 continued

Peak Nº	R. Time	Area %	Name
161	60.737	0.2	1,3,6,10-Cyclotetradecatetraene, 3,7,11-trimethyl-14- (methy ethyl)-
162	60.934	0.42	Cycloheptane, 4-methylene-1-methyl-2-(2-methyl-1-propenyl)4-1.1-vinyl-
163	61.44	0.18	Cycloheptane, 4-methylene-1-methyl-2-(2-methyl-1-propenyl)1-1.1-vinyl-
164	61.635	0.11	1,3,6,10-Cyclotetradecatetraene, 3,7,11-trimethyl-14-(15-methylethyl)-
165	61.725	0.38	Sulfurous acid, cyclohexylmethyl octadecyl ester
166	62.006	0.72	1,4-Benzenediamine, N-(1,3-dimethylbutyl)-N'-phenyl-
167	62.313	0.08	Cyclohexane, 1-ethenyl-1-methyl-2,4-bis(1-methylethenyl)-,
168	62.492	0.16	Cyclohexane, 1-ethenyl-1-methyl-2,4-bis(1-methyletheny l)-
169	62.615	0.2	3-Heptene, 2,2,4,6,6-pentamethyl-
170	62.933	0.08	Cyclohexane, 1-ethenyl-1-methyl-2,4-bis(1-methylethenyl)-,
171	63.324	0.14	Dotriacontane, 1-iodo-
172	65.254	0.13	Tetratriacontane
173	66.513	0.1	Sulfurous acid, cyclohexylmethyl pentadecyl ester
174	67.013	0.12	Dotriacontane
175	67.267	0.12	Sulfurous acid, cyclohexylmethyl pentadecyl ester
176	67.665	0.14	4,4'-((p-Phenylene)diisopropylidene)diphenol
177	67.835	0.15	1,3,6,10-Cyclotetradecatetraene, 3,7,11-trimethyl-14- (12-methyl ethyl)-
178	67.947	0.12	Thunbergol
179	68.088	0.31	Sulfurous acid, cyclohexylmethyl octadecyl ester
180	68.221	0.26	Squalene
181	68.341	0.24	1,6,10,14,18-Tetracosahexaen-3-ol, 2,6,10,15,19,2 930- hexamethyl-0,
182	68.594	0.17	1,3,6,10-Cyclotetradecatetraene, 3,7,11-trimethyl-14- (12-methylethyl)- ,
183	68.704	0.53	(R,1E,5E,9E)-1,5,9-Trimethyl-12-(prop-1-en-2-yl)cyclotetrade 2c7a4-1.1,55, 9-triene
184	68.755	0.18	2,4,4,6,6,8,8-Heptamethyl-1-nonene
185	68.815	0.08	.psi.,.psi.-Carotene, 7,8,11,11',12,12',15,15'-decahydro-
186	68.962	0.36	5-Phenyl-2,4-pyrimidinediamine, 2TMS derivative
187	69.178	0.06	1-Cycloheptene, 1,4-dimethyl-3-(2-methyl-1-propene-11-yl)-4-vinyl.-
188	69.838	0.06	Cyclohexane, 1-ethenyl-1-methyl-2,4-bis(1-methylethenyl)-,
189	69.935	0.08	Cyclohexane, 1-ethenyl-1-methyl-2,4-bis(1-methylethenyl)-,
190	70.183	0.2	Dotriacontane, 1-iodo-
191	70.527	0.09	1-Naphthalenecarboxylic acid, decahydro-1,4a-dimet hy -6-methylene- 5-(3-methyl-2,4-pentadienyl)-, methyl ester,
192	71.639	0.33	Dotriacontane
193	73.234	0.14	Tetracontane
194	73.336	0.15	Bis(2-ethylhexyl) methylphosphonate
195	73.969	0.06	(3S,8S,9S,10R,13R,14S,17R)-17-((2R,5R)-5-Ethyl-6 8-methylheptan-yl)-3-methoxy-10,13-dimethyl-2,3,4,7,8,9,10,11,12,13,14,15,16,1
196	74.105	0.12	Heptyl triacontyl ether
197	74.51	0.21	9,19-Cycloergost-24(28)-en-3-ol, 4,14-dimethyl-,
198	74.621	0.37	Stigmast-5-en-3-ol, oleate
199	74.932	0.14	Squalene
200	75.102	0.1	Dotriacontane